Melt/rock reaction at oceanic peridotite/gabbro transition as revealed by trace element chemistry of olivine

Elisabetta Rampone, Giulio Borghini, Marguerite Godard, Benoit Ildefonse, Laura Crispini, Patrizia Fumagalli

Elsevier Editorial System(tm) for Geochimica et Cosmochimica Acta

Manuscript Draft

Manuscript Number: GCA-D-15-00758R1

Title: Melt/rock reaction at oceanic peridotite/gabbro transition as revealed by trace element chemistry of olivine

Article Type: Article

Corresponding Author: Prof. Elisabetta Rampone,

Corresponding Author's Institution: University of Genova

First Author: Elisabetta Rampone

Order of Authors: Elisabetta Rampone; Giulio Borghini; Marguerite Godard; Benoit Ildefonse; Laura Crispini; Patrizia Fumagalli

Abstract: Several recent studies have documented that reactions between melt and crystal mush in primitive gabbroic rocks (via reactive porous flow) have an important control in the formation of the lower oceanic crust and the evolution of MORBs. In this context, olivine-rich rocks can form either by fractional crystallization of primitive melts or by open system reactive percolation of pre-existing (possibly mantle-derived) olivine matrix. To address this question, we performed in-situ trace element analyses (by LA-ICP-MS) of olivine from the Erro-Tobbio ophiolite Unit (Ligurian Alps), where mantle peridotites show gradational contacts with an hectometer-scale body of troctolites and plagioclase wehrlites, and both are cut by later decameter-wide lenses and dykes of olivine gabbros. Previous studies inferred that troctolites and olivine gabbros represent variably differentiated crystallization products from primitive MORB-type melts. Olivines in the three rock types (mantle peridotites, troctolites, olivine gabbros) exhibit distinct geochemical signature and well-defined elemental correlations. As expected, compatible elements (e.g. Ni) show the highest concentrations in peridotites (2580-2730 ppm), intermediate in troctolites (2050-2230 ppm) and lowest in gabbros (1355-1420 ppm), whereas moderate incompatible elements (e.g. Mn, Zn) show the opposite behaviour. By contrast, highly incompatible elements like Zr, Hf, Ti, HREE are variably enriched in olivines of troctolites, and the enrichment in absolute concentrations is coupled to development of significant HFSE/REE fractionation (ZrN/NdN up to 80). AFC modeling shows that such large ZrN/NdN ratios in olivines are consistent with a process of olivine assimilation and plagioclase crystallization at decreasing melt mass, in agreement with textural observations. In-situ trace element geochemistry of olivine, combined with microstructural investigations, thus appears a powerful tool to investigate reactive percolation and the origin of olivine-rich rocks in the lower oceanic crust.

Melt/rock reaction at oceanic peridotite/gabbro transition as revealed by trace element chemistry of olivine

Elisabetta Rampone[1], Giulio Borghini[2], Marguerite Godard[3], Benoit Ildefonse[3] Laura Crispini[1,] Patrizia Fumagalli[2]

, **http://dx.doi.org/10.1016/j.gca.2016.06.029**

[1]DISTAV, University of Genova, Corso Europa 26, I-16132 Genova, Italy

[2]Dipartimento di Scienze della Terra, University of Milano, via Botticelli 23, 20133 Milano, Italy

[3]Géosciences Montpellier, Université de Montpellier, CNRS UMR 5243, 34095 Montpellier cedex 05, France

Corresponding Author

Elisabetta Rampone
Dipartimento di Scienze della Terra, dell'Ambiente e della Vita (DISTAV)
Università degli Studi di Genova
Corso Europa 26
I-16132 Genova (Italy)

Tel. 0039 10 3538315
Fax. 0039 10 352169
Email: betta@dipteris.unige.it

Abstract

Several recent studies have documented that reactions between melt and crystal mush in primitive gabbroic rocks (via reactive porous flow) have an important control in the formation of the lower oceanic crust and the evolution of MORBs. In this context, olivine-rich rocks can form either by fractional crystallization of primitive melts or by open system reactive percolation of pre-existing (possibly mantle-derived) olivine matrix. To address this question, we performed in-situ trace element analyses (by LA-ICP-MS) of olivine from the Erro-Tobbio ophiolite Unit (Ligurian Alps), where mantle peridotites show gradational contacts with an hectometer-scale body of troctolites and plagioclase wehrlites, and both are cut by later decameter-wide lenses and dykes of olivine gabbros. Previous studies inferred that troctolites and olivine gabbros represent variably differentiated crystallization products from primitive MORB-type melts. Olivines in the three rock types (mantle peridotites, troctolites, olivine gabbros) exhibit distinct geochemical signature and well-defined elemental correlations. As expected, compatible elements (e.g. Ni) show the highest concentrations in peridotites (2580-2730 ppm), intermediate in troctolites (2050-2230 ppm) and lowest in gabbros (1355-1420 ppm), whereas moderate incompatible elements (e.g. Mn, Zn) show the opposite behaviour. By contrast, highly incompatible elements like Zr, Hf, Ti, HREE are variably enriched in olivines of troctolites, and the enrichment in absolute concentrations is coupled to development of significant HFSE/REE fractionation (Zr_N/Nd_N up to 80). AFC modeling shows that such large Zr_N/Nd_N ratios in olivines are consistent with a process of olivine assimilation and plagioclase crystallization at decreasing melt mass, in agreement with textural observations. In-situ trace element geochemistry of olivine, combined with microstructural investigations, thus appears a powerful tool to investigate reactive percolation and the origin of olivine-rich rocks in the lower oceanic crust.

1. INTRODUCTION

Several lines of evidence have stressed that melt/rock reactions acting at the oceanic mantle-crust boundary play an important role in the chemical evolution of MORBs and the formation of the primitive (olivine-rich) lower oceanic crust (Bedard et al., 2000; Coogan et al., 2000; Drouin et al., 2009, 2010; Gao et al., 2007; Dick et al., 2008; Lissenberg and Dick, 2008; Kvassnes and Grove, 2008; Eason and Sinton, 2009; Godard et al., 2009; Collier and Kelemen, 2010; Renna and Tribuzio, 2011; Sanfilippo and Tribuzio, 2011, 2012; Lissenberg et al., 2013; Sanfilippo et al., 2013, 2014, 2015a,b; Saper and Liang 2014). Specific chemical features in MORBs, such as the spread in MgO contents at given CaO values, cannot be easily reconciled with processes of fractional crystallization of heterogeneous parental melts occurring at variable pressure. Based on this observation, a series of papers inferred that the composition of MORBs can be modified by melt/rock reactions taking place either in the primitive lower oceanic crust, or in the uppermost lithospheric mantle (e.g. Lissenberg and Dick, 2008; Collier and Kelemen, 2010; Lissenberg et al., 2013). Collier and Kelemen (2010) described this process as reactive crystallization, linking the peculiar chemical signatures of MORBs to the diffuse evidence of melt percolation and impregnation in the oceanic mantle (e.g. Dick, 1989; Cannat et al., 1990; Rampone et al., 1997, 2008; Godard et al., 2000; Tartarotti et al., 2002; Dijkstra et al., 2003; Niu, 2004; Chazot et al., 2005; Piccardo et al. 2007; Kelemen et al., 2007; Müntener et al., 2010).

Parallel chemical and microstructural studies on olivine-rich intrusive rocks (troctolites, werhlites, olivine gabbros) from modern ridge settings and ophiolites (Lissenberg and Dick, 2008; Drouin et al., 2009, 2010; Renna and Tribuzio, 2011; Sanfilippo and Tribuzio, 2011, 2012; Lissenberg et al., 2013; Sanfilippo et al., 2013, 2014, 2015a,b) have suggested a composite "hybrid" origin of these rocks, likely related to open-system melt impregnation of an olivine crystal framework. An open issue thus concerns the origin of oceanic troctolites, whether they formed by fractional crystallization of primitive melts or by reactive percolation of pre-existing (possibly mantle-derived) olivine matrix.

Olivine is an ubiquitous mineral in both mantle and primitive lower crustal rocks, and largely involved in melt/rock reaction processes. Consequently, it has become increasingly important to improve knowledge about its trace element composition, and to test the existence of geochemical signatures to distinguish a magmatic versus a mantle origin. Foley et al. (2013) proposed a large compilation of trace element data in olivine from mantle peridotites and Mediterranean volcanics. They outlined the great potential of olivine as a petrogenetic tracer of mantle melting and early igneous crystallization, and the need of further studies on natural olivines, in order to improve the current database, lacking many promising elements.

Many studies have been devoted to determining diffusion and partition coefficients for minor and trace elements in olivine (e.g. Irving, 1978; Shimizu et al., 1982; Kinzler et al., 1990; Beattie (1994); Dunn and Sen, 1994; Eggins et al., 1998; Taura et al., 1998; Gregoire et al., 2000; Petry et al., 2004; Zanetti et al., 2004; Bedard, 2005; Coogan et al., 2005; Witt-Eickschen and O'Neill, 2005; Holzapfel et al., 2007; Lee et al., 2007; Spandler et al., 2007; Brady and Cherniak, 2010; Chakraborty, 2010; Cherniak, 2010; Dohmen et al., 2010; Spandler and O'Neill, 2010; Cherniak and Watson, 2012; Burgess and Cooper, 2013; Girona and Costa, 2013; Cherniak and Liang, 2014; Cherniak and Van Orman, 2014; Jolland et al., 2014; Kennedy et al., 1993; Zhukova et al., 2014), and a very robust data set exists on selected minor element abundances (e.g. Ni, Co, Mn, Cr) of olivine phenochrysts in basalts from different tectonic environments (Sobolev et al., 2005, 2007; Foley et al., 2013). Other studies have determined selected minor, trace elements concentrations in mantle olivines (e.g. O'Reilly et al., 1997; Normann, 1998; see also the data compilations in De Hoog et al., 2010, Foley et al., 2013). However, only a few studies provide a complete set of trace element compositions measured in olivine from mantle peridotite (Sun and Kerrick, 1995; Eggins et al., 1998; Bedini and Bodinier, 1999; Garrido et al., 2000; Gregoire et al., 2000; De Hoog et al., 2010) and gabbroic rocks (Drouin et al., 2009; Sanfilippo et al., 2014). This is mostly due to the difficulty to get reliable analyses, due to the extremely low abundances of many trace elements (e.g. REE, Ti, Zr, Hf) in this mineral.

We have selected peridotite, troctolite and gabbro samples from the ophiolitic Erro-Tobbio Unit (Ligurian Alps, Italy; Borghini et al., 2007, Borghini and Rampone, 2008), and performed a set of in-situ trace element analyses (by LA-ICP-MS) on olivine in both mantle and crustal rocks, with the objective to provide a first "baseline" dataset on olivine trace element chemistry in associated rocks of different origins (mantle and magmatic), and to exploit the potential of olivine geochemistry to get insights into processes of reactive melt percolation at the oceanic peridotite/gabbro transition. A major outcome of this work is that olivine in most of the troctolites has unexpected trace element compositions, indicative of melt/rock reactions likely involving concomitant olivine dissolution and plagioclase crystallization. Furthermore, discrepancies between the compositions of melts in equilibrium with olivine and coexisting minerals, in both mantle and gabbroic rocks, point to the need for a better understanding of the mechanisms of incorporation and diffusion of trace elements in olivine.

2. FIELD RELATIONS AND SAMPLES

The Erro-Tobbio Unit (ET, Voltri Massif, Ligurian Alps, Italy, Fig. 1) consists of predominant mantle peridotites, intruded by discrete gabbroic bodies and dykes, and represent remnants of the Jurassic Ligurian Tethys oceanic lithosphere. These rocks, in spite of the Alpine

overprint, preserve kilometre-scale structural and chemical records of their pre-Alpine evolution (Bezzi and Piccardo, 1971; Chiesa et al., 1975; Ernst and Piccardo, 1979; Ottonello et al., 1979; Piccardo et al., 1990; 1992; Hoogerdujin Strating et al., 1990; 1993; Vissers et al., 1991; Borsi et al., 1996; Capponi et al., 1999; Piccardo et al., 2004; Rampone et al., 2004, 2005).

The extension-related exhumation of the Erro-Tobbio mantle from deep lithospheric depths (P > 15–20 kbar) to a shallow level (P < 5 kbar) was accompanied by a composite history of melt migration and intrusion marked by i) open-system melt migration and reactive porous flow at spinel-facies depths, ii) melt/rock reaction at shallower and colder lithospheric level, leading to the formation of plagioclase-enriched impregnated peridotites, iii) multiple gabbroic intrusions (Piccardo et al., 2004; Rampone et al., 2004, 2005; Piccardo and Vissers, 2007; Borghini et al., 2007; Borghini and Rampone, 2007; Rampone and Borghini, 2008).

Samples investigated in this work were collected in the Southern sector of the Erro Tobbio Unit (Fig. 1), where plagioclase-rich impregnated peridotites are intruded by a discrete hundred-metre-scale magmatic body, mostly consisting of troctolites, and minor plagioclase-bearing dunites and wehrlites. This compositional variability often defines a magmatic layering. The contact between host mantle rocks and troctolites is gradational, in places marked by troctolite and wehrlite apophyses within the peridotites (Fig. 2a). Inside the troctolite body, the layering is also defined by a textural variability of olivine, ranging from granular to harrisitic (Fig. 2 b,c,d), with skeletal olivine crystals up to dm-scale size. Similar textures have been already documented in ophiolites and in layered intrusions (e.g. O'Driscoll et al., 2007; Renna and Tribuzio, 2011), and interpreted as primary magmatic disequilibrium texture related to open-system episodic melt influx. Subsequent olivine-gabbro lenses and thin dykelets intruded both peridotites and troctolites, crosscutting the peridotite foliation and the magmatic layering in the troctolite body (Borghini et al., 2007).

The studied samples are two peridotites (MF40, P1), five troctolites (MF21, MF51, MF72Ga, MF72Ha, MF73Ga) and one olivine gabbro (MF22). Samples MF22, MF40, MF21, MF51 were studied earlier (Borghini et al. 2007; Borghini and Rampone, 2007; Rampone et al., 2014) for major and trace element mineral chemistry (olivine and associated pyroxenes and plagioclase). Based on their bulk and mineral chemical compositions, troctolites and olivine gabbros were interpreted as crystallization products of variably evolved N-MORB-type melts (Borghini et al., 2007). The N-MORB affinity of parental melts is also indicated by Nd isotopic composition of gabbros (average initial ε_{Nd} of 9.25 ± 0.25; Rampone et al., 2014). A brief summary of salient petrographic and chemical characteristics of these samples is given below. The new samples included in this study are three troctolites showing variable olivine texture, from granular (MF72Ga, MF73Ga) to harrisitic (MF72Ha), and one mantle peridotite (P1). Troctolites MF72Ga and MF72Ha represent different textural domains in one single sample (MF72).

Peridotites (MF40, P1) are low-strain spinel tectonites showing diffuse plagioclase enrichment related to melt impregnation. This is illustrated by reactive dissolution and replacement of clinopyroxene by orthopyroxene + plagioclase intergrowth, and reactive dissolution of kinked mantle olivine by poikilitic orthopyroxene (see Borghini et al., 2007).

Troctolites (MF21, MF51, MF72Ga, MF73Ga) are made of dominant subidiomorphic granular olivine, idiomorphic Cr-spinel, interstitial plagioclase and subordinate clinopyroxene (Fig. 3a). They also contain small interstitial accessory minerals (Ti-rich pargasitic amphibole, ilmenite, orthopyroxene) as thin rims around Cr-rich spinel and olivine, related to late-stage crystallization of small fractions of trapped melt (Borghini and Rampone, 2007). The interstitial clinopyroxene and plagioclase often show lobate contacts against olivine, indicative of partial olivine resorption. Reactive dissolution of olivine is even more evident in the coarse-grained harrisitic types (MF73H, MF72Ha), where cm-size hopper olivine crystals are significantly corroded by plagioclase crystallization (Fig. 3c). In the troctolite apophysis MF51, olivine occurs either as euhedral undeformed crystals, or as large and irregular kinked grains, partly resorbed by plagioclase (Fig. 3b).

Olivine gabbro MF22 displays coarse- to medium-grained hypidiomorphic texture, with euhedral to subhedral olivine (about 10% by vol.), euhedral to subhedral plagioclase and anhedral to poikilitic clinopyroxene (Fig. 3d). The crystallization sequence, olivine–plagioclase–clinopyroxene, is typical of low-P oceanic gabbros. Olivine mostly exhibits rather regular contacts against plagioclase and clinopyroxene.

3. ANALYTICAL METHODS

The major element compositions of minerals in most of studied samples were provided in previous papers (Borghini et al., 2007; Borghini and Rampone, 2007). Here we report complementary analyses (in addition to data for the new samples P1, MF72Ga, MF72Ha, MF73Ga) for all mineral spots analysed in-situ for trace element chemistry.

Major element compositions of minerals were analysed using a JEOL JXA 8200 Superprobe equipped with five wavelength-dispersive (WDS) spectrometers, an energy dispersive (EDS) spectrometer, and a cathodoluminescence detector (accelerating potential 15 kV, beam current 15 nA), operating at the Dipartimento di Scienze della Terra, University of Milano.

In situ trace element compositions were determined by LA-ICPMS at Géosciences Montpellier (AETE, University of Montpellier, France). Plagioclase, clinopyroxene, orthopyroxene and olivine were analyzed using 120 μm thick polished sections. Sites of analysis were carefully selected optically to discard those affected by alteration. Analysed trace elements (and corresponding m/z values) were: ^{7}Li, ^{11}B, ^{45}Sc, ^{47}Ti, ^{51}V, ^{55}Mn, ^{59}Co, ^{62}Ni, ^{66}Zn, ^{88}Sr, ^{89}Y, ^{90}Zr,

^{93}Nb, ^{137}Ba, rare earth elements (REEs: ^{139}La, ^{140}Ce, ^{141}Pr, ^{146}Nd, ^{147}Sm, ^{151}Eu, ^{157}Gd, ^{159}Tb, ^{163}Dy, ^{165}Ho, ^{167}Er, ^{169}Tm, ^{173}Yb, ^{175}Lu), ^{177}Hf, ^{181}Ta, ^{208}Pb, ^{232}Th and ^{238}U. Analyses were performed with a Thermo Scientific Element XR (eXtended Range) high resolution ICPMS. The ICP-MS was coupled to a laser ablation system consisting of a Geolas (Microlas) automated platform with a 193 nm Excimer Compex 102 laser from LambdaPhysik. Ablation analyses were performed using an in-house modified 30 cm^3 ablation cell with a helium atmosphere to enhance sensitivity and reduce inter-element fractionation (Günther and Heinrich, 1999). Helium gas and ablated sample material were mixed with argon gas before entering the plasma. The laser energy density was set to 12 J cm^{-2} at a frequency of 8 Hz and the beam size was set to 102 μm. Data were collected in time resolved acquisition mode, with the background signal collected for 2 min followed by 1 min of sample ablation.

Data were reduced with the GLITTER software package (Van Achterberg et al., 2001), using the linear fit to ratio method. Data were filtered for spikes on an element by element basis. Internal standardization relative to EPMA data was done using ^{29}Si for all minerals. Detection limits were <1 ppb for most highly incompatible elements except for Ba, Zr and Sr (<2 ppb); they were <15 ppb for Sb, V, Cu, Zn, Co, Sc, Li and B and <200 ppb for Mn, Ti and Ni (Supplementary Table 1). Values that were within 1σ of the detection limit were excluded during data reduction. Data reported in Tables 1, 2, 3 are single-spot analyses, whereas averages of trace element compositions in olivine for each sample (data in Figures 6 and 7) are reported in Supplementary Table 2). Supplementary Table 3 reports 1σ error values of olivine analyses reported in Table 1. A typical time series for the analysis of trace elements in olivine is reported in the Supplementary Note 1. Instrument sensitivity due to analytical conditions was determined from the average across all days of repeat measurements of the synthetic NIST 612 glass (Pearce et al., 1997). Sensitivities were 800 cps/ppm for Ni, 2000-4000 cps/ppm for Ti, B and Zn, 6000-15000 cps/ppm for Li, Cu, Sb, Ba, Nd, Sm, Gd, Dy, Yb and Pb and >20000 cps/ppm for all other elements. Precision and accuracy were constrained by 8 analyses of reference basalt BIR 1-G (Supplementary Table 1): reproducibility was better than 5% for most elements except for Pb (16%), B and Ta (<10%) and measured values were comparable within analytical uncertainties to GEOREM accepted values (Jochum et al., 2005).

4. MAJOR AND TRACE ELEMENT MINERAL CHEMISTRY

Major and trace element compositions of olivine, plagioclase, clinopyroxene and orthopyroxene are shown in Tables 1, 2, 3. In most analysed olivines, we observed acceptable correlations between the Ni, Mn and Ca abundances analysed by EPMA and LA-ICPMS (see Supplementary Figure 1). Overall, the major and trace element chemistry data that are reported here

for clinopyroxene and plagioclase in samples MF22, MF40, MF21, MF51 are similar to previously published datasets (Borghini et al., 2007).

4.1. Peridotites

Olivines in peridotites have forsterite contents ranging Fo_{89}-Fo_{90}. They display the highest Ni (2570-2725 ppm) coupled to the lowest Mn (1170-1210 ppm), Zn (56-61 ppm), Hf, Ti and Li abundances, of all investigated (peridotite-troctolite-gabbro) samples (Figs. 4, 5, 6). REE patterns define regular trends for the H- (heavy) REE, but tend to be more disperse for the M- (middle) and especially the L- (light) REE (Fig.7). They show strong MREE/HREE fractionation (Tb_N/Yb_N = 0.004-0.042, normalized to C1-chondrite of Sun and McDonough, 1989), more pronounced than in the majority of available literature data on trace element chemistry of mantle olivines in orogenic massifs and xenoliths (see compositional field and references reported in Figure 7). However, published data mostly refer to metasomatized peridotites, as indicated by their enrichment in LREE and other highly incompatible elements (see fields in Figures 7c, 8c). Note also that all previous data are bulk analyses of olivine separates, thus possibly incorporating trace elements hosted in inclusions. On the other hand, D'Errico et al., 2015 recently documented similar MREE/HREE fractionation in olivine from Gakkel Ridge peridotites (see the compositional field in Figures 7c, 8c).

Plagioclase in peridotites is fully replaced by low-grade alteration products. Clinopyroxenes are partly dissolved and replaced by (orthopyroxene + plagioclase) intergrowths crystallized from the infiltrating melts. Their major and trace element compositions (Figs. 7,8 and Table 3) are consistent with previously published data (Borghini et al., 2007). Melt-rock interaction has modified their trace element composition (Borghini et al., 2007), causing an overall REE increase (M- to H-REE up to > 10xC1, see Fig. 7a), coupled to Zr, Y, Sc, V enrichment and strong Sr depletion (see Fig. 8a), compared to clinopyroxenes in those Erro-Tobbio spinel peridotites that represent the mantle protolith before melt impregnation (Rampone et al., 2004; 2005). Similar changes in clinopyroxene composition have been largely documented in plagioclase-rich impregnated peridotites of the Alpine–Apennine system (Rampone et al., 1997, 2008; Piccardo et al., 2004; Zanetti et al., 2007). They are interpreted as resulting from the combined effects of equilibration with enriched melts modified during reactive percolation at decreasing melt mass, and crystallization of small trapped melt fractions. In spite of the overall REE increase, clinopyroxenes preserve marked LREE depletion (La_N/Yb_N = 0.008-0.016), more pronounced than in clinopyroxenes from troctolites and gabbros (see Figure 7a). On this basis, Borghini et al. (2007) and Rampone and Borghini (2008) inferred that melt impregnation in the Erro-Tobbio peridotites

was caused by reactive porous flow of orthopyroxene-saturated depleted MORB-type melts, unrelated to subsequent intrusion of N-MORB-type magmas.

The analyzed orthopyroxenes represent melt-rock reaction products, crystallized together with plagioclase and replacing mantle clinopyroxene (see description above). They display low REE abundances (M-, H-REE below 2-3x C1, Fig. 7a), significant LREE/HREE fractionation (Ce_N/Yb_N = 0.003-0.005), and negative Sr and Eu anomalies coupled to Zr and Hf enrichment relative to the neighbouring REE (Fig. 8a).

4.2. Troctolites and Gabbro

Olivines from troctolites have high forsterite contents (Fo_{88}-Fo_{89}). The lowest forsterite values (Fo_{88}) are observed in samples with variable (granular and harrisitic) texture. They also display relatively high Ni (2050-2280 ppm), Mn (1010-1625 ppm) and moderate Zn (45-70 ppm) contents (see Fig. 4,5). The Co abundances are more scattered, and similar to those of olivines in peridotites. Troctolite olivines display a negative correlation between Mg# (Mg/(Mg+Fe)) and Mn content (Fig. 4b), with the lowest Mg# and highest Mn values observed in the composite granular-harrisitic samples. As expected, olivines in gabbro MF22 have the lowest forsterite contents (Fo_{83}-Fo_{84}), combined with the lowest Ni (1355-1415 ppm) and higher Mn (1890-1970 ppm), Zn (93-102 ppm) and Co (165-170 ppm) abundances. For all these elements (i.e. Mn, Zn, Co, Ni), troctolite olivines show intermediate concentrations compared to those of olivines in peridotites and gabbro. In contrast, their Hf, Ti and Zr concentrations are more variable (progressive enrichment), and extend beyond those of olivines in the gabbro (Figs. 6,7). Li abundances show the same behaviour, although the data are slightly more scattered (see Fig. 6d). Olivines in troctolites also exhibit the highest REE contents (HREE up to 0.8-1xC1, Fig. 7c), coupled to strong MREE/HREE fractionation (Tb_N/Yb_N = 0.004-0.042) and development of significant positive Zr-Hf anomalies relative to the neighbouring REE (Fig. 8c). Drouin et al. (2009) documented similar REE compositions in olivine from Mid Atlantic Ridge (MAR) olivine-rich troctolites (see the grey field in Fig. 8c).

Plagioclases in the studied troctolites and gabbro have similar anorthite contents (An_{58-63} in troctolites, An_{62} in gabbro, see Table 2). In the troctolites, the lowest anorthite values (An_{58-59}) are observed in composite granular-harrisite samples. Overall, plagioclases display LREE-enriched REE patterns (La_N/Sm_N = 1.23-2.56, Fig. 7a), positive Sr and Eu anomalies, and strong negative Zr-Hf anomalies relative to the neighbouring REE (Fig. 8b). In gabbro MF22, plagioclases exhibit the lowest REE abundances (LREE < 1 x C1), whereas in troctolites they show a larger LREE variability, with LREE up to 4xC1 in plagioclases of composite granular-harrisite troctolites (Fig.

7a). Similar REE compositions were documented by Borghini et al. (2007) (see the grey field in Fig. 7b).

The major and trace element compositions of clinopyroxenes reported in Table 3 were measured in cores of large crystals. For the purpose of this study, we did not consider within-crystal major-trace element variations related to late-stage crystallization of interstitial trapped melts. The reader can refer to Borghini and Rampone (2007) for this specific issue. Troctolite clinopyroxenes have high Mg# (0.89-0.90) coupled to relatively Al_2O_3 (3.04-4.82 wt%), Na_2O (0.43-0.61 wt%) and Cr_2O_3 (1.02-1.50 wt%) concentrations (Table 3), similar to those of clinopyroxenes from oceanic and ophiolitic troctolites (Drouin et al., 2009; Sanfilippo and Tribuzio, 2012). Lower Mg# (0.86) and Al_2O_3, Cr_2O_3 contents are found in clinopyroxenes of gabbro MF22. Overall, clinopyroxenes display moderate LREE depletion (La_N/Sm_N = 0.11-0.14 in troctolites and gabbro) and almost flat MREE to HREE patterns. As described above for plagioclase, gabbro clinopyroxenes have the lowest REE abundances (M-H-REE below 10 x C1, Fig.7a), whereas troctolite clinopyroxenes exhibit a general REE increase (M-H-REE up to 20 x C1) at nearly constant LREE fractionation (Fig. 7a). The REE increase is coupled to the development of negative Eu and Sr anomalies relative to neighbouring REE (Fig. 8a).

5. DISCUSSION

5.1. Mineral/mineral REE partitioning

A number of studies have shown that the distribution of trace elements between olivine, orthopyroxene and clinopyroxene depends on temperature, pressure and mineral compositions (e.g. Witt-Eickschen et al., 2005; Lee et al., 2007; Sun and Liang, 2012, 2013, 2014). For REE, the effect of decreasing temperature is to redistribute these elements into clinopyroxene, thus lowering the olivine/clinopyroxene and orthopyroxene/clinopyroxene partition coefficients. Also, this effect is stronger for the LREE relative to the HREE, possibly resulting in significant changes of the LREE/HREE fractionation in low-T (< 1000 °C) re-equilibrated minerals (Sun and Liang, 2014).

Lee et al. (2007) predicted Ol/Cpx and Opx/Cpx REE partition coefficients at variable temperatures based on lattice strain theory. Sun and Liang (2014) developed parameterized lattice strain models for REE and Y distribution among mantle minerals in a wide range of T conditions (800-1300°C), using mineral/melt partitioning models calibrated against experimentally determined mineral/melt partition coefficients (Sun and Liang, 2012, 2013). In order to test the distribution of REE between olivine, clinopyroxene and orthopyroxene in the Erro-Tobbio peridotites, troctolites and gabbro, and derive information about equilibration temperatures, we computed Ol/Cpx and Opx/Cpx REE partition coefficients in our samples, and compared them with i) predicted trends by Lee et al. (2007) (Fig. 9), ii) computed olivine/cpx trends, according to Sun and Liang (2012, 2013,

2014) modeling. This approach allows to calculate Ol/Cpx partition coefficients at varying T for a specific sample, using proper major element mineral compositions (Fig. 10; see figure caption for more details). The two sets of modelled temperature contours, shown in Figures 9 and 10, are similar, with a modest shift at higher Ol/Cpx partitioning values, at a given T, of trends computed according to Sun and Liang (2014) (see Figs. 9a and 10).

In all samples, Ol/Cpx partition coefficients regularly decrease from Lu to Dy, whereas they tend to define concave trends from MREE to LREE (Figs. 9a, 10). Similar "U-shaped" Ol/Cpx partitioning was already documented in previous studies (e.g. Agranier and Lee, 2007; Lee et al., 2007) and was ascribed to the difficulty to get accurate analyses of LREE in olivine, due to the extremely low concentrations in these elements, and/or to the occurrence of LREE-bearing fluid inclusions. However, it is remarkable that the Ol/Cpx partition coefficients for Gd, Eu and Nd in most samples are consistent with predicted trends (see Figs. 9a and 10), pointing to the reliability of our olivine data set for the majority of REE. Overall, the Ol/Cpx H- to M-REE distribution in most investigated samples defines arrays that are slightly steeper than computed trends. As already outlined in the results section, this is likely a consequence of the strong MREE/HREE fractionation shown by olivines in this study, more pronounced than the large majority of published data. Except for Dy and Tb, most Ol/Cpx partitioning data for the HREE indicate rather high equilibration temperatures (> 1100 °C). The highest values are observed in the troctolites, relative to peridotites and gabbro, and are probably related to the high HREE concentrations in olivines of troctolites resulting from melt/rock reaction processes (see the discussion below)

In Figure 9b, we also show the Opx/Cpx REE distribution coefficients for the two peridotite samples, compared with modelled trends by Lee et al. (2007). They define almost linear arrays, monotonically decreasing from HREE to LREE. Remarkably, these trends are mostly consistent with predicted Opx/Cpx partitioning at high temperature (> 1300 °C). In these samples, high-T estimates (1350-1400 °C) were also obtained by the REE in two-pyroxene thermometer of Liang et al (2013).

In summary, mineral/mineral REE partitioning in the Erro-Tobbio samples are mostly indicative of high temperature of equilibration (> 1100-1200 °C). Accordingly, we infer that the REE concentrations in olivine, clinopyroxene and orthopyroxene were not significantly modified by subsolidus re-equilibration, hence potentially recording information about the chemical signature of equilibrium melts. Nevertheless, the possible effect of decreasing temperature on olivine/clinopyroxene REE re-distribution is further discussed in the following section.

5.2. Paradoxical chemical signatures in olivine

394 The comparison of olivine compositions in the three investigated rock types, peridotite,
395 troctolite and gabbro reveals both expected and unexpected behaviour for trace elements.
396 Remarkably, olivines in the three rock types exhibit distinct geochemical signature and
397 define systematic elemental correlations for a series of minor (Ni, Mn) and trace elements (Zn, Co,
398 Ti, Zr, Hf , HREE). Similar correlations (at least for Ni, Mn, Ti, Zr, Yb) have been documented by
399 Sanfilippo et al. (2013) in a study of troctolites and mantle peridotites from the Alpine ophiolites
400 (see data reported in Figs. 4,5,6). These data provide the evidence that olivine, although being a
401 very minor reservoir for many trace elements, can record magmatic processes.
402 As expected, highly compatible elements in olivine such as Ni (Lee et al., 2007; Spandler et
403 al., 2010, and references therein) show the highest contents in peridotite, intermediate in troctolite
404 and lowest in gabbro, whereas Mn, Zn and Co show the opposite behaviour. Data on the
405 partitioning of Mn, Zn and Co in olivine (Ehlers et al., 1992; Kennedy et al., 1993; Beattie, 1994;
406 Gaetani and Grove, 1997; Kohn and Schofield, 1994; Bedard, 2005; Mysen, 2007; Spandler and
407 O'Neill, 2010) indicate a moderately incompatible to compatible behaviour. De Hoog et al. (2010),
408 in a comprehensive study of the trace element composition of mantle olivines from different origins
409 and settings, found negative correlations between Mn, Zn abundances and forsterite contents, thus
410 confirming their moderately incompatible behaviour. They also documented little systematic
411 variation of Co with forsterite values, indicative of a $K_D^{ol/melt}$ very close to 1. In our study, the
412 overall increase of Mn, Zn and Co abundances in olivines from mantle peridotites to gabbro further
413 demonstrate a moderately incompatible behaviour of these elements. Moreover, in the Mg# versus
414 Ni diagram of Figure 4a, the compositional array defined by the Erro-Tobbio peridotite-troctolite-
415 gabbro olivines is roughly consistent with computed trends for fractional crystallization at low
416 pressure (< 5 Kb) of a primary MORB melt (e.g. Drouin et al., 2009; grey lines in Fig. 4a). In
417 addition, Mn and Ni abundances of troctolite olivines fall within the compositional field defined by
418 MORB phenocrysts (see Figs. 4a,b; data from Sobolev et al., 2007). These features are in agreement
419 with previous inference by Borghini et al. (2007) that troctolites and gabbros reflect crystallization
420 products of variably evolved MORB magmas.
421 Zr, Hf, Ti and HREE display unforeseen behaviours. The concentrations of these elements
422 in troctolite olivines define enrichment trends that start from abundances similar to those in gabbro
423 olivines, and go up to one order of magnitude higher values (Fig. 6). These elements are all highly
424 incompatible in olivine (Lee et al., 2007; Spandler and O'Neill, 2010; De Hoog et al., 2010; and
425 references therein). If the composition of olivine in troctolites and gabbros were simply reflecting
426 fractionation from a variably evolved melt, we would expect the highest contents in incompatible
427 elements in the gabbro olivines. Moreover, the HREE enrichment in troctolite olivine is coupled to
428 the development of pronounced Zr-Hf positive anomalies and Zr/Nd fractionation (Zr_N/Nd_N up to

100). The same selective Zr-Hf enrichment was described in olivines from oceanic troctolites by Drouin et al. (2009). All these features indicate that the behaviour of these elements in the studied olivine data set does not conform to a simple magmatic crystallization process, and melt/rock reaction processes likely have occurred (see the discussion section below).

Another unexpected chemical characteristic in olivine is its ubiquitous (even in the gabbro) depleted REE composition (Fig. 7c). Similar REE patterns were documented by Drouin et al. (2009) in olivines from oceanic troctolites. These authors observed that computed melts in equilibrium with such olivines are significantly more depleted than melts in equilibrium with associated plagioclase and clinopyroxene. Hence, they proposed that the trace element depleted signature of olivine in the troctolites could reflect a mantle origin, whereas plagioclase and clinopyroxene crystallized from impregnating MORB-type melts.

The REE composition of melts computed in equilibrium with olivine, clinopyroxene, orthopyroxene and plagioclase from the Erro-Tobbio peridotites, troctolites and gabbro are shown in Figure 11. Following Drouin et al. (2009), melts were computed using clinopyroxene/liquid, orthopyroxene/liquid, and olivine/liquid partition coefficients from Lee et al. (2007), and plagioclase/liquid partition coefficients from Aigner-Torres et al. (2007). As previously documented by Drouin et al. (2009), computed melts in equilibrium with olivine in all investigated lithotypes exhibit lower REE abundances than melts in equilibrium with clinopyroxene. An exception to this behaviour is provided by Yb, which shows similar values in most computed melts (Fig. 11a,b,c). In troctolites, melts in equilibrium with plagioclase and clinopyroxenes display large variation in absolute REE contents, related to late-stage crystallization of interstitial melts (Borghini and Rampone, 2007). In spite of such variation, computed melts exhibit similar composition, with nearly flat REE patterns, indicative of a MORB affinity (Borghini et al., 2007). In contrast, melts in equilibrium with olivine display strong MREE/HREE fractionation (Dy_N/Yb_N = 0.17-0.39). Although such decoupling in the troctolites could reflect a different origin between olivine (possibly mantle derived) and associated plagioclase/clinopyroxene, this can be ruled out in gabbro MF22 (Fig. 11c), for which microstructural and major-minor element chemical features of olivine (and field relations) clearly indicate a magmatic origin.

In order to test whether the adopted partition coefficients could have a role in generating such contrasting signature, we also calculated the equilibrium melts using the following sets of partition coefficients: i) the compilation proposed in Bedard (2001), derived on the basis of empirical relationships between ln(Kd) and composition, and adopted by Lissenberg et al. (2013) to model reactive melt migration in the lower oceanic crust of Hess Deep (EPR), ii) the olivine/melt and clinopyroxene/melt partition coefficients computed for our samples at T = 1200 °C, according to Sun and Liang (2012, 2013) mineral/melt REE partitioning models. The resulting REE

compositions of equilibrium melts are reported in Figures 12 and 13. In spite of differences in absolute concentrations, we observed the same decoupling between the M-H-REE composition of melts in equilibrium with plagioclase and clinopyroxene, and those in equilibrium with olivine, the latter being even more fractionated (Dy_N/Yb_N = 0.043-0.098) when using the Bedard (2001) Kds. Finally, in order to check whether the observed decoupling of equilibrium melts compositions could be related to subsolidus redistribution of REE between olivine and clinopyroxene at lower temperature, we computed apparent melt compositions using the Kds sets obtained at 1100°C, by using Sun and Liang (2012,2013) models. The results are shown in Supplementary Figure 2. Again, the major effect is a difference in absolute concentrations, with a general shift at lower REE contents of computed melts in equilibrium with clinopyroxene, and higher REE abundances of computed melts in equilibrium with olivine. On the other hand, the decoupling of M-H-REE composition in clinopyroxene and olivine equilibrium melts largely persists, although the latter are slightly less fractionated (Dy_N/Yb_N = 0.13-0.29 at 1200°C, and 0.15-0.34 at 1100 °C). Therefore, re-distribution of REE between olivine and other minerals at subsolidus conditions is not sufficient to explain the observed decoupling.

A robust explanation of such chemical discrepancies between melts computed in equilibrium with olivine and those in equilibrium with all other minerals is presently lacking, and possibly lies in the inhibited incorporation of REE into the olivine crystal lattice, due to their high ionic radius relative to the M1 and M2 sites dimensions (Zanetti et al., 2004; Foley et al., 2013). This, in turn, can explain the uncertainties and variability of available partition and diffusion coefficients for REE and other highly incompatible elements in olivine.

Available experimental studies on the diffusion of trace elements in olivine have provided contrasting results. Spandler et al. (2007) and Spandler and O'Neill (2010) documented fast re-equilibration of REE in olivine, at rates similar to Mg-Fe exchange. By contrast, Cherniak (2010) and Remmert et al. (2008) found much lower (more than three order of magnitude) REE diffusion coefficients. They showed that REE diffusion in olivine is faster than in orthopyroxene and clinopyroxene, but slow enough to preserve REE heterogeneities in melt inclusions in olivine phenocrysts, at time scales of geologic processes. Cherniak (2010) also documented similar diffusivities for M- and H-REE (La, Dy, Yb), indicating no correlation between REE diffusion coefficients and ionic radius (consistent with Spandler and O'Neill, 2010), and little dependence of REE diffusion rates on crystallographic orientation. This behaviour differs from the pronounced anisotropy (more rapid diffusion parallel to *c* axis) documented for Fe-Mg and many trace elements (e.g. Ni, Cr, Zr, Hf) in olivine (Chakraborty, 1997; Petry et al., 2004; Ito and Ganguly, 2006; Spandler and O'Neill, 2010; Jollands et al., 2014).

More recently, Burgess and Cooper (2013) explained the discrepancies between the results of Cherniak (2010) and Spandler and O'Neill (2010) as a consequence of different diffusion mechanisms acting in olivine, with "lattice diffusion" in the former, and "fast-path diffusion" promoted by formation of extended defects, in the latter. Specifically, Burgess and Cooper (2013), in a combined experimental-TEM study on olivine in equilibrium with a TiO_2-rich MORB (similar to that used by Spandler and O'Neill, 2010), showed that the nucleation and growth of planar defects in olivine is enhanced by large TiO_2 chemical potential gradients at the olivine-melt boundary (leading to substitution of Ti^{4+} for divalent cations in the olivine octahedral site, and formation of octahedral vacancies). These authors outlined the need for a re-evaluation of the "simple" lattice diffusion mechanism, especially in the case of natural reacting systems governed by significant chemical potential gradients (e.g. metasomatism or magma mixing), and the importance of detailed analysis of natural and experimental samples for a better understanding of trace element diffusion in olivine.

In spite of such contrasting results, all studies provide consistent evidence of similar diffusion coefficients in olivine from HREE to LREE. Therefore, the ubiquitous strong MREE/HREE fractionation observed in all the analysed olivines cannot be easily related to modifications of the REE profile acquired by subsolidus diffusion and re-equilibration, as a consequence of different M- to H-REE diffusion rates. On the other hand, the large variation of available partition coefficients for REE (one to two orders of magnitude, especially for the LREE and MREE; see Bedard, 2001; Lee et al., 2007; Spandler and O'Neill, 2010) indicates the difficulty to get reliable values, and sheds light on the caution that is needed in using olivine REE contents to derive information about the compositions of equilibrum melts. The main factors influencing the REE partitioning between olivine and melt have been discussed in a series of papers. Bedard (2005) examined published natural and experimental $^{olivine/liquid}D$, and found a general tendency to increase with decreasing temperature and MgO content in the melt. Evans et al. (2008), in an experimental study in the CMAS system, documented strong inverse correlation between olivine-melt partition coefficients and SiO_2 contents in melt. Finally, Sun and Liang (2013), through the development of parameterized lattice strain models, found that the primary variables determining the REE and Y partitioning between olivine and melt are pressure, Forsterite and Al contents in olivine.

Overall, the results of our study further emphasize the need of enlarging the trace element olivine data set in natural mantle and gabbroic samples, as well as the importance of parallel experimental work. Based on present knowledge, the REE composition of olivine cannot be easily adopted to discriminate between mantle versus magmatic origin. Nevertheless, the peculiar and systematic trace element signature documented in olivine of troctolites points to a more complex origin than a simple fractional crystallization.

5.3. Evidence of melt/rock reaction in troctolites

The studied troctolites show microstructural and chemical evidence of mineral/melt reaction and disequilibrium. In most samples, olivine displays irregular and lobate contacts against interstitial minerals (plagioclase and subordinate clinopyroxene) indicative of reactive dissolution and resorbtion. Reactive dissolution of olivine is even more evident in coarse-grained harrisitic troctolites (e.g. sample MF72Ha), where centimetre-size hopper olivine crystals are significantly corroded by plagioclase crystallization (Fig. 3c). Similar granular to hopper to harrisitic textures in olivine are described in the literature in layered intrusions and ophiolites (e.g. Donaldson et al., 1982; O'Driscoll et al., 2007; Renna and Tribuzio, 2011), and are considered to result from open-system processes causing variations in melt composition and, consequently, in the degree of undercooling (e.g. Faure et al., 2003). Moreover, in the troctolite apophysis MF51 olivine occurs both as euhedral crystals and as large and irregular kinked grains, partly resorbed by plagioclase (Fig. 3b). All these features point to disequilibrium and reaction between the olivine framework (at least part of it) and the melt that crystallized the interstitial minerals.

Specific chemical characteristics also provide the same information. As outlined by Borghini et al. (2007), the overall major element compositions of minerals in Erro-Tobbio troctolites and gabbros define a variational trend at rather low An contents in plagioclase at given Fo in olivine and Mg# of clinopyroxene, as observed in some gabbroic rock suites from the Mid-Atlantic Ridge (e.g. Ross and Elton, 1997). Troctolites, specifically, display variable An contents in plagioclase at rather constant Fo value in olivine. The new troctolite samples analysed in this study with granular to harrisitic textures further confirm the lack of Fo-An correlation in the troctolites, being characterized by very low An values in plagioclase (An_{58-59}) at high Fo contents in olivine ($Fo_{87.5-88.5}$) and high Mg# in clinopyroxene (100*Mg# = 88-89.8)(see Tables 1,2,3). Although part of such chemical features, namely the low An contents in plagioclase and high Mg# in clinopyroxene, can be ascribed to crystallization at moderate P conditions (3-5 kbar, see Borghini et al., 2007), the large compositional range defined by plagioclase in the troctolites (An_{58-66}; Borghini et al 2007 and this study) at rather constant olivine composition rules out a simple process of fractional crystallization. This in turn calls for melt-rock reaction processes, in which exotic input of more evolved melts in a previously crystallized olivine framework, and/or crystallization of intercumulus liquid evolving upon cooling and partially trapped within the crystal mush, could have played a role.

Both textural and mineral chemistry features in the Erro-Tobbio troctolites thus point to melt-rock reaction involving olivine dissolution and concomitant plagioclase crystallization. In order to test, with a simple but effective approach, whether the observed trace element variations

and geochemical signature in olivine of troctolites, namely the selective HFSE (Zr, Hf, Ti) and HREE enrichment, can be explained by such process, we performed an Assimilation Fractional Crystallization (AFC) model (using the equation of De Paolo, 1981), assuming the following reaction:

$$\text{olivine}_1 + \text{melt}_1 = \text{olivine}_2 + \text{plagioclase} + \text{melt}_2,$$

in which "olivine$_2$" represents the olivine reequilibrated with the reacted melt$_2$. For clarity, we emphasize that in this study we were not able to distinguish two olivine generations in a specific troctolite sample, both in terms of textural occurrence and chemical composition. We often observed corroded olivine grains that texturally represent the "olivine$_1$" of the above reaction, but possess geochemical characteristics of "olivine$_2$". We further discuss this point below.

The results of AFC modeling are shown in Figure 14, in terms of Zr_N/Nd_N versus Yb_N in olivine computed in equilibrium with the reacted melt$_2$ (i.e. olivine$_2$). A major difficulty in performing geochemical modeling is the choice of appropriate mineral/liquid partition coefficients. This is especially crucial in the case of olivine and plagioclase, for which complete $^{\text{mineral/liquid}}D$ sets including REE and HFSE are poorly available in literature (see discussion above). We thus performed two distinct AFC models (Models A and B of Fig.14a,b), keeping fixed all the parameters except the partition coefficients, in order to highlight the variability of computed trends resulting from the choice of D values. In both models, the assimilated mass (Ma) is equal to 100% olivine, whereas the crystallized mass (Mc) is 100% plagioclase. The composition of the starting melt (C_0, reacting with olivine$_1$) is equal to the melt computed in equilibrium with the troctolite clinopyroxene showing the lowest REE concentrations (i.e. clinopyroxene in sample MF21; see Figs. 7a, 8a). This melt is very similar (at least for the L- and M- REE) to the composition of melt computed in equilibrium with troctolite plagioclase with the lowest REE abundances (i.e. plagioclase in sample MF51, see Figs. 7b, 8b), and we considered it as the best proxy of the composition of the interstitial melt before reactive crystallization. For the assimilated olivine, we used the composition of olivine in peridotite MF40, showing the lowest Yb and HFSE concentrations among all the investigated data set. It is remarkable, however, that olivine in gabbro MF22 also show low Zr_N/Nd_N fractionation and REE (see Figs. 7c, 8c), being likely less affected by melt-rock reaction processes than the troctolites. As clearly shown in Figure 14, the two (peridotite and gabbro) olivine compositions almost overlap. Therefore, using the gabbro olivine as Ma would have produced the same results discussed below.

Computed trends reported in Figure 14 show the compositions of olivine in equilibrium with residual liquids (melt$_2$) at decreasing melt mass (F = 0.95-0.10). The four different trends refer to different values of r (where r is equal to the Ma/Mc ratio). The models A and B (Fig. 14a,b) differ only in terms of adopted partition coefficients (see figure caption for details and references).

Keeping in mind the uncertainties resulting from the adopted parameters (partition coefficients, composition of initial melt C_0 and assimilated olivine Ma), and the very simplified approach, the model clearly suggests that the observed enrichment in Zr in olivine of the troctolites can be explained by a melt-rock reaction process involving dissolution of olivine and crystallization of plagioclase (in almost equal amounts, best consistency with Ma/Mc = 0.95) at progressively decreasing melt mass. This is due to the fact that olivine has higher $^{mineral/liquid}D_{Zr,Hf}$ relative to plagioclase, consistent with the significant Zr-Hf negative anomalies in plagioclase compositions, especially in plagioclase of gabbro MF22 (see Fig. 8b). This behaviour of olivine, i.e. $^{olivine/liquid}D_{HFSE} > {}^{olivine/liquid}D_{REE}$, has been invoked by Kelemen et al. (1990) to explain the development of arc-like signature in basaltic melt during reactive percolation through the lithospheric mantle, and it has been confirmed by the study of Bedard (2005), who highlighted the ubiquitous presence of positive $D_{Ti,Zr,Hf}$ anomalies in experimental olivine/melt partitioning data for a wide range of basaltic compositions.

As mentioned above, there is an apparent decoupling between the reaction considered in the AFC model, and our textural and geochemical observations. The reaction involves an $olivine_1$, likely possessing a higher forsterite content and low incompatible trace element abundances, and an $olivine_2$, supposed to crystallized from the reacted melt. However, in our study troctolite olivines which are significantly resorbed by plagioclase (i.e. texturally representing $olivine_1$), have enriched trace element signature, i.e. that expected for $olivine_2$. This could be explained assuming that $olivine_1$ has reset its composition, by interaction with the melt, rather than crystallizing in new grains.

In this study, we aimed to provide a first trace element data set in olivine from associated peridotite, troctolite and gabbro samples, in order to document major geochemical differences, if any, between the different rock types, and test the potential of trace element chemistry in olivine to track melt-rock reaction processes. Therefore, we did not focus the analytical work to detect within-grain elemental variations. The results of this study clearly indicate that the troctolites hold a more complex magmatic history than previously documented (Borghini et al., 2007; Borghini and Rampone, 2007). Borghini and Rampone (2007) found significant trace element zoning in poikilitic clinopyroxenes, correlated with the microstructural site (e.g. core to rims of large crystals, to very thin interstitial grains). They ascribed this feature to late-stage crystallization of interstitial trapped melts, and assumed olivine dissolution to explain the development of positive Zr, Hf anomalies in the very late-stage clinopyroxene. Here we show that olivine records the geochemical signature of such melt-mineral reaction. Detailed microstructural and geochemical investigations, involving Crystallographic Preferred Orientation (CPO) analyses (e.g. Drouin et al., 2010) combined to major-trace element traverses and mapping in selected olivine grains, will be essential to check the

existence of different generations of olivine within a single troctolite sample, and the preservation (or absence) of major, trace element zoning in a specific olivine crystal.

Records of compositional zoning in minerals largely depend on element diffusion rates, temperature conditions of crystallization and cooling rates. Major and minor element variations in olivine, such as decrease in NiO, Mg# and increase in TiO_2, have been documented in experiments of formation of plagioclase-bearing peridotites and wehrlites by reactive crystallization, and ascribed to the effects of dissolution and reprecipitation from the basaltic melt (Saper and Liang, 2014). Moreover, Welsch et al. (2014) recently documented surprising dendritic zoning of phosphorous in volcanic, experimental, and also plutonic olivine crystals (by electron probe microanalysis and mapping), and Burgess and Cooper (2013) shed lights on the diffusion mechanisms in olivine by combined experimental and TEM investigations. Overall, these works illustrate the usefulness of micro- and nano-scale detailed studies to get insights on combined processes of olivine deformation, dissolution and growth. Textural and geochemical variability documented in this study in troctolite olivines further confirms the relevance of such approaches.

6. CONCLUDING REMARKS

In-situ LA-ICP-MS analyses of a large set of trace elements in olivines of depleted mantle peridotites and associated primitive gabbroic rocks (troctolites and olivine gabbros) from the Ligurian ophiolites (Erro-Tobbio Unit, Italy) have revealed that olivines define systematic and reliable compositional trends that can be used to unravel their history of melt-rock reaction and magmatic crystallization.

In contrast with olivine gabbros, olivines in the troctolites display significant enrichment in incompatible elements like Zr, Hf, Ti, HREE, coupled to development of significant HFSE/REE fractionation. Such geochemical features are indicative of dissolution-precipitation processes and re-equilibration with reacted enriched melts. AFC modeling shows that the large Zr_N/Nd_N ratios in olivines of troctolites are consistent with a process of olivine assimilation and plagioclase crystallization at decreasing melt mass, in agreement with textural observations. Detailed in-situ trace element geochemistry of olivine, possibly combined with focused microstructural analysis, thus appears to be a powerful tool to investigate reactive percolation and the origin of olivine-rich rocks in the lower oceanic crust.

Compositional contrasts between computed melts in equilibrium with olivine and coexisting minerals, in both mantle peridotites and MORB-type gabbroic rocks, point to the need for a better understanding of the mechanisms of incorporation and diffusion of trace elements in olivine.

ACKNOWLEDGEMENTS

We thank Andrea Risplendente (Dipartimento di Scienze della Terra, University of Milano) for his assistance with the EPMA analyses, and Carlotta Ferrando (PhD student in Montpellier) who performed part of the LA-ICP-MS analyses. J.C.M de Hoog and C. Sun are greatly acknowledged for their constructive reviews. We also thank editorial advise and handling by W. van Westrenen and M. Norman. This study was supported by the University of Genova (grant PRA 2014), and the CNRS-INSU program SYSTER.

REFERENCES

Agranier A. and Lee C.-T.A. (2007) Quantifying trace element disequilibria in mantle xenoliths and abyssal peridotites. Earth Planet. Sci. Lett. 257, 290–298.

Aigner-Torres M., Blundy J., Ulmer P. and Pettke T. (2007) Laser Ablation ICPMS study of trace element partitioning between plagioclase and basaltic melts: an experimental approach. *Contrib. Mineral. Petrol.* **153**, 647–667.

Beattie P. (1994) Systematics and energetics of trace-element partitioning between olivine and silicate melts: implications for the nature of mineral/melt partitioning. *Chem Geol* **117**, 57–71.

Bédard J. (2001) Parental magmas of the Nain Plutonic Suite anorthosites and mafic cumulates: a trace element modelling approach. *Contrib. Mineral. Petrol.* **141**, 747–771.

Bédard J. (2005) Partitioning coefficients between olivine and silicate melts. *Lithos* **83**, 394–419.

Bédard J.H., Hebert R., Berclaz A. and Varfalvy V. (2000) Synthesis and the genesis of lower oceanic crust. *Geol. Soc. Am.* **349**, 105–119.

Bedini R.-M. and Bodinier J.-L. (1999) Distribution of incompatible trace elements between the constituents of spinel peridotite xenoliths: ICP-MS data from the East African Rift. *Geochim. Cosmochim. Acta* **63**, 3883–3900.

Bezzi A. and Piccardo G.B. (1971) Structural features of the Ligurian ophiolites: petrologic evidence for the 'oceanic' floor of the Northern Apennine geosyncline: a contribution to the alpine-type gabbro–peridotite associations. *Mem. Soc. Geol. It.* **10**, 55–63.

Borghini G. and Rampone E. (2007) Postcumulus processes in oceanic-type olivine-rich cumulates: the role of trapped melt crystallization versus melt-rock interaction. *Contrib. Mineral. Petrol.* **154**, 619–633.

Borghini G., Rampone E., Crispini L., De Ferrari R. and Godard M. (2007) Origin and emplacement of ultramafic-mafic intrusions in the Erro-Tobbio mantle peridotites (Ligurian Alps, Italy). *Lithos* **94**,210–229.

Borsi L., Scharer U., Gaggero L. and Crispini L. (1996) Age, origin and geodynamic significance of plagiogranites in lherzolites and gabbros of the Piedmont–Ligurian ocean basin. *Earth Planet. Sci. Lett.* **140**, 227–241.

Brady J.B. and Cherniak D.J. (2010) Diffusion in minerals: An overview of published experimental diffusion data. In: *Reviews in Mineralogy & Geochemistry*, Mineralogical Society of America **72**, 899–920.

Burgess K.D. and Cooper R.F. (2013) Extended planar defects and the rapid incorporation of Ti4+ into olivine. *Contrib. Mineral. Petrol.* **166**, 122–1233.

Cannat M., Bideau D. and Hebert R. (1990) Plastic deformation and magmatic impregnation in serpentinized ultramafic rocks from the Garrett transform fault (East Pacific Rise). *Earth Planet. Sci. Lett.* **101**, 216–232.

Capponi G., Crispini L., Silvestri R. and Vigo E. (1999). The role of Early Miocene thrust tectonics in the structural arrangement of the Voltri Group (Ligurian Alps, Italy): evidence of Bandita area. *Ofioliti* **24**, 13–19.

Chakraborty S. (1997) Rates and mechanisms of Fe-Mg interdiffusion in olivine at 980–1300 °C. J *Geophys. Res.* **102**, 12317–12331.

Chakraborty S. (2010) Diffusion coefficients in olivine, wadsleyite and ringwoodite. *Rev. Miner. Geochem.* **72**, 603–639.

Chazot C., Charpentier S., Kornprobst J., Vannucci R. and Luais B. (2005) Lithospheric mantle evolution during continental break-up: The West Iberia non-volcanic passive margin. *J. Petrol.* **46**, 2527–2568.

Cherniak D. J. (2010). REE Diffusion in Olivine. *Am. Mineral.* **95**, 362–368.

Cherniak D.J. and Liang Y. (2014) Titanium diffusion in olivine. *Geochim. Cosmochim. Acta* **147**, 43–57.

Chiesa S., Cortesogno L., Forcella F., Galli M., Messiga B., Pasquarè G., Pedemonte G.M., Piccardo G.B. and Rossi P.M. (1975) Assetto strutturale ed interpretazione geodinamica del Gruppo di Voltri. *Boll. Soc. Geol. It.* **94**, 555–581.

Collier M.L. and Kelemen P.B. (2010) The case for reactive crystallization at mid-ocean ridges. *J. Petrol*. **51**, 1913–1940.

Coogan L.A., Hain A., Stahl S. and Chakraborty S. (2005) Experimental determination of the diffusion coefficient for calcium in olivine between 900°C and 1500°C. *Geochim. Cosmochim. Acta* **69**, 3683–3694.

Coogan L.A., Saunders A.D., Kempton P.D. and Norry M.J. (2000) Evidences from oceanic gabbros for porous melt migration within a crystal mush beneath the Mid-Atlantic Ridge. *Geochem. Geophys. Geosys.* **1**, 2000GC00007.

D'Errico M., Warren J.M. and Godard M (2015) Evidence for chemically heterogeneous Artic mantle beneath the GakkelRidge. *Geochim. Cosmochim. Acta* **174**, 291-312.

De Hoog J. C. M., Gall L. and Cornell D. H. (2010) Trace-element geochemistry of mantle olivine and application to mantle petrogenesis and geothermobarometry. *Chem. Geol.* **270**, 196–215.

De Paolo D.J. (1981) Trace elements and isotopic effects of combined wall rock assimilation and fractional crystallization. *Earth Planet. Sci. Lett.* **53**, 189–202.

Dick H.J.B. (1989) Abyssal peridotites, very low spreading ridges and ocean ridge magmatism. In *Magmatism in the Ocean Basins* Saunders AD, Norry MJ (eds). Geol. Soc. Spec. Publ. **42**, Oxford, 71–105.

Dick H.J.B., Tivey M.A. and Tucholke B.E. (2008) Plutonic foundation of a slow-spread ridge segment: the oceanic core complex at Kane Megamullion, 23°30'N, 45°20'W. *Geochem. Geophys. Geosyst.* **9**, Q05014.

Dijkstra A.H., Barth M.G., Drury M.R., Mason P.R.D. and Vissers R.M.L. (2003) Diffuse porous melt flow and melt-rock reaction in the mantle lithosphere at the slow-spreading ridge: a structural petrology amd LA-ICP-MS study of the Othris Peridotite Massif (Greece). *Geochem. Geophys. Geosys.* **4**, 1–24.

Dohmen R., Kasemann S.A., Coogan L. and Chakraborty S. (2010) Diffusionof Li in olivine. Part I: experimental observations and a multispecies diffusion model. *Geochim. Cosmochim. Acta* **74**, 274–292.

Donaldson C.H. (1982) Origin of some of the Rhum harrisite by segregation of intercumulus liquid. *Min. Mag.* **45**, 201-209.

Drouin M., Godard M., Ildefonse B., Bruguier O. and Garrido C.J. (2009) Geochemical and petrographic evidence for magmatic impregnation in the oceanic lithosphere at Atlantis Massif, Mid-Atlantic Ridge (IODP Hole U1309D, 30°N). *Chem. Geol.* **264**, 71–88.

Drouin M., Ildefonse B and Godard M. (2010) A microstructure imprint of melt impregnation in slow spreading lithosphere: olivine-rich troctolites from the Atlantis Massif, Mid-Atlantic Ridge, 30 N, IOPD Hole U1309D. *Geochem. Geophys. Geosyst.* **11**, Q06003.doi:10.1029/2009GC002995.

Dunn T. and Sen C. (1994) Mineral/matrix partition coefficients for orthopyroxene, plagioclase and olivine in basaltic to andesitic systems: a combined analytical and experimental study. *Geochim. Cosmochim. Acta* **58**, 717–733.

Eason D.E. and Sinton J.M. (2009) Lava shields and fissure eruptions of the Western Volcanic Zone, Iceland, evidence for magma chambers and crustal interaction. *J. Volcanol. Geotherm. Res.* **186**, 331–348.

Eggins S.M., Rudnick R.L. and McDonoughet al., W.F. (1998) The composition of peridotites and their minerals: a laser-ablation ICP-MS study. *Earth Planet. Sci. Lett.* **154**, 53–71.

Ehlers K., Grove T.L., Sisson T.W., Recca S.I. and Zervas D.A. (1992) The effect of oxygen fugacity on the partitioning of nickel and cobalt between olivine, silicate melt and metal. *Geochim. Cosmochim. Acta* **56**, 3733–3743.

Ernst W.G. and Piccardo G. B., (1979) Petrogenesis of some Ligurian peridotites: I. Mineral and bulk rock chemistry. *Geochim. Cosmochim. Acta* **43**, 219–237.

Evans T.M., O'Neill H.St.C. and Tuff J. (2008) The influence of melt composition on the partitioning of REEs, Y, Sc, Zr and Al between forsterite and melt in the system CMAS. *Geochim. Cosmochim. Acta* **72**, 5708-5721.

Faure F., Trolliard G., Nicollet C. and Montel J.M. (2003) A developmental model of olivine morphology as a function of the cooling rate and the degree of undercooling. *Contrib. Miner. Petrol.* **145**, 251–263.

Federico L., Capponi G., Crispini L. and Scambelluri M. (2004) Exhumation of alpine high-pressure rocks: insights from petrology of eclogite clasts in the Tertiary Piedmontese basin (Ligurian Alps, Italy). *Lithos* **74**, 21–40.

Foley S. F., Prelevic D., Rehfeldt T. and Jacob D.E. (2013) Minor and trace elements in olivines as probes into early igneous and mantle melting processes. *Earth Planet. Sci. Lett.* **363**, 181–191.

Gaetani G.A. and Grove T.L. (1997) Partitioning of moderately siderophile elements among olivine, silicate melt and sulfide melt: constraints on core formation in the Earth and Mars. *Geochim. Cosmochim. Acta* **61**, 1829–1846.

Gao Y., Hoefs J., Hellebrand E., von der Andt A. and Snow J.E. (2007) Trace element zoning in pyroxenes from ODP Hole 735B gabbros: diffuse exchange or synkinematic crystal fractionation. *Contrib. Mineral. Petrol.* **153**, 429–442.

Garrido C.J., Bodinier J.-L. and Alard O. (2000) Distribution of LILE, REE and HFSE in anhydrous spinel peridotite and websterite minerals from the Ronda massif: insights into the nature of trace element reservoirs in the subcontinental lithospheric mantle. *Earth Planet. Sci. Lett.* **181**, 341–358.

Girona T. and Costa F. (2013) DIPRA: A user-friendly program to model multi-elementdiffusion in olivine with applications to timescales of magmatic processes. *Geochem. Geophys. Geosystems.* **14**, doi:10.1029/2012GC004427.

Godard M., Jousselin D. and Bodinier J.L. (2000) Relationships between geochemistry and structure beneath a paleo-spreading centre: a study of the mantle section in the Oman ophiolite. *Earth Planet. Sci. Lett.* **180**, 133–148.

Godard M., Awaji S., Hansen H., Hellebrand E., Brunelli D., Johnson K., Yamasaki T., Maeda J., Abratis M., Christie D., Kato Y., Mariet C. and Rosner M. (2009) Geochemistry of a long in-situ section of intrusive slow-spread oceanic lithosphere:Results from IODP Site U1309 (Atlantis Massif, 30°N Mid-Atlantic-Ridge). *Earth Planet. Sci. Lett.* **279**, 110–122.

Gregoire M., Moine B.N., O'Reilly S.Y., Cottin J.Y. and Giret A. (2000) Trace element residence and partitioning in mantle xenoliths metasomatized by highly alkaline, silicate- and carbonate-rich melts (Kerguelen Islands, Indian Ocean). *J. Petrol.* **41**, 477–509.

Günther D. and Heinrich C. (1999) Enhanced sensitivity in laser ablation-ICP mass spectrometry using helium-argon mixtures as aerosol carrier. J. *Anal. At. Spectrom.* **14**, 1363–1368.

Holzapfel C., Chakraborty S., Rubie D.C. and Frost D.J. (2007) Effect of pressure on Fe–Mg, Ni and Mn diffusion in $(Fex Mg1{-}x)_2SiO_4$ olivine. Physics of the Earth and Planetary Interiors **162**, 186–198.

Hoogerduijn Strating E.H., Piccardo G.B., Rampone E., Scambelluri M. and Vissers R.L.M. (1990) The structure and petrology of the Erro-Tobbio peridotite (Voltri Massif, Ligurian Alps): a two day excursion with emphasis on processes in the upper mantle. *Ofioliti* **15**, 119–184.

Hoogerduijn Strating E.H., Rampone E., Piccardo G.B., Drury M.R. and Vissers R.L.M. (1993) Subsolidus emplacement of mantle peridotities during incipient oceanic rifting and opening of the

Mesozoic Tethys (Voltri Massif, NW Italy). *J. Petrol.* **34**, 901–927.

Irving A.J. (1978) A review of experimental studies of crystal/liquid trace element partitioning. *Geochim. Cosmochim. Acta* **42**, 743–770.

Ito M. and Ganguly J. (2006) Diffusion kinetics of Cr in olivine and the 53Mn–53Cr thermochronology of early solar system objects. *Geochim. Cosmochim. Acta* **70**, 799–809.

Jochum K.P., Nohl U., Herwig K., Lammel E., Stoll B. and Hofmann A.W. (2005) GeoReM: A New Geochemical Database for Reference Materials and Isotopic Standards. *Geostand. Geoanalytical Res.* **29**, 333–338.

Jollands M.C., O'Neill H.S.C. and Hermann J. (2014) The importance of defining chemical potentials, substitution mechanisms and solubility in trace element diffusion studies: the case of Zr and Hf in olivine. *Contrib. Mineral. Petrol.* **168**, 1055–1073.

Kelemen P.B. (1990) Reaction between ultramafic rock and fractionating basaltic magma I. Phase relations, the origin of calcalkaline magma series, and the formation of discordant dunite. *J. Petrol* **31**, 51–98.

Kelemen P.B., Kikawa E. and Miller D.J. (2007) Leg 209 summary: processes in a 20-km-thick conductive boundary layer beneath the Mid-Atlantic Ridge, 14_–16_N. In: Kelemen PB, Kikawa E, Miller DJ (eds) *Proceedings of the ODP, science results* **209**, College Station, TX (Ocean Drilling Program), 1–33. doi:10.2973/odp.proc.sr.209.001.2007.

Kennedy A.K., Lofgren G.E. and Wasserburg G.J. (1993) An experimental study of trace element partitioning between olivine, orthopyroxene and melt in chondrules: equilibrium values and kinetic effects. *Earth Planet. Sci. Lett.* **115**, 177–195.

Kinzler R.J., Grove T.L. and Recca S.I. (1990) An experimental study on the effects of temperature and melt composition on the partitioning of nickel between olivine and silicate melt. *Geochim. Cosmochim. Acta* **54**, 1255–1266.

Kohn S.C. and Schofield P.F. (1994) The importance of melt composition in controlling trace-element behaviour — an experimental study of Mn and Zn partitioning between forsterite and silicate melts. *Chem. Geol.* **117**, 73–87.

Kvassnes A.J.S. and Grove T.L. (2008) How partial melts of mafic lower crust affect ascending magmas at ocean ridges. *Contrib. Mineral. Petrol.* **156**, 49–71.

Lee C.-T.A., Harbert A. and Leeman W.P. (2007) Extension of lattice strain theory to mineral/mineral rare-earth element partitioning: an approach for assessing disequilibrium and developing internally consistent partition coefficients between olivine, orthopyroxene, clinopyroxene and basaltic melt. *Geochim. Cosmochim. Acta* **71**, 481–496.

Liang Y., Sun C. and Yao L. (2013) A REE-in-two-pyroxene thermometer for mafic and ultramafic rocks. *Geochim. Cosmochim. Acta* **102**, 246–260.

Lissenberg C.J. and Dick H.J.B. (2008) Melt-rock reaction in the lower oceanic crust and its implications for the genesis of mid-ocean ridge basalt. *Earth Planet. Sci. Lett.* **271**, 311–325.

Lissenberg C.J., Howard K.A., MacLeod C.J. and Godard M. (2013) Pervasive reactive melt migration through fast-spreading lower oceanic crust (Hess Deep, Equatorial Pacific Ocean). *Earth Planet. Sci. Let.* **361**, 436–447.

Mysen B. (2007) Partitioning of calcium, magnesium, and transition metals between olivine and melt governed by the structure of the silicate melt at ambient pressure. *Am. Mineral.* **92**, 844–862.

Muentener O., Manatschal G., Laurent D. and Pettke T. (2010) Plagioclase peridotites in ocean-continent transitions: refertilized mantle domains generated by melt stagnation in the shallow mantle lithosphere. *J. Petrol* **51**, 255–294.

Niu Y. (2004) Bulk rock major and trace element compositions of abyssal peridotites: implications for mantle melting, melt extraction and post-melting processes beneath mid-ocean ridges. *J. Petrol.* **45**, 2423–2458.

Normann M.D. (1998) Melting and metasomatism in the continental lithosphere: laser ablation ICPMS analysis of minerals in spinel lherzolites from eastern Australia. *Contrib. Mineral. Petrol.* **130**, 240–255.

O'Driscoll B., Donaldson C.H., Troll V.R., Jerram D.A. and Emeleus C.H. (2007) An Origin for Harrisitic and Granular Olivine in the Rum Layered Suite, NW Scotland: a Crystal Size Distribution Study. *J.Petrol.* **48**, 253–270.

O'Reilly S.Y., Chen D., Griffin W.L. and Ryan C.G. (1997) Minor elements in olivine from spinel lherzolite xenoliths: implications for thermobarometry. *Mineral. Mag.* **61**, 257–269.

Ottonello G., Piccardo G.B. and Ernst W.G. (1979) Petrogenesis of some Ligurian peridotites – II rare earth element chemistry. *Geochim. Cosmochim. Acta* **43**, 1273–1284.

Pearce N.J.G., Perkins W.T., Westgate J.A., Gorton M.P., Jackson S.E., Neal C.R. and Chenery S.P. (1997) A compilation of new and published major and trace element data for NIST SRM 610 and NIST SRM 612 glass reference materials. *Geostand. Geoanalytical Res.* **21**, 115–144.

Petry C., Chakraborty S. and Palme H. (2004) Experimental determination of Ni diffusion coefficients in olivine and their dependence on temperature, composition, oxygen fugacity, and crystallographic orientation. *Geochim. Cosmochim. Acta* **68**, 4179–4188.

Piccardo G.B., Rampone E. and Vannucci R. (1990) Upper mantle evolution during continental rifting and ocean formation: evidence from peridotites bodies of the Western Alpine-Northern Appennine system. *Mem. Soc. Geol. Fr.* **156**, 323–333.

Piccardo G.B., Rampone E. and Vannucci R. (1992) Ligurian peridotites and ophiolites: from rift to ocean formation in the Jurassic Ligure-Piemontese basin. *Acta Vulcanol.* **2**, 313–325.

Piccardo G.B., Muentener O., Zanetti A. and Pettke T. (2004) Ophiolite peridotites of the Alpine-Apennine system: mantle processes and geodynamic relevance. *Int. Geol. Rev.* **40**, 1119–1159.

Piccardo G.B. and Vissers R.L.M. (2007) The pre-oceanic evolution of the Erro-Tobbio peridotite (Voltri Massif - Ligurian Alps, Italy). *J. Geodynam.* **43**, 41 –449.

Piccardo G.B., Zanetti A. and Muentener O. (2007) Melt/peridotite interaction in the Southern Lanzo peridotite: Field, textural and geochemical evidence. *Lithos* **94**, 181–209.

978 Rampone E. and Borghini G. (2008) Melt migration and intrusion in the Erro-Tobbio peridotites
979 (Ligurian Alps, Italy): Insights on magmatic processes in extending lithospheric mantle. *Eur. J.*
980 *Min.* **20**, 573–585.
981
982 Rampone E., Piccardo G.B., Vannucci R. and Bottazzi P. (1997) Chemistry and origin of trapped
983 melts in ophiolitic peridotites. *Geochim. Cosmochim. Acta* **61**, 4557–4569.
984
985 Rampone E., Romairone A. and Hofmann A.W. (2004) Contrasting bulk and mineral chemistry in
986 depleted peridotites : evidence for reactive porous flow. *Earth Planet. Sci. Lett.* **218**, 491–506.
987
988 Rampone E., Romairone A., Abouchami W., Piccardo G.B. and Hofmann A.W. (2005) Chronology,
989 petrology and isotope geochemistry of the Erro-Tobbio peridotites (Ligurian Alps, Italy): records of
990 late Paleozoic lithospheric extension. *J. Petrol.* **46**, 799–827.
991
992 Rampone E., Piccardo G.B. and Hofmann A.W. (2008) Multi-stage melt-rock interaction in the Mt.
993 Maggiore (Corsica, France) ophiolitic peridotites: microstructural and geochemical evidence.
994 *Contrib. Mineral. Petrol.* **156**, 453–475.
995
996 Rampone E., Borghini G., Romairone A., Abouchami W., Class C. and Goldstein S.L. (2014) Sm–
997 Nd geochronology of the Erro-Tobbio gabbros (Ligurian Alps, Italy): Insights into the evolution of
998 the Alpine Tethys. *Lithos* **205**, 236–246.
999
1000 Remmert P., Dohmen R. and Chakraborty S. (2008) Diffusion of REE, Hf e Sr in olivine. Eos
1001 Transactions, AGU, 89(53) Fall Meeting Supplement Abstract. MR33A-1844.
1002
1003 Renna M.R. and Tribuzio R. (2011) Olivine-richTroctolites from Ligurian Ophiolites (Italy):
1004 Evidence for Impregnation of Replacive Mantle Conduits by MORB-type Melts. *J. Petrol.* **52**,
1005 1763–1790.
1006
1007 Ross K. and Elthon D. (1997) Cumulus and postcumulus crystallization in the ocean crust: major-
1008 and trace-element geochemistry of leg 153 gabbroic rocks. In: Karson, J.A., Cannat, M., Millet,
1009 D.J., Elton, D., (Eds.), *Proceedings of the Ocean Drilling Program, Scientific Results* **153**. Ocean
1010 Drilling Program, College Station, Texas, 333–350.
1011
1012 Sanfilippo A. and Tribuzio R. (2011) Melt transport and deformation history in a nonvolcanic
1013 ophiolitic section, northern Apennines, Italy: implications for crustal accretion at slow spreading
1014 settings. *Geochem. Geophys. Geosyst.* **12**, Q0AG04.
1015
1016 Sanfilippo A. and Tribuzio R. (2013a) Building of the deepest crust at a fossil slow-spreading
1017 centre (Pineto gabbroic sequence, Alpine Jurassic ophiolites). *Contrib. Mineral. Petrol.* **165**, 705–
1018 721.
1019
1020 Sanfilippo A. and Tribuzio R. (2013b) Origin of olivine-rich troctolites from the oceanic
1021 lithosphere: a comparison between the Alpine Jurassic ophiolites and modern slow spreading
1022 ridges. *Ofioliti* **38**, 89–99.
1023
1024 Sanfilippo A., Dick H.J.B. and Ohara Y. (2013) Melt–rock reaction in the mantle: mantle troctolites
1025 from the Parece Vela Ancient Backarcspreading center. *J. Petrol.* **54**, 861–885.
1026
1027 Sanfilippo A., Tribuzio R. and Tiepolo M. (2014) Mantle–crust interactions in the oceanic
1028 lithosphere: Constraints from minor and trace elements in olivine. *Geochim Cosmochim. Acta* **141**,
1029 423-439.

Sanfilippo A., Morishita T., Kumagai H., Nakamura K., Okino K., Hara K.B., Tamura A. and Arai S. (2015a) Hybrid troctolites from mid-ocean ridges: inherited mantle in the lower crust. *Lithos* **232**, 124–130.

Sanfilippo A., Tribuzio R., Tiepolo M. and Berno D. (2015b) Reactive flow as dominant evolution process in the lowermost oceanic crust: evidence from olivine of the Pineto ophiolite (Corsica). *Contrib. Mineral. Petrol.* **170**, 38.

Saper L. and Liang Y. (2014) Formation of plagioclase-bearing peridotite and plagioclase-bearing wehrlite and gabbro suite through reactive crystallization: an experimental study. *Contrib. Mineral. Petrol.* **167**, 985.

Shimizu H., Sangen K. and Masuda A. (1982) Experimental-Study on Rare-Earth Element Partitioning in Olivine and Clinopyroxene Formed at 10 and 20kb for Basaltic Systems. *Geochemical Journal* 16, 107–117.

Spandler C., O'Neill H.S.C. and Kamenetsky V.S. (2007) Survival times of anomalous melt inclusions: constraints from element diffusion in olivine and chromite. *Nature* **447**, 303–306.

Spandler C. and O'Neill H.S.C. (2010) Diffusion and partition coefficients of minor and trace elements in San Carlos olivine at 1,300°C with some geochemical implications. *Contrib. Mineral. Petrol.* **159**, 791–818.

Sobolev A.V., Hofmann A.W., Sobolev S.V. and Nikogosian I.K. (2005) An olivine-free mantle source of Hawaiian shield basalts. *Nature* **434**, 590–597.

Sobolev A.V., Hofmann A.W., Kuzmin D.V., Yaxley G.M., Arndt N.T., Chung S.-L., Danyushevsky L.V., Elliott T., Frey F.A., Garcia M.O., Gurenko A.A., Kamenetsky V.S., Kerr A.C., Krivolutskaya N.A., Matvienkov V.V., Nikogosian I.K., Rocholl A., Sigurdsson I.A., Sushchevskaya N.M. and Teklay M. (2007) The amount of recycled crust in sources of mantle-derived melts. *Science* **316**, 412–417.

Sun M. and Kerrich R. (1995) Rare earth element and high field strength element characteristics of whole rocks and mineral separates of ultramafic nodules in Cenozoic volcanic vents of southeastern British Columbia, Canada. *Geochim Cosmochim Acta* **59**, 4863–4879.

Sun S.S. and McDonough W.F. (1989) Chemical and isotopic systematics of oceanic basalts: implications for mantle composition and processes. In: Saunders A.D., Norry M.J. (Eds.), *Magmatism in the ocean basins*. Geological Society of London, 313–345.

Sun C. and Liang Y. (2012) Distribution of REE between clinopyroxene and basaltic melt along a mantle adiabat: effects of major element composition, water, and temperature. *Contrib. Mineral. Petrol.* **163**, 807–823.

Sun C. and Liang Y. (2013) The importance of crystal chemistry on REE partitioning between mantle minerals (garnet, clinopyroxene, orthopyroxene and olivine) and basaltic melts. *Chem. Geol.* **358**, 23–36.

Sun C. and Liang Y. (2014) An assessment of subsolidus re-equilibration on REE distribution among mantle minerals olivine, orthopyroxene, clinopyroxene, and garnet in peridotites. *Chem. Geol.* **372**, 80–91.

Tartarotti P., Susini S., Nimis P. and Ottolini L. (2002) Melt migration in the upper mantle along the Romanche Fracture Zone (Equatorial Atlantic). *Lithos* **63**, 125–149.

Taura H., Yurimoto H., Kurita K. and Sueno S. (1998) Pressure dependence on partition coefficients for trace elements between olivine and the coexisting melts. *Phys. Chem. Miner.* **25**, 469–484.

Van Achterbergh E., Griffin W.L. and Stiefenhofer J. (2001) Metasomatism in mantle xenoliths from the Letlhakane kimberlites: estimation of element fluxes. *Contrib. Mineral. Petrol.* **141**, 397–414.

Vissers R.L.M., Drury M.R., Hoogerduijn Strating E.H. and Van der Wal D. (1991) Shear zones in the upper mantle: a case study in an Alpine lherzoliti massif. *Geology* **19**, 990–993.

Zanetti A., Tiepolo M., Oberti R. and Vannucci R. (2004) Trace-element partitioning in olivine: modelling of a complete data set from a synthetic hydrous basanite melt. *Lithos* **75**, 39–54.

Zhukova I., O'Neill H.S.C., Cambell I.K. and Kilburn (2014) The effect of silica activity on the diffusion of Ni and Co in olivine. *Contrib. Mineral. Petrol.* **168**, 1029.

Welsch B., Hammer J. and Hellebrand E. (2014) Phosphorus zoning reveals dendritic architecture of olivine. *Geology* **42**, 867–870.

Witt-Eickschen G. and O'Neill H.S. (2005) The effect of temperature on the equilibrium distribution of trace elements between clinopyroxene, orthopyroxene, olivine and spinel in upper mantle peridotite. *Chem. Geol.* **221**, 65–101.

FIGURE CAPTIONS

Figure 1 – Sketch map of the Voltri Massif (VM), showing the Erro-Tobbio peridotite and surrounding units (redrawn after Federico et al., 2004): (1) Erro-Tobbio peridotite Unit (VM), (2) Calcschists and meta-volcanics (VM), (3) Serpentinites and metagabbros (VM), (4) Crystalline massifs, (5) Sestri-Voltaggio zone, (6) Flysch Units, (7) Post-orogenic and Tertiary Piedmont Basin deposits, (8) Montenotte Unit. The large red circle indicates the studied area. (For interpretation of the references to colour in this figure legend, the reader is referred to the web version of this article).

Figure 2 – Field features of studied troctolites and gabbros. **a** Troctolite apophysis within mantle peridotites. **b** Textural variations (from granular to harrisitic types) within the troctolite. **c** Olivin gabbro dyke intruded (with sharp contacts) within the troctolite. **d** Close-up of Fig.2b, showing the textural variation of olivine (the dark grey mineral) from fine-grained granular (in the left bottom corner) to harrisitic-skeletal.

Figure 3 – Microscopic textures of troctolites and gabbros (cross-polarized light). **a** Sub-idiomorphic rounded olivine grains (ol) surrounded by plagioclase (plag), in granular troctolite MF21; small black spinel grain (sp) included in plagioclase. **b** Large kinked olivine grain (kinked ol), with irregular lobate contacts against interstitial plagioclase, in troctolite apophysis MF51. **c** Large hopper-type olivine crystal (ol) with lobate resorbed contacts against interstitial plagioclase (plag) in troctolite MF73. **d** Subidiomorphic olivine grain surrounded by plagioclase crystals (in rather sharp contacts) in olivine gabbro MF22.

Figure 4 – Variation of Mg# vs. Ni [**a**] and Mn [**b**] in olivines of Erro-Tobbio peridotites, troctolites and gabbro (see the legend for symbols). We also show olivine data for peridotites, dunites and troctolites in other Alpine-Apennine ophiolites (from Sanfilippo et al., 2014), together with the compositional field defined by olivine phenochrysts in MORB (data from Sobolev et al., 2007). Computed trends reported in Fig.4A refer to the compositional variations in olivine for fractional (FC) and equilibrium (EC) crystallization of a primary MORB melt at low pressure (< 5 Kb) (after Drouin et al., 2009).

Figure 5 – Variation of Mn vs. Ni [**a**], Co [**b**] and Zn [**c**] in olivines of Erro-Tobbio peridotites, troctolites and gabbro. Also shown are peridotite, troctolite, ol-gabbro data from Sanfilippo et al. (2014, 2015b).

Figure 6 - Variation of Zr vs. Hf [**a**], Ti [**b**], Yb [**c**] and Li [**d**] of olivines in Erro-Tobbio peridotites, troctolites and gabbro. In [**b**] and [**c**]**,** we also reported peridotite-troctolite olivine data from Sanfilippo et al. (2014), and MAR troctolite olivine data from Drouin et al. (2009). The field refers to the compositional range defined by mantle olivines in orogenic massifs and xenoliths (see text for more explanation; data from Sun and Kerrick, 1995; Garrido et al., 2000; Bedini and Bodinier, 1999).

Figure 7 - Chondrite-normalized Rare-Earth-Elements (REE) abundances of [**a**] clinopyroxene, orthopyroxene, [**b**] plagioclase and [**c**] olivine of Erro-Tobbio peridotites, troctolites and gabbro (see the legend for symbols). The fields reported in [**a**] and [**b**] refer, respectively, to the composition of clinopyroxene and plagioclase in ET troctolites from Borghini et al. (2007). In [**c**], we also show the compositional fields defined by: i) olivines in Mid-Atlantic Ridge troctolites (Drouin et al., 2009); ii) mantle olivines in orogenic massifs and xenoliths (see text for more explanation; data from Sun and Kerrick, 1995; Eggins et al., 1998; Garrido et al., 2000; Gregoire et al., 2000; Bedini and Bodinier, 1999), iii) olivines in Gakkel Ridge peridotites (D'Errico et al., 2015). Normalizing values after Sun and McDonough (1989).

Figure 8 – Primitive mantle-normalized trace elements abundances of [**a**] clinopyroxene, orthopyroxene, [**b**] plagioclase and [**c**] olivine of Erro-Tobbio peridotites, troctolites and gabbro (see the legend for symbols). The field reported in [**a**] refers to the composition of clinopyroxene in ET troctolites from Borghini et al. (2007). In [**c**], we also show the compositional fields defined by: i) olivines in Mid-Atlantic Ridge troctolites (Drouin et al., 2009); ii) mantle olivines in orogenic massifs and xenoliths (see text for more explanation; data from Sun and Kerrick, 1995; Eggins et al., 1998; Garrido et al., 2000; Gregoire et al., 2000; Bedini and Bodinier, 1999), iii) olivines in Gakkel Ridge peridotites (D'Errico et al., 2015). Normalizing values after Sun and McDonough (1989).

Figure 9 – [**a**] Olivine/cpx and [**b**] opx/cpx REE partition coefficients in the Erro-Tobbio peridotites, troctolites and ol-gabbro. We also reported predicted ol/cpx and opx/cpx partitioning at 1000, 1300 and 1400°C, after Lee et al. (2007).

Figure 10 - Olivine/cpx REE partition coefficients plotted versus Ionic Radius in the Erro-Tobbio peridotites [**a**], troctolites and gabbro **[b**]. Also shown are olivine/cpx trends computed at varying temperatures (1000-1300°C) using the major element compositions of olivine and clinopyroxene in our samples (following the modelling procedure by Sun and Liang, 2012, 2013, 2014).

Figure 11 - Chondrite-normalized Rare-Earth-Elements (REE) abundances of computed melts in equilibrium with: [**a**] olivine, orthopyroxene and clinopyroxene in the peridotites, [**b**] olivine, clinopyroxene and plagioclase in troctolites, [**c**] olivine, clinopyroxene and plagioclase in gabbro (see the legend for symbols). Clinopyroxene/liquid, orthopyroxene/liquid and olivine/liquid partition coefficients are from Lee et al. (2007). Plagioclase/liquid partition coefficients are from Aignes-Torres et al. (2007). Normalizing values after Sun and McDonough (1989).

Figure 12 - Chondrite-normalized Rare-Earth-Elements (REE) abundances of computed melts in equilibrium with: [**a**] olivine, orthopyroxene and clinopyroxene in the peridotites, [**b**] olivine, clinopyroxene and plagioclase in troctolites, [**c**] olivine, clinopyroxene and plagioclase in gabbro (see the legend for symbols). Clinopyroxene/liquid, orthopyroxene/liquid, olivine/liquid and plagioclase/liquid partition coefficients are from Bedard (2001). Normalizing values after Sun and McDonough (1989).

Figure 13 – Chondrite-normalized Rare-Earth-Elements (REE) abundances of computed melts in equilibrium with: [**a**] olivine and clinopyroxene in the peridotites, [**b**] olivine and clinopyroxene in troctolites, [**c**] olivine and clinopyroxene in gabbro (see the legend for symbols). Clinopyroxene/liquid and olivine/liquid partition coefficients at 1200 °C have been calculated following Sun and Liang (2012, 2013) models. Normalizing values after Sun and McDonough (1989).

Figure 14 – Variation of Zr_N/Nd_N ratio vs Yb_N in olivine of troctolites and gabbro, compared to olivine compositions computed by AFC model (De Paolo, 1981) at decreasing melt mass (F = 0.95-0.10). The initial melt composition C_0 is equal to the melt computed in equilibrium with the clinopyroxene of troctolite MF21 showing the lowest REE concentrations (see Table 3). The model assumes that initial melt ($melt_1$) assimilate olivine (Ma = 100% olivine) and crystallize plagioclase (Mc = 100% plag). The composition of assimilated olivine is olivine in peridotite MF40. The four different trends refer to different values of r (r = Ma/Mc). Model A in [**a**] and Model B in [**b**] differ only for the adopted partition coefficients. Model A: compilation of REE, Zr partition coefficients for olivine, plagioclase and clinopyroxene proposed by Suhr (1998). Model B: olivine/liquid D_{REE} by Lee (2007); olivine/liquid D_{Zr} by Spandler and O'Neill (2010); clinopyroxene/liquid $D_{REE,Zr}$ by Suhr (1998); plagioclase/liquid $D_{REE,Zr}$ by Aignes-Torres et al., (2007).

Melt/rock reaction at oceanic peridotite/gabbro transition as revealed by trace element chemistry of olivine

Elisabetta Rampone[1], Giulio Borghini[2], Marguerite Godard[3], Benoit Ildefonse[3], Laura Crispini[1,] Patrizia Fumagalli[2]

[1]DISTAV, University of Genova, Corso Europa 26, I-16132 Genova, Italy

[2]Dipartimento di Scienze della Terra, University of Milano, via Botticelli 23, 20133 Milano, Italy

[3]Géosciences Montpellier, Université de Montpellier, CNRS UMR 5243, 34095 Montpellier cedex 05, France

Corresponding Author

Elisabetta Rampone
Dipartimento di Scienze della Terra, dell'Ambiente e della Vita (DISTAV)
Università degli Studi di Genova
Corso Europa 26
I-16132 Genova (Italy)

Tel. 0039 10 3538315
Fax. 0039 10 352169
Email: betta@dipteris.unige.it

Abstract

Several recent studies have documented that reactions between melt and crystal mush in primitive gabbroic rocks (via reactive porous flow) have an important control in the formation of the lower oceanic crust and the evolution of MORBs. In this context, olivine-rich rocks can form either by fractional crystallization of primitive melts or by open system reactive percolation of pre-existing (possibly mantle-derived) olivine matrix. To address this question, we performed in-situ trace element analyses (by LA-ICP-MS) of olivine from the Erro-Tobbio ophiolite Unit (Ligurian Alps), where mantle peridotites show gradational contacts with an hectometer-scale body of troctolites and plagioclase wehrlites, and both are cut by later decameter-wide lenses and dykes of olivine gabbros. Previous studies inferred that troctolites and olivine gabbros represent variably differentiated crystallization products from primitive MORB-type melts. Olivines in the three rock types (mantle peridotites, troctolites, olivine gabbros) exhibit distinct geochemical signature and well-defined elemental correlations. As expected, compatible elements (e.g. Ni) show the highest concentrations in peridotites (2580-2730 ppm), intermediate in troctolites (2050-2230 ppm) and lowest in gabbros (1355-1420 ppm), whereas moderate incompatible elements (e.g. Mn, Zn) show the opposite behaviour. By contrast, highly incompatible elements like Zr, Hf, Ti, HREE are variably enriched in olivines of troctolites, and the enrichment in absolute concentrations is coupled to development of significant HFSE/REE fractionation (Zr_N/Nd_N up to 80). AFC modeling shows that such large Zr_N/Nd_N ratios in olivines are consistent with a process of olivine assimilation and plagioclase crystallization at decreasing melt mass, in agreement with textural observations. In-situ trace element geochemistry of olivine, combined with microstructural investigations, thus appears a powerful tool to investigate reactive percolation and the origin of olivine-rich rocks in the lower oceanic crust.

1. INTRODUCTION

Several lines of evidence have stressed that melt/rock reactions acting at the oceanic mantle-crust boundary play an important role in the chemical evolution of MORBs and the formation of the primitive (olivine-rich) lower oceanic crust (Bedard et al., 2000; Coogan et al., 2000; Drouin et al., 2009, 2010; Gao et al., 2007; Dick et al., 2008; Lissenberg and Dick, 2008; Kvassnes and Grove, 2008; Eason and Sinton, 2009; Godard et al., 2009; Collier and Kelemen, 2010; Renna and Tribuzio, 2011; Sanfilippo and Tribuzio, 2011, 2012; Lissenberg et al., 2013; Sanfilippo et al., 2013, 2014, 2015a,b; Saper and Liang 2014). Specific chemical features in MORBs, such as the spread in MgO contents at given CaO values, cannot be easily reconciled with processes of fractional crystallization of heterogeneous parental melts occurring at variable pressure. Based on this observation, a series of papers inferred that the composition of MORBs can be modified by melt/rock reactions taking place either in the primitive lower oceanic crust, or in the uppermost lithospheric mantle (e.g. Lissenberg and Dick, 2008; Collier and Kelemen, 2010; Lissenberg et al., 2013). Collier and Kelemen (2010) described this process as reactive crystallization, linking the peculiar chemical signatures of MORBs to the diffuse evidence of melt percolation and impregnation in the oceanic mantle (e.g. Dick, 1989; Cannat et al., 1990; Rampone et al., 1997, 2008; Godard et al., 2000; Tartarotti et al., 2002; Dijkstra et al., 2003; Niu, 2004; Chazot et al., 2005; Piccardo et al. 2007; Kelemen et al., 2007; Müntener et al., 2010).

Parallel chemical and microstructural studies on olivine-rich intrusive rocks (troctolites, werhlites, olivine gabbros) from modern ridge settings and ophiolites (Lissenberg and Dick, 2008; Drouin et al., 2009, 2010; Renna and Tribuzio, 2011; Sanfilippo and Tribuzio, 2011, 2012; Lissenberg et al., 2013; Sanfilippo et al., 2013, 2014, 2015a,b) have suggested a composite "hybrid" origin of these rocks, likely related to open-system melt impregnation of an olivine crystal framework. An open issue thus concerns the origin of oceanic troctolites, whether they formed by fractional crystallization of primitive melts or by reactive percolation of pre-existing (possibly mantle-derived) olivine matrix.

Olivine is an ubiquitous mineral in both mantle and primitive lower crustal rocks, and largely involved in melt/rock reaction processes. Consequently, it has become increasingly important to improve knowledge about its trace element composition, and to test the existence of geochemical signatures to distinguish a magmatic versus a mantle origin. Foley et al. (2013) proposed a large compilation of trace element data in olivine from mantle peridotites and Mediterranean volcanics. They outlined the great potential of olivine as a petrogenetic tracer of mantle melting and early igneous crystallization, and the need of further studies on natural olivines, in order to improve the current database, lacking many promising elements.

Many studies have been devoted to determining diffusion and partition coefficients for minor and trace elements in olivine (e.g. Irving, 1978; Shimizu et al., 1982; Kinzler et al., 1990; Beattie (1994); Dunn and Sen, 1994; Eggins et al., 1998; Taura et al., 1998; Gregoire et al., 2000; Petry et al., 2004; Zanetti et al., 2004; Bedard, 2005; Coogan et al., 2005; Witt-Eickschen and O'Neill, 2005; Holzapfel et al., 2007; Lee et al., 2007; Spandler et al., 2007; Brady and Cherniak, 2010; Chakraborty, 2010; Cherniak, 2010; Dohmen et al., 2010; Spandler and O'Neill, 2010; Cherniak and Watson, 2012; Burgess and Cooper, 2013; Girona and Costa, 2013; Cherniak and Liang, 2014; Cherniak and Van Orman, 2014; Jolland et al., 2014; Kennedy et al., 1993; Zhukova et al., 2014), and a very robust data set exists on selected minor element abundances (e.g. Ni, Co, Mn, Cr) of olivine phenochrysts in basalts from different tectonic environments (Sobolev et al., 2005, 2007; Foley et al., 2013). Other studies have determined selected minor, trace elements concentrations in mantle olivines (e.g. O'Reilly et al., 1997; Normann, 1998; see also the data compilations in De Hoog et al., 2010, Foley et al., 2013). However, only a few studies provide a complete set of trace element compositions measured in olivine from mantle peridotite (Sun and Kerrick, 1995; Eggins et al., 1998; Bedini and Bodinier, 1999; Garrido et al., 2000; Gregoire et al., 2000; De Hoog et al., 2010) and gabbroic rocks (Drouin et al., 2009; Sanfilippo et al., 2014). This is mostly due to the difficulty to get reliable analyses, due to the extremely low abundances of many trace elements (e.g. REE, Ti, Zr, Hf) in this mineral.

We have selected peridotite, troctolite and gabbro samples from the ophiolitic Erro-Tobbio Unit (Ligurian Alps, Italy; Borghini et al., 2007, Borghini and Rampone, 2008), and performed a set of in-situ trace element analyses (by LA-ICP-MS) on olivine in both mantle and crustal rocks, with the objective to provide a first "baseline" dataset on olivine trace element chemistry in associated rocks of different origins (mantle and magmatic), and to exploit the potential of olivine geochemistry to get insights into processes of reactive melt percolation at the oceanic peridotite/gabbro transition. A major outcome of this work is that olivine in most of the troctolites has unexpected trace element compositions, indicative of melt/rock reactions likely involving concomitant olivine dissolution and plagioclase crystallization. Furthermore, discrepancies between the compositions of melts in equilibrium with olivine and coexisting minerals, in both mantle and gabbroic rocks, point to the need for a better understanding of the mechanisms of incorporation and diffusion of trace elements in olivine.

2. FIELD RELATIONS AND SAMPLES

The Erro-Tobbio Unit (ET, Voltri Massif, Ligurian Alps, Italy, Fig. 1) consists of predominant mantle peridotites, intruded by discrete gabbroic bodies and dykes, and represent remnants of the Jurassic Ligurian Tethys oceanic lithosphere. These rocks, in spite of the Alpine

overprint, preserve kilometre-scale structural and chemical records of their pre-Alpine evolution (Bezzi and Piccardo, 1971; Chiesa et al., 1975; Ernst and Piccardo, 1979; Ottonello et al., 1979; Piccardo et al., 1990; 1992; Hoogerdujin Strating et al., 1990; 1993; Vissers et al., 1991; Borsi et al., 1996; Capponi et al., 1999; Piccardo et al., 2004; Rampone et al., 2004, 2005).

The extension-related exhumation of the Erro-Tobbio mantle from deep lithospheric depths (P > 15–20 kbar) to a shallow level (P < 5 kbar) was accompanied by a composite history of melt migration and intrusion marked by i) open-system melt migration and reactive porous flow at spinel-facies depths, ii) melt/rock reaction at shallower and colder lithospheric level, leading to the formation of plagioclase-enriched impregnated peridotites, iii) multiple gabbroic intrusions (Piccardo et al., 2004; Rampone et al., 2004, 2005; Piccardo and Vissers, 2007; Borghini et al., 2007; Borghini and Rampone, 2007; Rampone and Borghini, 2008).

Samples investigated in this work were collected in the Southern sector of the Erro Tobbio Unit (Fig. 1), where plagioclase-rich impregnated peridotites are intruded by a discrete hundred-metre-scale magmatic body, mostly consisting of troctolites, and minor plagioclase-bearing dunites and wehrlites. This compositional variability often defines a magmatic layering. The contact between host mantle rocks and troctolites is gradational, in places marked by troctolite and wehrlite apophyses within the peridotites (Fig 2a). Inside the troctolite body, the layering is also defined by a textural variability of olivine, ranging from granular to harrisitic (Fig. 2 b,c,d), with skeletal olivine crystals up to dm-scale size. Similar textures have been already documented in ophiolites and in layered intrusions (e.g. O'Driscoll et al., 2007; Renna and Tribuzio, 2011), and interpreted as primary magmatic disequilibrium texture related to open-system episodic melt influx. Subsequent olivine-gabbro lenses and thin dykelets intruded both peridotites and troctolites, crosscutting the peridotite foliation and the magmatic layering in the troctolite body (Borghini et al., 2007).

The studied samples are two peridotites (MF40, P1), five troctolites (MF21, MF51, MF72Ga, MF72Ha, MF73Ga) and one olivine gabbro (MF22). Samples MF22, MF40, MF21, MF51 were studied earlier (Borghini et al. 2007; Borghini and Rampone, 2007; Rampone et al., 2014) for major and trace element mineral chemistry (olivine and associated pyroxenes and plagioclase). Based on their bulk and mineral chemical compositions, troctolites and olivine gabbros were interpreted as crystallization products of variably evolved N-MORB-type melts (Borghini et al., 2007). The N-MORB affinity of parental melts is also indicated by Nd isotopic composition of gabbros (average initial ε_{Nd} of 9.25 ± 0.25; Rampone et al., 2014). A brief summary of salient petrographic and chemical characteristics of these samples is given below. The new samples included in this study are three troctolites showing variable olivine texture, from granular (MF72Ga, MF73Ga) to harrisitic (MF72Ha), and one mantle peridotite (P1). Troctolites MF72Ga and MF72Ha represent different textural domains in one single sample (MF72).

Peridotites (MF40, P1) are low-strain spinel tectonites showing diffuse plagioclase enrichment related to melt impregnation. This is illustrated by reactive dissolution and replacement of clinopyroxene by orthopyroxene + plagioclase intergrowth, and reactive dissolution of kinked mantle olivine by poikilitic orthopyroxene (see Borghini et al., 2007).

Troctolites (MF21, MF51, MF72Ga, MF73Ga) are made of dominant subidiomorphic granular olivine, idiomorphic Cr-spinel, interstitial plagioclase and subordinate clinopyroxene (Fig. 3a). They also contain small interstitial accessory minerals (Ti-rich pargasitic amphibole, ilmenite, orthopyroxene) as thin rims around Cr-rich spinel and olivine, related to late-stage crystallization of small fractions of trapped melt (Borghini and Rampone, 2007). The interstitial clinopyroxene and plagioclase often show lobate contacts against olivine, indicative of partial olivine resorption. Reactive dissolution of olivine is even more evident in the coarse-grained harrisitic types (MF73H, MF72Ha), where cm-size hopper olivine crystals are significantly corroded by plagioclase crystallization (Fig. 3c). In the troctolite apophysis MF51, olivine occurs either as euhedral undeformed crystals, or as large and irregular kinked grains, partly resorbed by plagioclase (Fig. 3b).

Olivine gabbro MF22 displays coarse- to medium-grained hypidiomorphic texture, with euhedral to subhedral olivine (about 10% by vol.), euhedral to subhedral plagioclase and anhedral to poikilitic clinopyroxene (Fig. 3d). The crystallization sequence, olivine–plagioclase–clinopyroxene, is typical of low-P oceanic gabbros. Olivine mostly exhibits rather regular contacts against plagioclase and clinopyroxene.

3. ANALYTICAL METHODS

The major element compositions of minerals in most of studied samples were provided in previous papers (Borghini et al., 2007; Borghini and Rampone, 2007). Here we report complementary analyses (in addition to data for the new samples P1, MF72Ga, MF72Ha, MF73Ga) for all mineral spots analysed in-situ for trace element chemistry.

Major element compositions of minerals were analysed using a JEOL JXA 8200 Superprobe equipped with five wavelength-dispersive (WDS) spectrometers, an energy dispersive (EDS) spectrometer, and a cathodoluminescence detector (accelerating potential 15 kV, beam current 15 nA), operating at the Dipartimento di Scienze della Terra, University of Milano.

In situ trace element compositions were determined by LA-ICPMS at Géosciences Montpellier (AETE, University of Montpellier, France). Plagioclase, clinopyroxene, orthopyroxene and olivine were analyzed using 120 μm thick polished sections. Sites of analysis were carefully selected optically to discard those affected by alteration. Analysed trace elements (and corresponding m/z values) were: ^{7}Li, ^{11}B, ^{45}Sc, ^{47}Ti, ^{51}V, ^{55}Mn, ^{59}Co, ^{62}Ni, ^{66}Zn, ^{88}Sr, ^{89}Y, ^{90}Zr,

^{93}Nb, ^{137}Ba, rare earth elements (REEs: ^{139}La, ^{140}Ce, ^{141}Pr, ^{146}Nd, ^{147}Sm, ^{151}Eu, ^{157}Gd, ^{159}Tb, ^{163}Dy, ^{165}Ho, ^{167}Er, ^{169}Tm, ^{173}Yb, ^{175}Lu), ^{177}Hf, ^{181}Ta, ^{208}Pb, ^{232}Th and ^{238}U. Analyses were performed with a Thermo Scientific Element XR (eXtended Range) high resolution ICPMS. The ICP-MS was coupled to a laser ablation system consisting of a Geolas (Microlas) automated platform with a 193 nm Excimer Compex 102 laser from LambdaPhysik. Ablation analyses were performed using an in-house modified 30 cm^3 ablation cell with a helium atmosphere to enhance sensitivity and reduce inter-element fractionation (Günther and Heinrich, 1999). Helium gas and ablated sample material were mixed with argon gas before entering the plasma. The laser energy density was set to 12 J cm^{-2} at a frequency of 8 Hz and the beam size was set to 102 μm. Data were collected in time resolved acquisition mode, with the background signal collected for 2 min followed by 1 min of sample ablation.

Data were reduced with the GLITTER software package (Van Achterberg et al., 2001), using the linear fit to ratio method. Data were filtered for spikes on an element by element basis. Internal standardization relative to EPMA data was done using ^{29}Si for all minerals. Detection limits were <1 ppb for most highly incompatible elements except for Ba, Zr and Sr (<2 ppb); they were <15 ppb for Sb, V, Cu, Zn, Co, Sc, Li and B and <200 ppb for Mn, Ti and Ni (Supplementary Table 1). Values that were within 1σ of the detection limit were excluded during data reduction. Data reported in Tables 1, 2, 3 are single-spot analyses, whereas averages of trace element compositions in olivine for each sample (data in Figures 6 and 7) are reported in Supplementary Table 2). Supplementary Table 3 reports 1σ error values of olivine analyses reported in Table 1. A typical time series for the analysis of trace elements in olivine is reported in the Supplementary Note 1. Instrument sensitivity due to analytical conditions was determined from the average across all days of repeat measurements of the synthetic NIST 612 glass (Pearce et al., 1997). Sensitivities were 800 cps/ppm for Ni, 2000-4000 cps/ppm for Ti, B and Zn, 6000-15000 cps/ppm for Li, Cu, Sb, Ba, Nd, Sm, Gd, Dy, Yb and Pb and >20000 cps/ppm for all other elements. Precision and accuracy were constrained by 8 analyses of reference basalt BIR 1-G (Supplementary Table 1): reproducibility was better than 5% for most elements except for Pb (16%), B and Ta (<10%) and measured values were comparable within analytical uncertainties to GEOREM accepted values (Jochum et al., 2005).

4. MAJOR AND TRACE ELEMENT MINERAL CHEMISTRY

Major and trace element compositions of olivine, plagioclase, clinopyroxene and orthopyroxene are shown in Tables 1, 2, 3. In most analysed olivines, we observed acceptable correlations between the Ni, Mn and Ca abundances analysed by EPMA and LA-ICPMS (see Supplementary Figure 1). Overall, the major and trace element chemistry data that are reported here

for clinopyroxene and plagioclase in samples MF22, MF40, MF21, MF51 are similar to previously published datasets (Borghini et al., 2007).

4.1. Peridotites

Olivines in peridotites have forsterite contents ranging Fo_{89}-Fo_{90}. They display the highest Ni (2570-2725 ppm) coupled to the lowest Mn (1170-1210 ppm), Zn (56-61 ppm), Hf, Ti and Li abundances, of all investigated (peridotite-troctolite-gabbro) samples (Figs. 4, 5, 6). REE patterns define regular trends for the H- (heavy) REE, but tend to be more disperse for the M- (middle) and especially the L- (light) REE (Fig.7). They show strong MREE/HREE fractionation (Tb_N/Yb_N = 0.004-0.042, normalized to C1-chondrite of Sun and McDonough, 1989), more pronounced than in the majority of available literature data on trace element chemistry of mantle olivines in orogenic massifs and xenoliths (see compositional field and references reported in Figure 7). However, published data mostly refer to metasomatized peridotites, as indicated by their enrichment in LREE and other highly incompatible elements (see fields in Figures 7c, 8c). Note also that all previous data are bulk analyses of olivine separates, thus possibly incorporating trace elements hosted in inclusions. On the other hand, D'Errico et al., 2015 recently documented similar MREE/HREE fractionation in olivine from Gakkel Ridge peridotites (see the compositional field in Figures 7c, 8c).

Plagioclase in peridotites is fully replaced by low-grade alteration products. Clinopyroxenes are partly dissolved and replaced by (orthopyroxene + plagioclase) intergrowths crystallized from the infiltrating melts. Their major and trace element compositions (Figs. 7,8 and Table 3) are consistent with previously published data (Borghini et al., 2007). Melt-rock interaction has modified their trace element composition (Borghini et al., 2007), causing an overall REE increase (M- to H-REE up to > 10xC1, see Fig. 7a), coupled to Zr, Y, Sc, V enrichment and strong Sr depletion (see Fig. 8a), compared to clinopyroxenes in those Erro-Tobbio spinel peridotites that represent the mantle protolith before melt impregnation (Rampone et al., 2004; 2005). Similar changes in clinopyroxene composition have been largely documented in plagioclase-rich impregnated peridotites of the Alpine–Apennine system (Rampone et al., 1997, 2008; Piccardo et al., 2004; Zanetti et al., 2007). They are interpreted as resulting from the combined effects of equilibration with enriched melts modified during reactive percolation at decreasing melt mass, and crystallization of small trapped melt fractions. In spite of the overall REE increase, clinopyroxenes preserve marked LREE depletion (La_N/Yb_N = 0.008-0.016), more pronounced than in clinopyroxenes from troctolites and gabbros (see Figure 7a). On this basis, Borghini et al. (2007) and Rampone and Borghini (2008) inferred that melt impregnation in the Erro-Tobbio peridotites

was caused by reactive porous flow of orthopyroxene-saturated depleted MORB-type melts, unrelated to subsequent intrusion of N-MORB-type magmas.

The analyzed orthopyroxenes represent melt-rock reaction products, crystallized together with plagioclase and replacing mantle clinopyroxene (see description above). They display low REE abundances (M-, H-REE below 2-3x C1, Fig. 7a), significant LREE/HREE fractionation (Ce_N/Yb_N = 0.003-0.005), and negative Sr and Eu anomalies coupled to Zr and Hf enrichment relative to the neighbouring REE (Fig. 8a).

4.2. Troctolites and Gabbro

Olivines from troctolites have high forsterite contents (Fo_{88}-Fo_{89}). The lowest forsterite values (Fo_{88}) are observed in samples with variable (granular and harrisitic) texture. They also display relatively high Ni (2050-2280 ppm), Mn (1010-1625 ppm) and moderate Zn (45-70 ppm) contents (see Fig. 4,5). The Co abundances are more scattered, and similar to those of olivines in peridotites. Troctolite olivines display a negative correlation between Mg# (Mg/(Mg+Fe)) and Mn content (Fig. 4b), with the lowest Mg# and highest Mn values observed in the composite granular-harrisitic samples. As expected, olivines in gabbro MF22 have the lowest forsterite contents (Fo_{83}-Fo_{84}), combined with the lowest Ni (1355-1415 ppm) and higher Mn (1890-1970 ppm), Zn (93-102 ppm) and Co (165-170 ppm) abundances. For all these elements (i.e. Mn, Zn, Co, Ni), troctolite olivines show intermediate concentrations compared to those of olivines in peridotites and gabbro. In contrast, their Hf, Ti and Zr concentrations are more variable (progressive enrichment), and extend beyond those of olivines in the gabbro (Figs. 6,7). Li abundances show the same behaviour, although the data are slightly more scattered (see Fig. 6d). Olivines in troctolites also exhibit the highest REE contents (HREE up to 0.8-1xC1, Fig. 7c), coupled to strong MREE/HREE fractionation (Tb_N/Yb_N = 0.004-0.042) and development of significant positive Zr-Hf anomalies relative to the neighbouring REE (Fig. 8c). Drouin et al. (2009) documented similar REE compositions in olivine from Mid Atlantic Ridge (MAR) olivine-rich troctolites (see the grey field in Fig. 8c).

Plagioclases in the studied troctolites and gabbro have similar anorthite contents (An_{58-63} in troctolites, An_{62} in gabbro, see Table 2). In the troctolites, the lowest anorthite values (An_{58-59}) are observed in composite granular-harrisite samples. Overall, plagioclases display LREE-enriched REE patterns (La_N/Sm_N = 1.23-2.56, Fig. 7a), positive Sr and Eu anomalies, and strong negative Zr-Hf anomalies relative to the neighbouring REE (Fig. 8b). In gabbro MF22, plagioclases exhibit the lowest REE abundances (LREE < 1 x C1), whereas in troctolites they show a larger LREE variability, with LREE up to 4xC1 in plagioclases of composite granular-harrisite troctolites (Fig.

7a). Similar REE compositions were documented by Borghini et al. (2007) (see the grey field in Fig. 7b).

The major and trace element compositions of clinopyroxenes reported in Table 3 were measured in cores of large crystals. For the purpose of this study, we did not consider within-crystal major-trace element variations related to late-stage crystallization of interstitial trapped melts. The reader can refer to Borghini and Rampone (2007) for this specific issue. Troctolite clinopyroxenes have high Mg# (0.89-0.90) coupled to relatively Al_2O_3 (3.04-4.82 wt%), Na_2O (0.43-0.61 wt%) and Cr_2O_3 (1.02-1.50 wt%) concentrations (Table 3), similar to those of clinopyroxenes from oceanic and ophiolitic troctolites (Drouin et al., 2009; Sanfilippo and Tribuzio, 2012). Lower Mg# (0.86) and Al_2O_3, Cr_2O_3 contents are found in clinopyroxenes of gabbro MF22. Overall, clinopyroxenes display moderate LREE depletion (La_N/Sm_N = 0.11-0.14 in troctolites and gabbro) and almost flat MREE to HREE patterns. As described above for plagioclase, gabbro clinopyroxenes have the lowest REE abundances (M-H-REE below 10 x C1, Fig.7a), whereas troctolite clinopyroxenes exhibit a general REE increase (M-H-REE up to 20 x C1) at nearly constant LREE fractionation (Fig. 7a). The REE increase is coupled to the development of negative Eu and Sr anomalies relative to neighbouring REE (Fig. 8a).

5. DISCUSSION

5.1. Mineral/mineral REE partitioning

A number of studies have shown that the distribution of trace elements between olivine, orthopyroxene and clinopyroxene depends on temperature, pressure and mineral compositions (e.g. Witt-Eickschen et al., 2005; Lee et al., 2007; Sun and Liang, 2012, 2013, 2014). For REE, the effect of decreasing temperature is to redistribute these elements into clinopyroxene, thus lowering the olivine/clinopyroxene and orthopyroxene/clinopyroxene partition coefficients. Also, this effect is stronger for the LREE relative to the HREE, possibly resulting in significant changes of the LREE/HREE fractionation in low-T (< 1000 °C) re-equilibrated minerals (Sun and Liang, 2014).

Lee et al. (2007) predicted Ol/Cpx and Opx/Cpx REE partition coefficients at variable temperatures based on lattice strain theory. Sun and Liang (2014) developed parameterized lattice strain models for REE and Y distribution among mantle minerals in a wide range of T conditions (800-1300°C), using mineral/melt partitioning models calibrated against experimentally determined mineral/melt partition coefficients (Sun and Liang, 2012, 2013). In order to test the distribution of REE between olivine, clinopyroxene and orthopyroxene in the Erro-Tobbio peridotites, troctolites and gabbro, and derive information about equilibration temperatures, we computed Ol/Cpx and Opx/Cpx REE partition coefficients in our samples, and compared them with i) predicted trends by Lee et al. (2007) (Fig. 9), ii) computed olivine/cpx trends, according to Sun and Liang (2012, 2013,

2014) modeling. This approach allows to calculate Ol/Cpx partition coefficients at varying T for a specific sample, using proper major element mineral compositions (Fig. 10; see figure caption for more details). The two sets of modelled temperature contours, shown in Figures 9 and 10, are similar, with a modest shift at higher Ol/Cpx partitioning values, at a given T, of trends computed according to Sun and Liang (2014) (see Figs. 9a and 10).

In all samples, Ol/Cpx partition coefficients regularly decrease from Lu to Dy, whereas they tend to define concave trends from MREE to LREE (Figs. 9a, 10). Similar "U-shaped" Ol/Cpx partitioning was already documented in previous studies (e.g. Agranier and Lee, 2007; Lee et al., 2007) and was ascribed to the difficulty to get accurate analyses of LREE in olivine, due to the extremely low concentrations in these elements, and/or to the occurrence of LREE-bearing fluid inclusions. However, it is remarkable that the Ol/Cpx partition coefficients for Gd, Eu and Nd in most samples are consistent with predicted trends (see Figs. 9a and 10), pointing to the reliability of our olivine data set for the majority of REE. Overall, the Ol/Cpx H- to M-REE distribution in most investigated samples defines arrays that are slightly steeper than computed trends. As already outlined in the results section, this is likely a consequence of the strong MREE/HREE fractionation shown by olivines in this study, more pronounced than the large majority of published data. Except for Dy and Tb, most Ol/Cpx partitioning data for the HREE indicate rather high equilibration temperatures (> 1100 °C). The highest values are observed in the troctolites, relative to peridotites and gabbro, and are probably related to the high HREE concentrations in olivines of troctolites resulting from melt/rock reaction processes (see the discussion below)

In Figure 9b, we also show the Opx/Cpx REE distribution coefficients for the two peridotite samples, compared with modelled trends by Lee et al. (2007). They define almost linear arrays, monotonically decreasing from HREE to LREE. Remarkably, these trends are mostly consistent with predicted Opx/Cpx partitioning at high temperature (> 1300 °C). In these samples, high-T estimates (1350-1400 °C) were also obtained by the REE in two-pyroxene thermometer of Liang et al (2013).

In summary, mineral/mineral REE partitioning in the Erro-Tobbio samples are mostly indicative of high temperature of equilibration (> 1100-1200 °C). Accordingly, we infer that the REE concentrations in olivine, clinopyroxene and orthopyroxene were not significantly modified by subsolidus re-equilibration, hence potentially recording information about the chemical signature of equilibrium melts. Nevertheless, the possible effect of decreasing temperature on olivine/clinopyroxene REE re-distribution is further discussed in the following section.

5.2. Paradoxical chemical signatures in olivine

The comparison of olivine compositions in the three investigated rock types, peridotite, troctolite and gabbro reveals both expected and unexpected behaviour for trace elements.

Remarkably, olivines in the three rock types exhibit distinct geochemical signature and define systematic elemental correlations for a series of minor (Ni, Mn) and trace elements (Zn, Co, Ti, Zr, Hf , HREE). Similar correlations (at least for Ni, Mn, Ti, Zr, Yb) have been documented by Sanfilippo et al. (2013) in a study of troctolites and mantle peridotites from the Alpine ophiolites (see data reported in Figs. 4,5,6). These data provide the evidence that olivine, although being a very minor reservoir for many trace elements, can record magmatic processes.

As expected, highly compatible elements in olivine such as Ni (Lee et al., 2007; Spandler et al., 2010, and references therein) show the highest contents in peridotite, intermediate in troctolite and lowest in gabbro, whereas Mn, Zn and Co show the opposite behaviour. Data on the partitioning of Mn, Zn and Co in olivine (Ehlers et al., 1992; Kennedy et al., 1993; Beattie, 1994; Gaetani and Grove, 1997; Kohn and Schofield, 1994; Bedard, 2005; Mysen, 2007; Spandler and O'Neill, 2010) indicate a moderately incompatible to compatible behaviour. De Hoog et al. (2010), in a comprehensive study of the trace element composition of mantle olivines from different origins and settings, found negative correlations between Mn, Zn abundances and forsterite contents, thus confirming their moderately incompatible behaviour. They also documented little systematic variation of Co with forsterite values, indicative of a $K_D^{ol/melt}$ very close to 1. In our study, the overall increase of Mn, Zn and Co abundances in olivines from mantle peridotites to gabbro further demonstrate a moderately incompatible behaviour of these elements. Moreover, in the Mg# versus Ni diagram of Figure 4a, the compositional array defined by the Erro-Tobbio peridotite-troctolite-gabbro olivines is roughly consistent with computed trends for fractional crystallization at low pressure (< 5 Kb) of a primary MORB melt (e.g. Drouin et al., 2009; grey lines in Fig. 4a). In addition, Mn and Ni abundances of troctolite olivines fall within the compositional field defined by MORB phenocrysts (see Figs. 4a,b; data from Sobolev et al., 2007). These features are in agreement with previous inference by Borghini et al. (2007) that troctolites and gabbros reflect crystallization products of variably evolved MORB magmas.

Zr, Hf, Ti and HREE display unforeseen behaviours. The concentrations of these elements in troctolite olivines define enrichment trends that start from abundances similar to those in gabbro olivines, and go up to one order of magnitude higher values (Fig. 6). These elements are all highly incompatible in olivine (Lee et al., 2007; Spandler and O'Neill, 2010; De Hoog et al., 2010; and references therein). If the composition of olivine in troctolites and gabbros were simply reflecting fractionation from a variably evolved melt, we would expect the highest contents in incompatible elements in the gabbro olivines. Moreover, the HREE enrichment in troctolite olivine is coupled to the development of pronounced Zr-Hf positive anomalies and Zr/Nd fractionation (Zr_N/Nd_N up to

100). The same selective Zr-Hf enrichment was described in olivines from oceanic troctolites by Drouin et al. (2009). All these features indicate that the behaviour of these elements in the studied olivine data set does not conform to a simple magmatic crystallization process, and melt/rock reaction processes likely have occurred (see the discussion section below).

Another unexpected chemical characteristic in olivine is its ubiquitous (even in the gabbro) depleted REE composition (Fig. 7c). Similar REE patterns were documented by Drouin et al. (2009) in olivines from oceanic troctolites. These authors observed that computed melts in equilibrium with such olivines are significantly more depleted than melts in equilibrium with associated plagioclase and clinopyroxene. Hence, they proposed that the trace element depleted signature of olivine in the troctolites could reflect a mantle origin, whereas plagioclase and clinopyroxene crystallized from impregnating MORB-type melts.

The REE composition of melts computed in equilibrium with olivine, clinopyroxene, orthopyroxene and plagioclase from the Erro-Tobbio peridotites, troctolites and gabbro are shown in Figure 11. Following Drouin et al. (2009), melts were computed using clinopyroxene/liquid, orthopyroxene/liquid, and olivine/liquid partition coefficients from Lee et al. (2007), and plagioclase/liquid partition coefficients from Aigner-Torres et al. (2007). As previously documented by Drouin et al. (2009), computed melts in equilibrium with olivine in all investigated lithotypes exhibit lower REE abundances than melts in equilibrium with clinopyroxene. An exception to this behaviour is provided by Yb, which shows similar values in most computed melts (Fig. 11a,b,c). In troctolites, melts in equilibrium with plagioclase and clinopyroxenes display large variation in absolute REE contents, related to late-stage crystallization of interstitial melts (Borghini and Rampone, 2007). In spite of such variation, computed melts exhibit similar composition, with nearly flat REE patterns, indicative of a MORB affinity (Borghini et al., 2007). In contrast, melts in equilibrium with olivine display strong MREE/HREE fractionation (Dy_N/Yb_N = 0.17-0.39). Although such decoupling in the troctolites could reflect a different origin between olivine (possibly mantle derived) and associated plagioclase/clinopyroxene, this can be ruled out in gabbro MF22 (Fig. 11c), for which microstructural and major-minor element chemical features of olivine (and field relations) clearly indicate a magmatic origin.

In order to test whether the adopted partition coefficients could have a role in generating such contrasting signature, we also calculated the equilibrium melts using the following sets of partition coefficients: i) the compilation proposed in Bedard (2001), derived on the basis of empirical relationships between ln(Kd) and composition, and adopted by Lissenberg et al. (2013) to model reactive melt migration in the lower oceanic crust of Hess Deep (EPR), ii) the olivine/melt and clinopyroxene/melt partition coefficients computed for our samples at T = 1200 °C, according to Sun and Liang (2012, 2013) mineral/melt REE partitioning models. The resulting REE

compositions of equilibrium melts are reported in Figures 12 and 13. In spite of differences in absolute concentrations, we observed the same decoupling between the M-H-REE composition of melts in equilibrium with plagioclase and clinopyroxene, and those in equilibrium with olivine, the latter being even more fractionated (Dy_N/Yb_N = 0.043-0.098) when using the Bedard (2001) Kds. Finally, in order to check whether the observed decoupling of equilibrium melts compositions could be related to subsolidus redistribution of REE between olivine and clinopyroxene at lower temperature, we computed apparent melt compositions using the Kds sets obtained at 1100°C, by using Sun and Liang (2012,2013) models. The results are shown in Supplementary Figure 2. Again, the major effect is a difference in absolute concentrations, with a general shift at lower REE contents of computed melts in equilibrium with clinopyroxene, and higher REE abundances of computed melts in equilibrium with olivine. On the other hand, the decoupling of M-H-REE composition in clinopyroxene and olivine equilibrium melts largely persists, although the latter are slightly less fractionated (Dy_N/Yb_N = 0.13-0.29 at 1200°C, and 0.15-0.34 at 1100 °C). Therefore, re-distribution of REE between olivine and other minerals at subsolidus conditions is not sufficient to explain the observed decoupling.

A robust explanation of such chemical discrepancies between melts computed in equilibrium with olivine and those in equilibrium with all other minerals is presently lacking, and possibly lies in the inhibited incorporation of REE into the olivine crystal lattice, due to their high ionic radius relative to the M1 and M2 sites dimensions (Zanetti et al., 2004; Foley et al., 2013). This, in turn, can explain the uncertainties and variability of available partition and diffusion coefficients for REE and other highly incompatible elements in olivine.

Available experimental studies on the diffusion of trace elements in olivine have provided contrasting results. Spandler et al. (2007) and Spandler and O'Neill (2010) documented fast re-equilibration of REE in olivine, at rates similar to Mg-Fe exchange. By contrast, Cherniak (2010) and Remmert et al. (2008) found much lower (more than three order of magnitude) REE diffusion coefficients. They showed that REE diffusion in olivine is faster than in orthopyroxene and clinopyroxene, but slow enough to preserve REE heterogeneities in melt inclusions in olivine phenocrysts, at time scales of geologic processes. Cherniak (2010) also documented similar diffusivities for M- and H-REE (La, Dy, Yb), indicating no correlation between REE diffusion coefficients and ionic radius (consistent with Spandler and O'Neill, 2010), and little dependence of REE diffusion rates on crystallographic orientation. This behaviour differs from the pronounced anisotropy (more rapid diffusion parallel to *c* axis) documented for Fe-Mg and many trace elements (e.g. Ni, Cr, Zr, Hf) in olivine (Chakraborty, 1997; Petry et al., 2004; Ito and Ganguly, 2006; Spandler and O'Neill, 2010; Jollands et al., 2014).

More recently, Burgess and Cooper (2013) explained the discrepancies between the results of Cherniak (2010) and Spandler and O'Neill (2010) as a consequence of different diffusion mechanisms acting in olivine, with "lattice diffusion" in the former, and "fast-path diffusion" promoted by formation of extended defects, in the latter. Specifically, Burgess and Cooper (2013), in a combined experimental-TEM study on olivine in equilibrium with a TiO_2-rich MORB (similar to that used by Spandler and O'Neill, 2010), showed that the nucleation and growth of planar defects in olivine is enhanced by large TiO_2 chemical potential gradients at the olivine-melt boundary (leading to substitution of Ti^{4+} for divalent cations in the olivine octahedral site, and formation of octahedral vacancies). These authors outlined the need for a re-evaluation of the "simple" lattice diffusion mechanism, especially in the case of natural reacting systems governed by significant chemical potential gradients (e.g. metasomatism or magma mixing), and the importance of detailed analysis of natural and experimental samples for a better understanding of trace element diffusion in olivine.

In spite of such contrasting results, all studies provide consistent evidence of similar diffusion coefficients in olivine from HREE to LREE. Therefore, the ubiquitous strong MREE/HREE fractionation observed in all the analysed olivines cannot be easily related to modifications of the REE profile acquired by subsolidus diffusion and re-equilibration, as a consequence of different M- to H-REE diffusion rates. On the other hand, the large variation of available partition coefficients for REE (one to two orders of magnitude, especially for the LREE and MREE; see Bedard, 2001; Lee et al., 2007; Spandler and O'Neill, 2010) indicates the difficulty to get reliable values, and sheds light on the caution that is needed in using olivine REE contents to derive information about the compositions of equilibrum melts. The main factors influencing the REE partitioning between olivine and melt have been discussed in a series of papers. Bedard (2005) examined published natural and experimental $^{olivine/liquid}D$, and found a general tendency to increase with decreasing temperature and MgO content in the melt. Evans et al. (2008), in an experimental study in the CMAS system, documented strong inverse correlation between olivine-melt partition coefficients and SiO_2 contents in melt. Finally, Sun and Liang (2013), through the development of parameterized lattice strain models, found that the primary variables determining the REE and Y partitioning between olivine and melt are pressure, Forsterite and Al contents in olivine.

Overall, the results of our study further emphasize the need of enlarging the trace element olivine data set in natural mantle and gabbroic samples, as well as the importance of parallel experimental work. Based on present knowledge, the REE composition of olivine cannot be easily adopted to discriminate between mantle versus magmatic origin. Nevertheless, the peculiar and systematic trace element signature documented in olivine of troctolites points to a more complex origin than a simple fractional crystallization.

5.3. Evidence of melt/rock reaction in troctolites

The studied troctolites show microstructural and chemical evidence of mineral/melt reaction and disequilibrium. In most samples, olivine displays irregular and lobate contacts against interstitial minerals (plagioclase and subordinate clinopyroxene) indicative of reactive dissolution and resorbtion. Reactive dissolution of olivine is even more evident in coarse-grained harrisitic troctolites (e.g. sample MF72Ha), where centimetre-size hopper olivine crystals are significantly corroded by plagioclase crystallization (Fig. 3c). Similar granular to hopper to harrisitic textures in olivine are described in the literature in layered intrusions and ophiolites (e.g. Donaldson et al., 1982; O'Driscoll et al., 2007; Renna and Tribuzio, 2011), and are considered to result from open-system processes causing variations in melt composition and, consequently, in the degree of undercooling (e.g. Faure et al., 2003). Moreover, in the troctolite apophysis MF51 olivine occurs both as euhedral crystals and as large and irregular kinked grains, partly resorbed by plagioclase (Fig. 3b). All these features point to disequilibrium and reaction between the olivine framework (at least part of it) and the melt that crystallized the interstitial minerals.

Specific chemical characteristics also provide the same information. As outlined by Borghini et al. (2007), the overall major element compositions of minerals in Erro-Tobbio troctolites and gabbros define a variational trend at rather low An contents in plagioclase at given Fo in olivine and Mg# of clinopyroxene, as observed in some gabbroic rock suites from the Mid-Atlantic Ridge (e.g. Ross and Elton, 1997). Troctolites, specifically, display variable An contents in plagioclase at rather constant Fo value in olivine. The new troctolite samples analysed in this study with granular to harrisitic textures further confirm the lack of Fo-An correlation in the troctolites, being characterized by very low An values in plagioclase (An_{58-59}) at high Fo contents in olivine ($Fo_{87.5-88.5}$) and high Mg# in clinopyroxene (100*Mg# = 88-89.8)(see Tables 1,2,3). Although part of such chemical features, namely the low An contents in plagioclase and high Mg# in clinopyroxene, can be ascribed to crystallization at moderate P conditions (3-5 kbar, see Borghini et al., 2007), the large compositional range defined by plagioclase in the troctolites (An_{58-66}; Borghini et al 2007 and this study) at rather constant olivine composition rules out a simple process of fractional crystallization. This in turn calls for melt-rock reaction processes, in which exotic input of more evolved melts in a previously crystallized olivine framework, and/or crystallization of intercumulus liquid evolving upon cooling and partially trapped within the crystal mush, could have played a role.

Both textural and mineral chemistry features in the Erro-Tobbio troctolites thus point to melt-rock reaction involving olivine dissolution and concomitant plagioclase crystallization. In order to test, with a simple but effective approach, whether the observed trace element variations

and geochemical signature in olivine of troctolites, namely the selective HFSE (Zr, Hf, Ti) and HREE enrichment, can be explained by such process, we performed an Assimilation Fractional Crystallization (AFC) model (using the equation of De Paolo, 1981), assuming the following reaction:

$$\text{olivine}_1 + \text{melt}_1 = \text{olivine}_2 + \text{plagioclase} + \text{melt}_2,$$

in which "olivine$_2$" represents the olivine reequilibrated with the reacted melt$_2$. For clarity, we emphasize that in this study we were not able to distinguish two olivine generations in a specific troctolite sample, both in terms of textural occurrence and chemical composition. We often observed corroded olivine grains that texturally represent the "olivine$_1$" of the above reaction, but possess geochemical characteristics of "olivine$_2$". We further discuss this point below.

The results of AFC modeling are shown in Figure 14, in terms of Zr_N/Nd_N versus Yb_N in olivine computed in equilibrium with the reacted melt$_2$ (i.e. olivine$_2$). A major difficulty in performing geochemical modeling is the choice of appropriate mineral/liquid partition coefficients. This is especially crucial in the case of olivine and plagioclase, for which complete $^{\text{mineral/liquid}}D$ sets including REE and HFSE are poorly available in literature (see discussion above). We thus performed two distinct AFC models (Models A and B of Fig.14a,b), keeping fixed all the parameters except the partition coefficients, in order to highlight the variability of computed trends resulting from the choice of D values. In both models, the assimilated mass (Ma) is equal to 100% olivine, whereas the crystallized mass (Mc) is 100% plagioclase. The composition of the starting melt (C_0, reacting with olivine$_1$) is equal to the melt computed in equilibrium with the troctolite clinopyroxene showing the lowest REE concentrations (i.e. clinopyroxene in sample MF21; see Figs. 7a, 8a). This melt is very similar (at least for the L- and M- REE) to the composition of melt computed in equilibrium with troctolite plagioclase with the lowest REE abundances (i.e. plagioclase in sample MF51, see Figs. 7b, 8b), and we considered it as the best proxy of the composition of the interstitial melt before reactive crystallization. For the assimilated olivine, we used the composition of olivine in peridotite MF40, showing the lowest Yb and HFSE concentrations among all the investigated data set. It is remarkable, however, that olivine in gabbro MF22 also show low Zr_N/Nd_N fractionation and REE (see Figs. 7c, 8c), being likely less affected by melt-rock reaction processes than the troctolites. As clearly shown in Figure 14, the two (peridotite and gabbro) olivine compositions almost overlap. Therefore, using the gabbro olivine as Ma would have produced the same results discussed below.

Computed trends reported in Figure 14 show the compositions of olivine in equilibrium with residual liquids (melt$_2$) at decreasing melt mass (F = 0.95-0.10). The four different trends refer to different values of r (where r is equal to the Ma/Mc ratio). The models A and B (Fig. 14a,b) differ only in terms of adopted partition coefficients (see figure caption for details and references).

Keeping in mind the uncertainties resulting from the adopted parameters (partition coefficients, composition of initial melt C_0 and assimilated olivine Ma), and the very simplified approach, the model clearly suggests that the observed enrichment in Zr in olivine of the troctolites can be explained by a melt-rock reaction process involving dissolution of olivine and crystallization of plagioclase (in almost equal amounts, best consistency with Ma/Mc = 0.95) at progressively decreasing melt mass. This is due to the fact that olivine has higher $^{mineral/liquid}D_{Zr,Hf}$ relative to plagioclase, consistent with the significant Zr-Hf negative anomalies in plagioclase compositions, especially in plagioclase of gabbro MF22 (see Fig. 8b). This behaviour of olivine, i.e. $^{olivine/liquid}D_{HFSE} > {}^{olivine/liquid}D_{REE}$, has been invoked by Kelemen et al. (1990) to explain the development of arc-like signature in basaltic melt during reactive percolation through the lithospheric mantle, and it has been confirmed by the study of Bedard (2005), who highlighted the ubiquitous presence of positive $D_{Ti,Zr,Hf}$ anomalies in experimental olivine/melt partitioning data for a wide range of basaltic compositions.

As mentioned above, there is an apparent decoupling between the reaction considered in the AFC model, and our textural and geochemical observations. The reaction involves an $olivine_1$, likely possessing a higher forsterite content and low incompatible trace element abundances, and an $olivine_2$, supposed to crystallized from the reacted melt. However, in our study troctolite olivines which are significantly resorbed by plagioclase (i.e. texturally representing $olivine_1$), have enriched trace element signature, i.e. that expected for $olivine_2$. This could be explained assuming that $olivine_1$ has reset its composition, by interaction with the melt, rather than crystallizing in new grains.

In this study, we aimed to provide a first trace element data set in olivine from associated peridotite, troctolite and gabbro samples, in order to document major geochemical differences, if any, between the different rock types, and test the potential of trace element chemistry in olivine to track melt-rock reaction processes. Therefore, we did not focus the analytical work to detect within-grain elemental variations. The results of this study clearly indicate that the troctolites hold a more complex magmatic history than previously documented (Borghini et al., 2007; Borghini and Rampone, 2007). Borghini and Rampone (2007) found significant trace element zoning in poikilitic clinopyroxenes, correlated with the microstructural site (e.g. core to rims of large crystals, to very thin interstitial grains). They ascribed this feature to late-stage crystallization of interstitial trapped melts, and assumed olivine dissolution to explain the development of positive Zr, Hf anomalies in the very late-stage clinopyroxene. Here we show that olivine records the geochemical signature of such melt-mineral reaction. Detailed microstructural and geochemical investigations, involving Crystallographic Preferred Orientation (CPO) analyses (e.g. Drouin et al., 2010) combined to major-trace element traverses and mapping in selected olivine grains, will be essential to check the

existence of different generations of olivine within a single troctolite sample, and the preservation (or absence) of major, trace element zoning in a specific olivine crystal.

Records of compositional zoning in minerals largely depend on element diffusion rates, temperature conditions of crystallization and cooling rates. Major and minor element variations in olivine, such as decrease in NiO, Mg# and increase in TiO_2, have been documented in experiments of formation of plagioclase-bearing peridotites and wehrlites by reactive crystallization, and ascribed to the effects of dissolution and reprecipitation from the basaltic melt (Saper and Liang, 2014). Moreover, Welsch et al. (2014) recently documented surprising dendritic zoning of phosphorous in volcanic, experimental, and also plutonic olivine crystals (by electron probe microanalysis and mapping), and Burgess and Cooper (2013) shed lights on the diffusion mechanisms in olivine by combined experimental and TEM investigations. Overall, these works illustrate the usefulness of micro- and nano-scale detailed studies to get insights on combined processes of olivine deformation, dissolution and growth. Textural and geochemical variability documented in this study in troctolite olivines further confirms the relevance of such approaches.

6. CONCLUDING REMARKS

In-situ LA-ICP-MS analyses of a large set of trace elements in olivines of depleted mantle peridotites and associated primitive gabbroic rocks (troctolites and olivine gabbros) from the Ligurian ophiolites (Erro-Tobbio Unit, Italy) have revealed that olivines define systematic and reliable compositional trends that can be used to unravel their history of melt-rock reaction and magmatic crystallization.

In contrast with olivine gabbros, olivines in the troctolites display significant enrichment in incompatible elements like Zr, Hf, Ti, HREE, coupled to development of significant HFSE/REE fractionation. Such geochemical features are indicative of dissolution-precipitation processes and re-equilibration with reacted enriched melts. AFC modeling shows that the large Zr_N/Nd_N ratios in olivines of troctolites are consistent with a process of olivine assimilation and plagioclase crystallization at decreasing melt mass, in agreement with textural observations. Detailed in-situ trace element geochemistry of olivine, possibly combined with focused microstructural analysis, thus appears to be a powerful tool to investigate reactive percolation and the origin of olivine-rich rocks in the lower oceanic crust.

Compositional contrasts between computed melts in equilibrium with olivine and coexisting minerals, in both mantle peridotites and MORB-type gabbroic rocks, point to the need for a better understanding of the mechanisms of incorporation and diffusion of trace elements in olivine.

ACKNOWLEDGEMENTS

We thank Andrea Risplendente (Dipartimento di Scienze della Terra, University of Milano) for his assistance with the EPMA analyses, and Carlotta Ferrando (PhD student in Montpellier) who performed part of the LA-ICP-MS analyses. J.C.M de Hoog and C. Sun are greatly acknowledged for their constructive reviews. We also thank editorial advise and handling by W. van Westrenen and M. Norman. This study was supported by the University of Genova (grant PRA 2014), and the CNRS-INSU program SYSTER.

REFERENCES

Agranier A. and Lee C.-T.A. (2007) Quantifying trace element disequilibria in mantle xenoliths and abyssal peridotites. Earth Planet. Sci. Lett. 257, 290–298.

Aigner-Torres M., Blundy J., Ulmer P. and Pettke T. (2007) Laser Ablation ICPMS study of trace element partitioning between plagioclase and basaltic melts: an experimental approach. *Contrib. Mineral. Petrol.* **153**, 647–667.

Beattie P. (1994) Systematics and energetics of trace-element partitioning between olivine and silicate melts: implications for the nature of mineral/melt partitioning. *Chem Geol* **117**, 57–71.

Bédard J. (2001) Parental magmas of the Nain Plutonic Suite anorthosites and mafic cumulates: a trace element modelling approach. *Contrib. Mineral. Petrol.* **141**, 747–771.

Bédard J. (2005) Partitioning coefficients between olivine and silicate melts. *Lithos* **83**, 394–419.

Bédard J.H., Hebert R., Berclaz A. and Varfalvy V. (2000) Synthesis and the genesis of lower oceanic crust. *Geol. Soc. Am.* **349**, 105–119.

Bedini R.-M. and Bodinier J.-L. (1999) Distribution of incompatible trace elements between the constituents of spinel peridotite xenoliths: ICP-MS data from the East African Rift. *Geochim. Cosmochim. Acta* **63**, 3883–3900.

Bezzi A. and Piccardo G.B. (1971) Structural features of the Ligurian ophiolites: petrologic evidence for the 'oceanic' floor of the Northern Apennine geosyncline: a contribution to the alpine-type gabbro–peridotite associations. *Mem. Soc. Geol. It.* **10**, 55–63.

Borghini G. and Rampone E. (2007) Postcumulus processes in oceanic-type olivine-rich cumulates: the role of trapped melt crystallization versus melt-rock interaction. *Contrib. Mineral. Petrol.* **154**, 619–633.

Borghini G., Rampone E., Crispini L., De Ferrari R. and Godard M. (2007) Origin and emplacement of ultramafic-mafic intrusions in the Erro-Tobbio mantle peridotites (Ligurian Alps, Italy). *Lithos* **94**,210–229.

Borsi L., Scharer U., Gaggero L. and Crispini L. (1996) Age, origin and geodynamic significance of plagiogranites in lherzolites and gabbros of the Piedmont–Ligurian ocean basin. *Earth Planet. Sci. Lett.* **140**, 227–241.

Brady J.B. and Cherniak D.J. (2010) Diffusion in minerals: An overview of published experimental diffusion data. In: *Reviews in Mineralogy & Geochemistry*, Mineralogical Society of America **72**, 899–920.

Burgess K.D. and Cooper R.F. (2013) Extended planar defects and the rapid incorporation of Ti4+ into olivine. *Contrib. Mineral. Petrol.* **166**, 122–1233.

Cannat M., Bideau D. and Hebert R. (1990) Plastic deformation and magmatic impregnation in serpentinized ultramafic rocks from the Garrett transform fault (East Pacific Rise). *Earth Planet. Sci. Lett.* **101**, 216–232.

Capponi G., Crispini L., Silvestri R. and Vigo E. (1999). The role of Early Miocene thrust tectonics in the structural arrangement of the Voltri Group (Ligurian Alps, Italy): evidence of Bandita area. *Ofioliti* **24**, 13–19.

Chakraborty S. (1997) Rates and mechanisms of Fe-Mg interdiffusion in olivine at 980–1300 °C. J *Geophys. Res.* **102**, 12317–12331.

Chakraborty S. (2010) Diffusion coefficients in olivine, wadsleyite and ringwoodite. *Rev. Miner. Geochem.* **72**, 603–639.

Chazot C., Charpentier S., Kornprobst J., Vannucci R. and Luais B. (2005) Lithospheric mantle evolution during continental break-up: The West Iberia non-volcanic passive margin. *J. Petrol.* **46**, 2527–2568.

Cherniak D. J. (2010). REE Diffusion in Olivine. *Am. Mineral.* **95**, 362–368.

Cherniak D.J. and Liang Y. (2014) Titanium diffusion in olivine. *Geochim. Cosmochim. Acta* **147**, 43–57.

Chiesa S., Cortesogno L., Forcella F., Galli M., Messiga B., Pasquarè G., Pedemonte G.M., Piccardo G.B. and Rossi P.M. (1975) Assetto strutturale ed interpretazione geodinamica del Gruppo di Voltri. *Boll. Soc. Geol. It.* **94**, 555–581.

Collier M.L. and Kelemen P.B. (2010) The case for reactive crystallization at mid-ocean ridges. *J. Petrol*. **51**, 1913–1940.

Coogan L.A., Hain A., Stahl S. and Chakraborty S. (2005) Experimental determination of the diffusion coefficient for calcium in olivine between 900°C and 1500°C. *Geochim. Cosmochim. Acta* **69**, 3683–3694.

Coogan L.A., Saunders A.D., Kempton P.D. and Norry M.J. (2000) Evidences from oceanic gabbros for porous melt migration within a crystal mush beneath the Mid-Atlantic Ridge. *Geochem. Geophys. Geosys.* **1**, 2000GC00007.

D'Errico M., Warren J.M. and Godard M (2015) Evidence for chemically heterogeneous Artic mantle beneath the GakkelRidge. *Geochim. Cosmochim. Acta* **174**, 291-312.

De Hoog J. C. M., Gall L. and Cornell D. H. (2010) Trace-element geochemistry of mantle olivine and application to mantle petrogenesis and geothermobarometry. *Chem. Geol.* **270**, 196–215.

De Paolo D.J. (1981) Trace elements and isotopic effects of combined wall rock assimilation and fractional crystallization. *Earth Planet. Sci. Lett.* **53**, 189–202.

Dick H.J.B. (1989) Abyssal peridotites, very low spreading ridges and ocean ridge magmatism. In *Magmatism in the Ocean Basins* Saunders AD, Norry MJ (eds). Geol. Soc. Spec. Publ. **42**, Oxford, 71–105.

Dick H.J.B., Tivey M.A. and Tucholke B.E. (2008) Plutonic foundation of a slow-spread ridge segment: the oceanic core complex at Kane Megamullion, 23°30'N, 45°20'W. *Geochem. Geophys. Geosyst.* **9**, Q05014.

Dijkstra A.H., Barth M.G., Drury M.R., Mason P.R.D. and Vissers R.M.L. (2003) Diffuse porous melt flow and melt-rock reaction in the mantle lithosphere at the slow-spreading ridge: a structural petrology amd LA-ICP-MS study of the Othris Peridotite Massif (Greece). *Geochem. Geophys. Geosys.* **4**, 1–24.

Dohmen R., Kasemann S.A., Coogan L. and Chakraborty S. (2010) Diffusionof Li in olivine. Part I: experimental observations and a multispecies diffusion model. *Geochim. Cosmochim. Acta* **74**, 274–292.

Donaldson C.H. (1982) Origin of some of the Rhum harrisite by segregation of intercumulus liquid. *Min. Mag.* **45**, 201-209.

Drouin M., Godard M., Ildefonse B., Bruguier O. and Garrido C.J. (2009) Geochemical and petrographic evidence for magmatic impregnation in the oceanic lithosphere at Atlantis Massif, Mid-Atlantic Ridge (IODP Hole U1309D, 30°N). *Chem. Geol.* **264**, 71–88.

Drouin M., Ildefonse B and Godard M. (2010) A microstructure imprint of melt impregnation in slow spreading lithosphere: olivine-rich troctolites from the Atlantis Massif, Mid-Atlantic Ridge, 30 N, IOPD Hole U1309D. *Geochem. Geophys. Geosyst.* **11**, Q06003.doi:10.1029/2009GC002995.

Dunn T. and Sen C. (1994) Mineral/matrix partition coefficients for orthopyroxene, plagioclase and olivine in basaltic to andesitic systems: a combined analytical and experimental study. *Geochim. Cosmochim. Acta* **58**, 717–733.

Eason D.E. and Sinton J.M. (2009) Lava shields and fissure eruptions of the Western Volcanic Zone, Iceland, evidence for magma chambers and crustal interaction. *J. Volcanol. Geotherm. Res.* **186**, 331–348.

Eggins S.M., Rudnick R.L. and McDonoughet al., W.F. (1998) The composition of peridotites and their minerals: a laser-ablation ICP-MS study. *Earth Planet. Sci. Lett.* **154**, 53–71.

Ehlers K., Grove T.L., Sisson T.W., Recca S.I. and Zervas D.A. (1992) The effect of oxygen fugacity on the partitioning of nickel and cobalt between olivine, silicate melt and metal. *Geochim. Cosmochim. Acta* **56**, 3733–3743.

Ernst W.G. and Piccardo G. B., (1979) Petrogenesis of some Ligurian peridotites: I. Mineral and bulk rock chemistry. *Geochim. Cosmochim. Acta* **43**, 219–237.

Evans T.M., O'Neill H.St.C. and Tuff J. (2008) The influence of melt composition on the partitioning of REEs, Y, Sc, Zr and Al between forsterite and melt in the system CMAS. *Geochim. Cosmochim. Acta* **72**, 5708-5721.

Faure F., Trolliard G., Nicollet C. and Montel J.M. (2003) A developmental model of olivine morphology as a function of the cooling rate and the degree of undercooling. *Contrib. Miner. Petrol.* **145**, 251–263.

Federico L., Capponi G., Crispini L. and Scambelluri M. (2004) Exhumation of alpine high-pressure rocks: insights from petrology of eclogite clasts in the Tertiary Piedmontese basin (Ligurian Alps, Italy). *Lithos* **74**, 21–40.

Foley S. F., Prelevic D., Rehfeldt T. and Jacob D.E. (2013) Minor and trace elements in olivines as probes into early igneous and mantle melting processes. *Earth Planet. Sci. Lett.* **363**, 181–191.

Gaetani G.A. and Grove T.L. (1997) Partitioning of moderately siderophile elements among olivine, silicate melt and sulfide melt: constraints on core formation in the Earth and Mars. *Geochim. Cosmochim. Acta* **61**, 1829–1846.

Gao Y., Hoefs J., Hellebrand E., von der Andt A. and Snow J.E. (2007) Trace element zoning in pyroxenes from ODP Hole 735B gabbros: diffuse exchange or synkinematic crystal fractionation. *Contrib. Mineral. Petrol.* **153**, 429–442.

Garrido C.J., Bodinier J.-L. and Alard O. (2000) Distribution of LILE, REE and HFSE in anhydrous spinel peridotite and websterite minerals from the Ronda massif: insights into the nature of trace element reservoirs in the subcontinental lithospheric mantle. *Earth Planet. Sci. Lett.* **181**, 341–358.

Girona T. and Costa F. (2013) DIPRA: A user-friendly program to model multi-elementdiffusion in olivine with applications to timescales of magmatic processes. *Geochem. Geophys. Geosystems.* **14**, doi:10.1029/2012GC004427.

Godard M., Jousselin D. and Bodinier J.L. (2000) Relationships between geochemistry and structure beneath a paleo-spreading centre: a study of the mantle section in the Oman ophiolite. *Earth Planet. Sci. Lett.* **180**, 133–148.

Godard M., Awaji S., Hansen H., Hellebrand E., Brunelli D., Johnson K., Yamasaki T., Maeda J., Abratis M., Christie D., Kato Y., Mariet C. and Rosner M. (2009) Geochemistry of a long in-situ section of intrusive slow-spread oceanic lithosphere:Results from IODP Site U1309 (Atlantis Massif, 30°N Mid-Atlantic-Ridge). *Earth Planet. Sci. Lett.* **279**, 110–122.

Gregoire M., Moine B.N., O'Reilly S.Y., Cottin J.Y. and Giret A. (2000) Trace element residence and partitioning in mantle xenoliths metasomatized by highly alkaline, silicate- and carbonate-rich melts (Kerguelen Islands, Indian Ocean). *J. Petrol.* **41**, 477–509.

Günther D. and Heinrich C. (1999) Enhanced sensitivity in laser ablation-ICP mass spectrometry using helium-argon mixtures as aerosol carrier. J. *Anal. At. Spectrom.* **14**, 1363–1368.

Holzapfel C., Chakraborty S., Rubie D.C. and Frost D.J. (2007) Effect of pressure on Fe–Mg, Ni and Mn diffusion in $(FexMg1-x)_2SiO_4$ olivine. Physics of the Earth and Planetary Interiors **162**, 186–198.

Hoogerduijn Strating E.H., Piccardo G.B., Rampone E., Scambelluri M. and Vissers R.L.M. (1990) The structure and petrology of the Erro-Tobbio peridotite (Voltri Massif, Ligurian Alps): a two day excursion with emphasis on processes in the upper mantle. *Ofioliti* **15**, 119–184.

Hoogerduijn Strating E.H., Rampone E., Piccardo G.B., Drury M.R. and Vissers R.L.M. (1993) Subsolidus emplacement of mantle peridotities during incipient oceanic rifting and opening of the

Mesozoic Tethys (Voltri Massif, NW Italy). *J. Petrol.* **34**, 901–927.

Irving A.J. (1978) A review of experimental studies of crystal/liquid trace element partitioning. *Geochim. Cosmochim. Acta* **42**, 743–770.

Ito M. and Ganguly J. (2006) Diffusion kinetics of Cr in olivine and the 53Mn–53Cr thermochronology of early solar system objects. *Geochim. Cosmochim. Acta* **70**, 799–809.

Jochum K.P., Nohl U., Herwig K., Lammel E., Stoll B. and Hofmann A.W. (2005) GeoReM: A New Geochemical Database for Reference Materials and Isotopic Standards. *Geostand. Geoanalytical Res.* **29**, 333–338.

Jollands M.C., O'Neill H.S.C. and Hermann J. (2014) The importance of defining chemical potentials, substitution mechanisms and solubility in trace element diffusion studies: the case of Zr and Hf in olivine. *Contrib. Mineral. Petrol.* **168**, 1055–1073.

Kelemen P.B. (1990) Reaction between ultramafic rock and fractionating basaltic magma I. Phase relations, the origin of calcalkaline magma series, and the formation of discordant dunite. *J. Petrol* **31**, 51–98.

Kelemen P.B., Kikawa E. and Miller D.J. (2007) Leg 209 summary: processes in a 20-km-thick conductive boundary layer beneath the Mid-Atlantic Ridge, 14_–16_N. In: Kelemen PB, Kikawa E, Miller DJ (eds) *Proceedings of the ODP, science results* **209**, College Station, TX (Ocean Drilling Program), 1–33. doi:10.2973/odp.proc.sr.209.001.2007.

Kennedy A.K., Lofgren G.E. and Wasserburg G.J. (1993) An experimental study of trace element partitioning between olivine, orthopyroxene and melt in chondrules: equilibrium values and kinetic effects. *Earth Planet. Sci. Lett.* **115**, 177–195.

Kinzler R.J., Grove T.L. and Recca S.I. (1990) An experimental study on the effects of temperature and melt composition on the partitioning of nickel between olivine and silicate melt. *Geochim. Cosmochim. Acta* **54**, 1255–1266.

Kohn S.C. and Schofield P.F. (1994) The importance of melt composition in controlling trace-element behaviour — an experimental study of Mn and Zn partitioning between forsterite and silicate melts. *Chem. Geol.* **117**, 73–87.

Kvassnes A.J.S. and Grove T.L. (2008) How partial melts of mafic lower crust affect ascending magmas at ocean ridges. *Contrib. Mineral. Petrol.* **156**, 49–71.

Lee C.-T.A., Harbert A. and Leeman W.P. (2007) Extension of lattice strain theory to mineral/mineral rare-earth element partitioning: an approach for assessing disequilibrium and developing internally consistent partition coefficients between olivine, orthopyroxene, clinopyroxene and basaltic melt. *Geochim. Cosmochim. Acta* **71**, 481–496.

Liang Y., Sun C. and Yao L. (2013) A REE-in-two-pyroxene thermometer for mafic and ultramafic rocks. *Geochim. Cosmochim. Acta* **102**, 246–260.

Lissenberg C.J. and Dick H.J.B. (2008) Melt-rock reaction in the lower oceanic crust and its implications for the genesis of mid-ocean ridge basalt. *Earth Planet. Sci. Lett.* **271**, 311–325.

Lissenberg C.J., Howard K.A., MacLeod C.J. and Godard M. (2013) Pervasive reactive melt migration through fast-spreading lower oceanic crust (Hess Deep, Equatorial Pacific Ocean). *Earth Planet. Sci. Let.* **361**, 436–447.

Mysen B. (2007) Partitioning of calcium, magnesium, and transition metals between olivine and melt governed by the structure of the silicate melt at ambient pressure. *Am. Mineral.* **92**, 844–862.

Muentener O., Manatschal G., Laurent D. and Pettke T. (2010) Plagioclase peridotites in ocean-continent transitions: refertilized mantle domains generated by melt stagnation in the shallow mantle lithosphere. *J. Petrol* **51**, 255–294.

Niu Y. (2004) Bulk rock major and trace element compositions of abyssal peridotites: implications for mantle melting, melt extraction and post-melting processes beneath mid-ocean ridges. *J. Petrol.* **45**, 2423–2458.

Normann M.D. (1998) Melting and metasomatism in the continental lithosphere: laser ablation ICPMS analysis of minerals in spinel lherzolites from eastern Australia. *Contrib. Mineral. Petrol.* **130**, 240–255.

O'Driscoll B., Donaldson C.H., Troll V.R., Jerram D.A. and Emeleus C.H. (2007) An Origin for Harrisitic and Granular Olivine in the Rum Layered Suite, NW Scotland: a Crystal Size Distribution Study. *J.Petrol.* **48**, 253–270.

O'Reilly S.Y., Chen D., Griffin W.L. and Ryan C.G. (1997) Minor elements in olivine from spinel lherzolite xenoliths: implications for thermobarometry. *Mineral. Mag.* **61**, 257–269.

Ottonello G., Piccardo G.B. and Ernst W.G. (1979) Petrogenesis of some Ligurian peridotites – II rare earth element chemistry. *Geochim. Cosmochim. Acta* **43**, 1273–1284.

Pearce N.J.G., Perkins W.T., Westgate J.A., Gorton M.P., Jackson S.E., Neal C.R. and Chenery S.P. (1997) A compilation of new and published major and trace element data for NIST SRM 610 and NIST SRM 612 glass reference materials. *Geostand. Geoanalytical Res.* **21**, 115–144.

Petry C., Chakraborty S. and Palme H. (2004) Experimental determination of Ni diffusion coefficients in olivine and their dependence on temperature, composition, oxygen fugacity, and crystallographic orientation. *Geochim. Cosmochim. Acta* **68**, 4179–4188.

Piccardo G.B., Rampone E. and Vannucci R. (1990) Upper mantle evolution during continental rifting and ocean formation: evidence from peridotites bodies of the Western Alpine-Northern Appennine system. *Mem. Soc. Geol. Fr.* **156**, 323–333.

Piccardo G.B., Rampone E. and Vannucci R. (1992) Ligurian peridotites and ophiolites: from rift to ocean formation in the Jurassic Ligure-Piemontese basin. *Acta Vulcanol.* **2**, 313–325.

Piccardo G.B., Muentener O., Zanetti A. and Pettke T. (2004) Ophiolite peridotites of the Alpine-Apennine system: mantle processes and geodynamic relevance. *Int. Geol. Rev.* **40**, 1119–1159.

Piccardo G.B. and Vissers R.L.M. (2007) The pre-oceanic evolution of the Erro-Tobbio peridotite (Voltri Massif - Ligurian Alps, Italy). *J. Geodynam.* **43**, 41 –449.

Piccardo G.B., Zanetti A. and Muentener O. (2007) Melt/peridotite interaction in the Southern Lanzo peridotite: Field, textural and geochemical evidence. *Lithos* **94**, 181–209.

978 Rampone E. and Borghini G. (2008) Melt migration and intrusion in the Erro-Tobbio peridotites
979 (Ligurian Alps, Italy): Insights on magmatic processes in extending lithospheric mantle. *Eur. J.*
980 *Min.* **20**, 573–585.
981
982 Rampone E., Piccardo G.B., Vannucci R. and Bottazzi P. (1997) Chemistry and origin of trapped
983 melts in ophiolitic peridotites. *Geochim. Cosmochim. Acta* **61**, 4557–4569.
984
985 Rampone E., Romairone A. and Hofmann A.W. (2004) Contrasting bulk and mineral chemistry in
986 depleted peridotites : evidence for reactive porous flow. *Earth Planet. Sci. Lett.* **218**, 491–506.
987
988 Rampone E., Romairone A., Abouchami W., Piccardo G.B. and Hofmann A.W. (2005) Chronology,
989 petrology and isotope geochemistry of the Erro-Tobbio peridotites (Ligurian Alps, Italy): records of
990 late Paleozoic lithospheric extension. *J. Petrol.* **46**, 799–827.
991
992 Rampone E., Piccardo G.B. and Hofmann A.W. (2008) Multi-stage melt-rock interaction in the Mt.
993 Maggiore (Corsica, France) ophiolitic peridotites: microstructural and geochemical evidence.
994 *Contrib. Mineral. Petrol.* **156**, 453–475.
995
996 Rampone E., Borghini G., Romairone A., Abouchami W., Class C. and Goldstein S.L. (2014) Sm–
997 Nd geochronology of the Erro-Tobbio gabbros (Ligurian Alps, Italy): Insights into the evolution of
998 the Alpine Tethys. *Lithos* **205**, 236–246.
999
1000 Remmert P., Dohmen R. and Chakraborty S. (2008) Diffusion of REE, Hf e Sr in olivine. Eos
1001 Transactions, AGU, 89(53) Fall Meeting Supplement Abstract. MR33A-1844.
1002
1003 Renna M.R. and Tribuzio R. (2011) Olivine-richTroctolites from Ligurian Ophiolites (Italy):
1004 Evidence for Impregnation of Replacive Mantle Conduits by MORB-type Melts. *J. Petrol.* **52**,
1005 1763–1790.
1006
1007 Ross K. and Elthon D. (1997) Cumulus and postcumulus crystallization in the ocean crust: major-
1008 and trace-element geochemistry of leg 153 gabbroic rocks. In: Karson, J.A., Cannat, M., Millet,
1009 D.J., Elton, D., (Eds.), *Proceedings of the Ocean Drilling Program, Scientific Results* **153**. Ocean
1010 Drilling Program, College Station, Texas, 333–350.
1011
1012 Sanfilippo A. and Tribuzio R. (2011) Melt transport and deformation history in a nonvolcanic
1013 ophiolitic section, northern Apennines, Italy: implications for crustal accretion at slow spreading
1014 settings. *Geochem. Geophys. Geosyst.* **12**, Q0AG04.
1015
1016 Sanfilippo A. and Tribuzio R. (2013a) Building of the deepest crust at a fossil slow-spreading
1017 centre (Pineto gabbroic sequence, Alpine Jurassic ophiolites). *Contrib. Mineral. Petrol.* **165**, 705–
1018 721.
1019
1020 Sanfilippo A. and Tribuzio R. (2013b) Origin of olivine-rich troctolites from the oceanic
1021 lithosphere: a comparison between the Alpine Jurassic ophiolites and modern slow spreading
1022 ridges. *Ofioliti* **38**, 89–99.
1023
1024 Sanfilippo A., Dick H.J.B. and Ohara Y. (2013) Melt–rock reaction in the mantle: mantle troctolites
1025 from the Parece Vela Ancient Backarcspreading center. *J. Petrol.* **54**, 861–885.
1026
1027 Sanfilippo A., Tribuzio R. and Tiepolo M. (2014) Mantle–crust interactions in the oceanic
1028 lithosphere: Constraints from minor and trace elements in olivine. *Geochim Cosmochim. Acta* **141**,
1029 423-439.

Sanfilippo A., Morishita T., Kumagai H., Nakamura K., Okino K., Hara K.B., Tamura A. and Arai S. (2015a) Hybrid troctolites from mid-ocean ridges: inherited mantle in the lower crust. *Lithos* **232**, 124–130.

Sanfilippo A., Tribuzio R., Tiepolo M. and Berno D. (2015b) Reactive flow as dominant evolution process in the lowermost oceanic crust: evidence from olivine of the Pineto ophiolite (Corsica). *Contrib. Mineral. Petrol.* **170**, 38.

Saper L. and Liang Y. (2014) Formation of plagioclase-bearing peridotite and plagioclase-bearing wehrlite and gabbro suite through reactive crystallization: an experimental study. *Contrib. Mineral. Petrol.* **167**, 985.

Shimizu H., Sangen K. and Masuda A. (1982) Experimental-Study on Rare-Earth Element Partitioning in Olivine and Clinopyroxene Formed at 10 and 20kb for Basaltic Systems. *Geochemical Journal* 16, 107–117.

Spandler C., O'Neill H.S.C. and Kamenetsky V.S. (2007) Survival times of anomalous melt inclusions: constraints from element diffusion in olivine and chromite. *Nature* **447**, 303–306.

Spandler C. and O'Neill H.S.C. (2010) Diffusion and partition coefficients of minor and trace elements in San Carlos olivine at 1,300°C with some geochemical implications. *Contrib. Mineral. Petrol.* **159**, 791–818.

Sobolev A.V., Hofmann A.W., Sobolev S.V. and Nikogosian I.K. (2005) An olivine-free mantle source of Hawaiian shield basalts. *Nature* **434**, 590–597.

Sobolev A.V., Hofmann A.W., Kuzmin D.V., Yaxley G.M., Arndt N.T., Chung S.-L., Danyushevsky L.V., Elliott T., Frey F.A., Garcia M.O., Gurenko A.A., Kamenetsky V.S., Kerr A.C., Krivolutskaya N.A., Matvienkov V.V., Nikogosian I.K., Rocholl A., Sigurdsson I.A., Sushchevskaya N.M. and Teklay M. (2007) The amount of recycled crust in sources of mantle-derived melts. *Science* **316**, 412–417.

Sun M. and Kerrich R. (1995) Rare earth element and high field strength element characteristics of whole rocks and mineral separates of ultramafic nodules in Cenozoic volcanic vents of southeastern British Columbia, Canada. *Geochim Cosmochim Acta* **59**, 4863–4879.

Sun S.S. and McDonough W.F. (1989) Chemical and isotopic systematics of oceanic basalts: implications for mantle composition and processes. In: Saunders A.D., Norry M.J. (Eds.), *Magmatism in the ocean basins*. Geological Society of London, 313–345.

Sun C. and Liang Y. (2012) Distribution of REE between clinopyroxene and basaltic melt along a mantle adiabat: effects of major element composition, water, and temperature. *Contrib. Mineral. Petrol.* **163**, 807–823.

Sun C. and Liang Y. (2013) The importance of crystal chemistry on REE partitioning between mantle minerals (garnet, clinopyroxene, orthopyroxene and olivine) and basaltic melts. *Chem. Geol.* **358**, 23–36.

Sun C. and Liang Y. (2014) An assessment of subsolidus re-equilibration on REE distribution among mantle minerals olivine, orthopyroxene, clinopyroxene, and garnet in peridotites. *Chem. Geol.* **372**, 80–91.

Tartarotti P., Susini S., Nimis P. and Ottolini L. (2002) Melt migration in the upper mantle along the Romanche Fracture Zone (Equatorial Atlantic). *Lithos* **63**, 125–149.

Taura H., Yurimoto H., Kurita K. and Sueno S. (1998) Pressure dependence on partition coefficients for trace elements between olivine and the coexisting melts. *Phys. Chem. Miner.* **25**, 469–484.

Van Achterbergh E., Griffin W.L. and Stiefenhofer J. (2001) Metasomatism in mantle xenoliths from the Letlhakane kimberlites: estimation of element fluxes. *Contrib. Mineral. Petrol.* **141**, 397–414.

Vissers R.L.M., Drury M.R., Hoogerduijn Strating E.H. and Van der Wal D. (1991) Shear zones in the upper mantle: a case study in an Alpine lherzoliti massif. *Geology* **19**, 990–993.

Zanetti A., Tiepolo M., Oberti R. and Vannucci R. (2004) Trace-element partitioning in olivine: modelling of a complete data set from a synthetic hydrous basanite melt. *Lithos* **75**, 39–54.

Zhukova I., O'Neill H.S.C., Cambell I.K. and Kilburn (2014) The effect of silica activity on the diffusion of Ni and Co in olivine. *Contrib. Mineral. Petrol.* **168**, 1029.

Welsch B., Hammer J. and Hellebrand E. (2014) Phosphorus zoning reveals dendritic architecture of olivine. *Geology* **42**, 867–870.

Witt-Eickschen G. and O'Neill H.S. (2005) The effect of temperature on the equilibrium distribution of trace elements between clinopyroxene, orthopyroxene, olivine and spinel in upper mantle peridotite. *Chem. Geol.* **221**, 65–101.

FIGURE CAPTIONS

Figure 1 – Sketch map of the Voltri Massif (VM), showing the Erro-Tobbio peridotite and surrounding units (redrawn after Federico et al., 2004): (1) Erro-Tobbio peridotite Unit (VM), (2) Calcschists and meta-volcanics (VM), (3) Serpentinites and metagabbros (VM), (4) Crystalline massifs, (5) Sestri-Voltaggio zone, (6) Flysch Units, (7) Post-orogenic and Tertiary Piedmont Basin deposits, (8) Montenotte Unit. The large red circle indicates the studied area. (For interpretation of the references to colour in this figure legend, the reader is referred to the web version of this article).

Figure 2 – Field features of studied troctolites and gabbros. **a** Troctolite apophysis within mantle peridotites. **b** Textural variations (from granular to harrisitic types) within the troctolite. **c** Olivin gabbro dyke intruded (with sharp contacts) within the troctolite. **d** Close-up of Fig.2b, showing the textural variation of olivine (the dark grey mineral) from fine-grained granular (in the left bottom corner) to harrisitic-skeletal.

Figure 3 – Microscopic textures of troctolites and gabbros (cross-polarized light). **a** Sub-idiomorphic rounded olivine grains (ol) surrounded by plagioclase (plag), in granular troctolite MF21; small black spinel grain (sp) included in plagioclase. **b** Large kinked olivine grain (kinked ol), with irregular lobate contacts against interstitial plagioclase, in troctolite apophysis MF51. **c** Large hopper-type olivine crystal (ol) with lobate resorbed contacts against interstitial plagioclase (plag) in troctolite MF73. **d** Subidiomorphic olivine grain surrounded by plagioclase crystals (in rather sharp contacts) in olivine gabbro MF22.

Figure 4 – Variation of Mg# vs. Ni [**a**] and Mn [**b**] in olivines of Erro-Tobbio peridotites, troctolites and gabbro (see the legend for symbols). We also show olivine data for peridotites, dunites and troctolites in other Alpine-Apennine ophiolites (from Sanfilippo et al., 2014), together with the compositional field defined by olivine phenochrysts in MORB (data from Sobolev et al., 2007). Computed trends reported in Fig.4A refer to the compositional variations in olivine for fractional (FC) and equilibrium (EC) crystallization of a primary MORB melt at low pressure (< 5 Kb) (after Drouin et al., 2009).

Figure 5 – Variation of Mn vs. Ni [**a**], Co [**b**] and Zn [**c**] in olivines of Erro-Tobbio peridotites, troctolites and gabbro. Also shown are peridotite, troctolite, ol-gabbro data from Sanfilippo et al. (2014, 2015b).

Figure 6 - Variation of Zr vs. Hf [**a**], Ti [**b**], Yb [**c**] and Li [**d**] of olivines in Erro-Tobbio peridotites, troctolites and gabbro. In [**b**] and [**c**]**,** we also reported peridotite-troctolite olivine data from Sanfilippo et al. (2014), and MAR troctolite olivine data from Drouin et al. (2009). The field refers to the compositional range defined by mantle olivines in orogenic massifs and xenoliths (see text for more explanation; data from Sun and Kerrick, 1995; Garrido et al., 2000; Bedini and Bodinier, 1999).

Figure 7 - Chondrite-normalized Rare-Earth-Elements (REE) abundances of [**a**] clinopyroxene, orthopyroxene, [**b**] plagioclase and [**c**] olivine of Erro-Tobbio peridotites, troctolites and gabbro (see the legend for symbols). The fields reported in [**a**] and [**b**] refer, respectively, to the composition of clinopyroxene and plagioclase in ET troctolites from Borghini et al. (2007). In [**c**], we also show the compositional fields defined by: i) olivines in Mid-Atlantic Ridge troctolites (Drouin et al., 2009); ii) mantle olivines in orogenic massifs and xenoliths (see text for more explanation; data from Sun and Kerrick, 1995; Eggins et al., 1998; Garrido et al., 2000; Gregoire et al., 2000; Bedini and Bodinier, 1999), iii) olivines in Gakkel Ridge peridotites (D'Errico et al., 2015). Normalizing values after Sun and McDonough (1989).

Figure 8 – Primitive mantle-normalized trace elements abundances of [**a**] clinopyroxene, orthopyroxene, [**b**] plagioclase and [**c**] olivine of Erro-Tobbio peridotites, troctolites and gabbro (see the legend for symbols). The field reported in [**a**] refers to the composition of clinopyroxene in ET troctolites from Borghini et al. (2007). In [**c**], we also show the compositional fields defined by: i) olivines in Mid-Atlantic Ridge troctolites (Drouin et al., 2009); ii) mantle olivines in orogenic massifs and xenoliths (see text for more explanation; data from Sun and Kerrick, 1995; Eggins et al., 1998; Garrido et al., 2000; Gregoire et al., 2000; Bedini and Bodinier, 1999), iii) olivines in Gakkel Ridge peridotites (D'Errico et al., 2015). Normalizing values after Sun and McDonough (1989).

Figure 9 – [**a**] Olivine/cpx and [**b**] opx/cpx REE partition coefficients in the Erro-Tobbio peridotites, troctolites and ol-gabbro. We also reported predicted ol/cpx and opx/cpx partitioning at 1000, 1300 and 1400°C, after Lee et al. (2007).

Figure 10 - Olivine/cpx REE partition coefficients plotted versus Ionic Radius in the Erro-Tobbio peridotites [**a**], troctolites and gabbro **[b**]. Also shown are olivine/cpx trends computed at varying temperatures (1000-1300°C) using the major element compositions of olivine and clinopyroxene in our samples (following the modelling procedure by Sun and Liang, 2012, 2013, 2014).

Figure 11 - Chondrite-normalized Rare-Earth-Elements (REE) abundances of computed melts in equilibrium with: [**a**] olivine, orthopyroxene and clinopyroxene in the peridotites, [**b**] olivine, clinopyroxene and plagioclase in troctolites, [**c**] olivine, clinopyroxene and plagioclase in gabbro (see the legend for symbols). Clinopyroxene/liquid, orthopyroxene/liquid and olivine/liquid partition coefficients are from Lee et al. (2007). Plagioclase/liquid partition coefficients are from Aignes-Torres et al. (2007). Normalizing values after Sun and McDonough (1989).

Figure 12 - Chondrite-normalized Rare-Earth-Elements (REE) abundances of computed melts in equilibrium with: [**a**] olivine, orthopyroxene and clinopyroxene in the peridotites, [**b**] olivine, clinopyroxene and plagioclase in troctolites, [**c**] olivine, clinopyroxene and plagioclase in gabbro (see the legend for symbols). Clinopyroxene/liquid, orthopyroxene/liquid, olivine/liquid and plagioclase/liquid partition coefficients are from Bedard (2001). Normalizing values after Sun and McDonough (1989).

Figure 13 – Chondrite-normalized Rare-Earth-Elements (REE) abundances of computed melts in equilibrium with: [**a**] olivine and clinopyroxene in the peridotites, [**b**] olivine and clinopyroxene in troctolites, [**c**] olivine and clinopyroxene in gabbro (see the legend for symbols). Clinopyroxene/liquid and olivine/liquid partition coefficients at 1200 °C have been calculated following Sun and Liang (2012, 2013) models. Normalizing values after Sun and McDonough (1989).

Figure 14 – Variation of Zr_N/Nd_N ratio vs Yb_N in olivine of troctolites and gabbro, compared to olivine compositions computed by AFC model (De Paolo, 1981) at decreasing melt mass (F = 0.95-0.10). The initial melt composition C_0 is equal to the melt computed in equilibrium with the clinopyroxene of troctolite MF21 showing the lowest REE concentrations (see Table 3). The model assumes that initial melt ($melt_1$) assimilate olivine (Ma = 100% olivine) and crystallize plagioclase (Mc = 100% plag). The composition of assimilated olivine is olivine in peridotite MF40. The four different trends refer to different values of r (r = Ma/Mc). Model A in [**a**] and Model B in [**b**] differ only for the adopted partition coefficients. Model A: compilation of REE, Zr partition coefficients for olivine, plagioclase and clinopyroxene proposed by Suhr (1998). Model B: olivine/liquid D_{REE} by Lee (2007); olivine/liquid D_{Zr} by Spandler and O'Neill (2010); clinopyroxene/liquid $D_{REE,Zr}$ by Suhr (1998); plagioclase/liquid $D_{REE,Zr}$ by Aignes-Torres et al., (2007).

Table 1

Table 1 - Major and trace element compositions of olivines

	MF40			P1			MF21					
	peridotite			peridotite			troctolite					
SiO_2	39.98	40.39	40.54	41.11	41.29	41.13	39.89	40.36	40.72	40.52	40.55	40.27
FeO	10.18	10.30	10.22	9.72	9.80	9.85	11.00	10.73	10.99	10.87	10.47	10.58
MgO	49.23	48.27	48.66	48.58	48.66	48.27	48.42	48.73	48.16	47.87	48.16	48.37
MnO	0.12	0.12	0.14	0.15	0.16	0.17	0.09	0.20	0.20	0.21	0.20	0.15
NiO	0.36	0.33	0.32	0.37	0.36	0.37	0.23	0.28	0.31	0.37	0.28	0.37
CaO	0.06	0.07	0.06	0.06	0.09	0.10	0.05	0.04	0.05	0.06	0.04	0.03
Tot.	99.92	99.48	99.94	99.98	100.36	99.89	99.68	100.34	100.42	99.90	99.70	99.78
Mg#	0.896	0.893	0.895	0.899	0.899	0.897	0.887	0.890	0.887	0.887	0.891	0.891
ppm												
Li	1.13	1.05	1.45	0.38	1.02	0.39	2.21	2.68	1.87	1.99	1.26	1.52
B	0.18		0.32	0.45	0.36	0.37	0.53	0.41	0.41	1.24	7.02	1.37
Ca	446	457	434	695	388	679	298	267	388	306	423	257
Sc	5.4	5.3	4.7	5.3	4.8	5.5	5.3	4.4	5.6	5.8	5.6	5.7
Ti	59	57	50	59	46	54	70	58	144	97	109	93
V	4.4	4.6	3.7	5.2	4.2	5.0	3.0	3.2	3.1	3.0	3.0	2.8
Mn	1151	1158	1186	1179	1158	1177	1374	1399	1381	1279	991	1306
Co	136.7	138.5	141.3	150.0	147.5	147.3	143.5	145.1	143.4	141.5	137.8	139.2
Ni	2523	2534	2583	2734	2711	2739	2149	2178	2145	2173	2115	2198
Cu	0.11	0.11	0.11	0.34	0.31	0.30	0.07	1.71	n.d.	0.09	1.24	0.13
Zn	56.6	56.3	60.0	57.7	57.1	56.0	61.0	62.4	60.3	56.1	43.6	56.2
Sr	n.d.	n.d.	n.d.	0.09	n.d.	n.d.	n.d.	n.d.	n.d.	n.d.	0.12	n.d.
Y	0.07	0.08	0.07	0.08	0.05	0.08	0.07	0.04	0.08	0.08	0.07	0.06
Zr	0.01	0.02	0.01	0.02	0.01	0.01	0.03	0.09	0.17	0.07	0.07	0.05
Nb	n.d.	n.d.	n.d.	0.0009	0.0003	0.0011	0.0007	0.0040	0.0017		0.0011	0.0006
Ba	n.d.	n.d.	n.d.	n.d.	n.d.	n.d.	n.d.	n.d.	n.d.	0.0144	0.0468	0.0134
La	n.d.	0.00024	0.00045	n.d.	n.d.	n.d.	n.d.	0.00037	n.d.	0.00051	0.00025	n.d.
Ce	n.d.	0.00016	0.00230	n.d.	n.d.	n.d.	0.00042	0.00095	0.00037	0.00112	0.00027	0.00060
Pr	n.d.	n.d.	n.d.	n.d.	n.d.	0.00017	0.00009	0.00005	n.d.	n.d.	n.d.	n.d.
Nd	n.d.	0.00033	n.d.	n.d.	n.d.	n.d.	n.d.	n.d.	n.d.	n.d.	n.d.	n.d.
Sm	n.d.	n.d.	n.d.	n.d.	n.d.	n.d.	0.00297	0.00226	n.d.	n.d.	n.d.	n.d.
Eu	n.d.	n.d.	n.d.	0.00028	n.d.	n.d.	n.d.	0.00024	0.00031	n.d.	0.00022	n.d.
Gd	n.d.	n.d.	n.d.	0.00100	0.00080	0.00036	n.d.	n.d.	n.d.	n.d.	0.00154	n.d.
Tb	n.d.	0.00052	0.00015	n.d.	n.d.	0.00028	0.00026	n.d.	0.00030	0.00032	n.d.	n.d.
Dy	0.00474	0.00579	0.00255	0.00605	0.00318	0.00356	0.00500	0.00228	0.00549	0.00402	0.00344	0.00191
Ho	0.00242	0.00262	0.00230	0.00257	0.00183	0.00275	0.00237	0.00099	0.00231	0.00269	0.00204	0.00182
Er	0.01330	0.01330	0.01210	0.01810	0.01190	0.02030	0.01660	0.00865	0.01700	0.01570	0.01570	0.01540
Tm	0.00481	0.00455	0.00392	0.00503	0.00345	0.00491	0.00398	0.00308	0.00612	0.00559	0.00614	0.00505
Yb	0.05090	0.05440	0.04010	0.05000	0.03410	0.05390	0.05230	0.04600	0.06540	0.06280	0.06200	0.05920
Lu	0.01204	0.01226	0.01045	0.01207	0.01054	0.01279	0.01441	0.01146	0.01758	0.01841	0.01778	0.01839
Hf	0.00061	n.d.	n.d.	0.00041	0.00077	0.00055	0.00152	0.00261	0.00493	0.00134	0.00159	0.00128
Ta	0.00057	0.00027	n.d.	n.d.	n.d.	0.00030	n.d.	n.d.	n.d.	0.00036	n.d.	n.d.
Pb	0.00221	0.01295	0.00276	0.01068	0.00185	0.00700	0.00341	0.00465	0.00131	0.00142	0.00637	0.01780
Th	n.d.	n.d.	n.d.	n.d.	n.d.	n.d.		0.00042	n.d.	n.d.	n.d.	0.00027
U	n.d.	n.d.	n.d.	n.d.	n.d.	n.d.	0.00040	0.00022	n.d.	n.d.	n.d.	0.00006

Table 1 - Continued

	MF51				MF72Ga			MF72Ha			
	troctolite				troctolite			troctolite			
SiO_2	40.23	40.30	40.29	40.36	40.48	40.32	40.32	40.21	40.41	40.57	40.38
FeO	11.33	11.35	11.09	11.15	11.54	11.51	11.40	11.60	11.19	11.15	11.21
MgO	47.92	47.73	47.93	47.88	47.65	47.51	47.48	48.18	47.79	47.96	47.81
MnO	0.21	0.19	0.18	0.21	0.15	0.17	0.24	0.15	0.20	0.19	0.24
NiO	0.23	0.30	0.34	0.30	0.21	0.28	0.28	0.25	0.27	0.24	0.35
CaO	0.06	0.05	0.05	0.05	0.05	0.03	0.08	0.04	0.06	0.02	0.03
Tot.	99.98	99.92	99.88	99.95	100.08	99.82	99.79	100.43	99.91	100.12	100.01
Mg#	0.883	0.882	0.885	0.884	0.880	0.880	0.881	0.881	0.884	0.885	0.884
ppm											
Li	2.26	2.30	2.36	2.09	1.88	2.40	1.99	2.01	0.72	1.85	0.73
B	0.32	0.31	0.35	0.32	0.74	1.53	0.44	0.91	1.63	12.56	2.49
Ca	566	398	290	334	398	351	393	510	538	383	294
Sc	5.0	5.9	7.1	7.3	10.2	8.9	8.9	7.1	6.9	6.7	6.0
Ti	73	293	197	171	136	128	128	85	165	107	246
V	2.9	6.4	5.0	4.6	3.3	3.2	3.5	3.8	4.9	3.0	4.0
Mn	1456	1496	1478	1475	1533	1535	1509	1554	1538	1341	1547
Co	143.7	146.1	146.0	146.6	139.9	139.8	141.3	142.0	136.4	129.8	139.6
Ni	2037	2056	2094	2133	2142	2119	2152	2155	2116	2027	2265
Cu	0.07	0.08	0.07	0.06	0.02	0.04	0.12	n.d.	0.01	0.27	0.03
Zn	67.9	68.7	69.0	70.8	58.1	57.3	61.4	60.2	53.4	43.7	61.1
Sr	n.d.	n.d.	n.d.	n.d.	0.00	0.01	0.08	0.01	0.03	0.41	0.05
Y	0.07	0.14	0.12	0.17	0.21	0.15	0.16	0.14	0.18	0.08	0.06
Zr	0.07	0.32	0.23	0.18	0.13	0.09	0.25	0.19	0.30	0.16	0.43
Nb	0.0013	0.0146	n.d.	0.0011	0.0010	0.0010	0.0011	0.0009	0.0035	0.0011	0.0071
Ba	0.0045	n.d.	0.0096	n.d.	n.d.	0.0075	0.0034	n.d.	0.0076	0.6890	0.0057
La	0.00027	n.d.	n.d.	0.00019	n.d.	n.d.	0.00047	0.00024	0.00032	0.00071	n.d.
Ce	n.d.	0.00039	n.d.	n.d.	n.d.	n.d.	0.00209	0.00049	0.00089	0.00084	n.d.
Pr	0.00007	0.00016	n.d.	n.d.	n.d.	n.d.	0.00028	n.d.	n.d.	n.d.	n.d.
Nd	n.d.	n.d.	n.d.	0.00189	n.d.	n.d.	0.00033	n.d.	0.00069	0.00044	0.00048
Sm	n.d.	n.d.	n.d.	n.d.	n.d.	n.d.	n.d.	0.00147	0.00063	n.d.	n.d.
Eu	0.00015	n.d.	n.d.	n.d.	n.d.	n.d.	n.d.	n.d.	n.d.	n.d.	n.d.
Gd	n.d.	0.00166	n.d.	n.d.	n.d.	0.00166	n.d.	n.d.	0.00365	n.d.	0.00076
Tb	n.d.	0.00029	n.d.	0.00042	0.00078	0.00033	0.00013	0.00046	0.00068	0.00009	n.d.
Dy	0.00317	0.01010	0.00324	0.00959	0.01045	0.00655	0.00390	0.00472	0.01380	0.00345	0.00325
Ho	0.00193	0.00438	0.00353	0.00563	0.00628	0.00470	0.00422	0.00412	0.00596	0.00253	0.00242
Er	0.01630	0.02850	0.02930	0.03740	0.04640	0.03840	0.03680	0.03590	0.03230	0.02400	0.01760
Tm	0.00591	0.00781	0.01116	0.01222	0.01605	0.01269	0.01414	0.01234	0.01106	0.00841	0.00623
Yb	0.06720	0.09090	0.11690	0.12660	0.17420	0.14640	0.16120	0.14520	0.11920	0.10880	0.07890
Lu	0.01733	0.02360	0.03120	0.03050	0.03940	0.03620	0.03940	0.03710	0.03000	0.03070	0.02280
Hf	0.00208	0.01140	0.00435	0.00357	0.00224	0.00177	0.00554	0.00639	0.00352	0.00323	0.00787
Ta	n.d.	0.00118	n.d.	n.d.	n.d.	n.d.	n.d.	n.d.	0.00038	n.d.	n.d.
Pb	0.00269	0.00138	0.00280	n.d.	0.01082	0.00733	0.00734	0.00748	0.01268	0.01214	0.00306
Th	n.d.	0.00010	n.d.	n.d.	n.d.	n.d.	n.d.	n.d.	n.d.	n.d.	n.d.
U	0.01475	n.d.	n.d.	n.d.	n.d.	n.d.	n.d.	n.d.	0.00007	n.d.	n.d.

Table 1 - Continued

	MF73Ga		MF22		
	troctolite		ol-gabbro		
SiO_2	40.51	39.99	39.63	39.42	39.77
FeO	11.45	11.79	15.38	15.55	15.28
MgO	47.27	48.09	44.85	44.24	44.31
MnO	0.18	0.22	0.28	0.24	0.31
NiO	0.29	0.25	0.16	0.17	0.10
CaO	0.04	0.05	0.03	0.03	0.04
Tot.	99.74	100.39	100.33	99.64	99.81
Mg#	0.880	0.879	0.839	0.835	0.838
ppm					
Li	2.51	2.45	1.85	1.75	1.81
B	0.29	0.34	0.86	1.34	0.26
Ca	495	358	183	181	283
Sc	8.4	6.5	5.1	5.5	5.5
Ti	194	105	59	52	67
V	6.9	3.8	2.5	2.4	2.8
Mn	1553	1609	1913	1949	1874
Co	139.2	134.5	168.0	167.4	163.6
Ni	2023	2062	1401	1389	1341
Cu	0.12	0.19	0.07	0.20	0.06
Zn	67.2	69.8	100.8	99.7	92.5
Sr	5.29	n.d.	0.07	0.06	0.00
Y	0.18	0.07	0.03	0.04	0.04
Zr	0.18	0.11	0.05	0.05	0.03
Nb	0.0014	0.0008	0.0031	0.0034	0.0007
Ba	0.0066	n.d.	0.0229	0.0315	n.d.
La	n.d.	n.d.	0.00088	0.00042	n.d.
Ce	0.00867	0.00191	0.00314	0.00315	0.00043
Pr	0.00121	n.d.	0.0003	n.d.	n.d.
Nd	n.d.	n.d.	0.00114	n.d.	0.00042
Sm	0.00086	n.d.	n.d.	n.d.	n.d.
Eu	0.00018	n.d.	n.d.	n.d.	n.d.
Gd	0.00365	n.d.	0.00079	n.d.	n.d.
Tb	0.00097	n.d.	n.d.	n.d.	0.00011
Dy	0.01260	0.00253	0.00238	0.00121	0.00229
Ho	0.00597	0.00216	0.00109	0.00109	0.00163
Er	0.03120	0.01730	0.00771	0.00883	0.00985
Tm	0.00953	0.00686	0.00260	0.00296	0.00307
Yb	0.10350	0.09570	0.03600	0.04850	0.04750
Lu	0.03060	0.02530	0.01290	0.01372	0.01372
Hf	0.00379	0.00443	0.00082	0.00155	0.00107
Ta	n.d.	n.d.	n.d.	n.d.	n.d.
Pb	0.00897	0.00476	0.00646	0.00303	0.00855
Th	n.d.	n.d.	0.00019	n.d.	n.d.
U	0.01920	0.00040	n.d.	n.d.	0.00008

Table 2

Table 2 - Major and trace element compositions of plagioclases

	MF51*	MF21	MF73H	MF22	MF73Ga
	troctolite	troctolite	troctolite	ol-gabbro	troctolite
SiO_2	51.93	52.55	52.66	53.09	53.32
TiO_2	0.08	0.10	0.13	0.10	0.07
Al_2O_3	31.20	30.67	30.05	29.83	29.69
FeO	0.11	0.12	0.22	0.26	0.18
MgO	0.00	0.03	0.02	0.06	0.06
MnO	0.03	0.00	0.00	0.00	0.01
CaO	12.97	12.66	11.88	12.38	11.86
Na_2O	4.36	4.19	4.44	4.31	4.66
K_2O	0.04	0.02	0.03	0.02	0.03
Tot.	100.72	100.33	99.43	100.04	99.89
Anorthite	0.62	0.625	0.597	0.613	0.584
ppm					
Li	0.473	b.d.l.	b.d.l.	1.36	b.d.l.
Sc	0.761	0.349	b.d.l.	0.94	1.112
Ti	220.2	632.5	626.4	246.6	698.0
V	2.57	2.24	3.74	2.59	5.88
Cr	2.39	3.45	4.81	b.d.l.	b.d.l.
Co	0.211	0.32	0.267	0.19	0.11
Ni	b.d.l.	b.d.l.	b.d.l.	b.d.l.	b.d.l.
Mn	n.d	n.d	n.d	19.6	10.1
Cu	0.414	0.61	0.433	0.67	0.49
Zn	0.889	1.23150	0.977	1.80	1.10
Rb	0.0499	0.16200	0.299	n.d	n.d
Sr	256.0	275.4	271.0	237.4	250.5
Y	0.2470	0.4600	0.5040	0.1920	1.0870
Zr	0.0759	0.0492	0.0650	0.0346	0.2001
Nb	0.0037	b.d.l.	b.d.l.	0.0045	0.0020
Ba	0.8900	3.6750	1.8190	1.1320	2.4130
La	0.1667	0.6820	0.3500	0.1531	0.4310
Ce	0.4010	1.9645	0.9210	0.4510	1.2050
Pr	0.0626	0.2520	0.1296	0.0616	0.1813
Nd	0.2820	1.1255	0.6300	0.2820	0.8720
Sm	0.0860	0.2175	0.1830	0.0584	0.2145
Eu	0.3130	0.4260	0.3230	0.3230	0.4120
Gd	0.0612	0.1710	0.1130	0.0695	0.2582
Tb	0.0088	0.0181	0.0134	0.0107	0.0369
Dy	0.0414	0.0949	0.1100	0.0410	0.2117
Ho	0.0097	0.0141	0.0209	0.0081	0.0448
Er	0.0182	0.0344	0.0461	0.0156	0.1126
Tm	0.0031	0.0037	0.0051	0.0033	0.0142
Yb	0.0209	b.d.l.	0.0310	0.0111	0.0818
Lu	0.0023	0.0036	0.0034	0.0017	0.0116
Hf	b.d.l.	0.0066	b.d.l.	0.0012	0.0059
Ta	b.d.l.	b.d.l.	b.d.l.	b.d.l.	0.0011
Pb	0.1482	0.1597	0.1110	0.1077	0.1374
Th	b.d.l.	b.d.l.	b.d.l.	0.0008	b.d.l.
U	b.d.l.	b.d.l.	b.d.l.	0.0087	b.d.l.

* Data from Borghini et al. (2007)

Table 3

Table 3 - Major and trace element compositions of clinopyroxenes and orthopyroxenes

	MF22	MF40		P1		MF51	MF72Ga	MF72Ha	MF73Ga	MF21
	ol-gabbro	peridotite		peridotite		troctolite	troctolite	troctolite	troctolite	troctolite
	cpx	opx	cpx	opx	cpx	cpx	cpx	cpx	cpx	cpx
SiO_2	52.31	55.54	51.41	55.64	51.43	52.28	52.23	52.77	52.21	52.17
TiO_2	0.37	0.19	0.51	0.20	0.45	0.95	0.81	0.54	0.56	0.38
Al_2O_3	2.87	2.66	4.54	2.29	4.82	3.04	3.34	3.62	3.80	3.57
Cr_2O_3	0.88	0.78	1.40	0.68	1.23	1.02	1.45	1.06	1.50	1.56
FeO	4.63	6.89	3.14	6.61	3.30	3.81	4.10	3.41	3.29	3.21
MgO	16.91	32.47	16.01	32.32	16.16	17.19	16.99	16.65	16.24	16.33
MnO	0.17	0.08	0.10	0.14	0.14	0.18	0.06	0.06	0.09	0.09
NiO	0.05	0.12	0.07	0.16	0.06	0.05	0.07	0.01	0.10	0.10
CaO	20.79	1.44	22.71	1.39	21.87	20.79	20.26	21.18	21.92	22.15
Na_2O	0.40	0.00	0.33	0.00	0.26	0.43	0.52	0.60	0.61	0.59
Tot.	99.39	100.16	100.22	99.44	99.72	99.75	99.83	99.89	100.31	100.15
Mg#	0.867	0.894	0.901	0.897	0.897	0.889	0.881	0.897	0.898	0.901
ppm										
Li	1.89	0.34	1.25	3.54	2.63	1.23	b.d.l.	b.d.l.	0.10	0.46
B	0.63	0.37	0.34	1.00	0.41	0.63	0.39	0.30	0.30	0.48
Sc	88.3	38.6	70.4	35.5	66.5	115.6	126.7	94.1	107.3	77.8
Ti	2749	1525	3378	1348	2964	6825	5874	3311	2952	2893
V	276.7	161.0	345.8	140.1	310.1	409.2	362.5	297.7	260.3	269.3
Mn	1169	1188	907	1201	871	1097	1005	891	846	907
Co	30.0	57.6	30.8	57.8	29.5	26.8	27.1	28.7	28.2	28.3
Ni	210	683	424	683	423	308	326	365	338	353
Cu	3.86	b.d.l.	0.06	0.13	0.20	0.13	0.51	0.15	0.12	0.14
Zn	21.14	45.93	17.74	39.99	14.15	17.60	17.72	15.52	14.42	16.38
Sr	12.12	0.02	0.72	0.23	0.56	11.31	13.79	13.68	12.64	12.08
Y	15.07	4.61	25.94	3.96	25.23	45.37	32.85	14.61	16.35	12.98
Zr	11.90	2.46	14.46	2.11	15.28	41.56	25.84	11.12	11.46	9.43
Nb	0.0965	0.0189	0.0278	0.0173	0.0318	0.0585	0.1131	0.0385	0.0408	0.0962
Sb	0.0103	b.d.l.	b.d.l.	b.d.l.	b.d.l.	0.0021	0.0023	b.d.l.	b.d.l.	b.d.l.
Ba	0.0831	b.d.l.	b.d.l.	0.194	b.d.l.	0.0766	0.0561	0.0024	0.0074	0.0158
La	0.2856	0.0004	0.0301	b.d.l.	0.0504	0.644	0.537	0.2378	0.1999	0.2620
Ce	1.6540	0.0143	0.6510	0.0084	0.837	4.26	2.941	1.514	1.1910	1.4880
Pr	0.4030	0.0074	0.3290	0.0039	0.359	1.098	0.745	0.395	0.3092	0.3650
Nd	2.7900	0.0985	3.2330	0.0650	3.39	7.9	5.66	2.866	2.4370	2.5300
Sm	1.2960	0.1070	2.0840	0.0706	2.02	3.68	2.734	1.384	1.2170	1.2200
Eu	0.4770	0.0377	0.7040	0.0270	0.646	0.857	0.858	0.526	0.4470	0.4780
Gd	2.2148	0.3041	4.0680	0.1948	3.55	5.89	4.42	2.061	2.2453	2.0103
Tb	0.4180	0.0737	0.7140	0.0558	0.695	1.191	0.885	0.419	0.4140	0.3680
Dy	2.9500	0.6610	4.9900	0.5640	4.82	8.59	6.24	2.91	3.0300	2.6260
Ho	0.6670	0.1904	1.0890	0.1573	1.051	1.923	1.406	0.63	0.6710	0.5850
Er	1.8450	0.6530	2.9650	0.5560	2.84	5.39	3.91	1.77	1.8190	1.5690
Tm	0.2810	0.1178	0.4240	0.1056	0.404	0.77	0.554	0.243	0.2682	0.2257
Yb	1.7900	0.8770	2.5610	0.8090	2.299	4.69	3.41	1.575	1.6770	1.3990
Lu	0.2639	0.1477	0.3530	0.1350	0.329	0.669	0.506	0.2257	0.2526	0.2042
Hf	0.4660	0.1921	0.9660	0.1662	1.027	1.43	1.225	0.52	0.5510	0.4580
Ta	0.0073	b.d.l.	b.d.l.	b.d.l.	b.d.l.	0.0093	0.00447	0.00068	0.0008	0.0017
Pb	0.0150	0.0053	0.0034	0.0129	0.0084	0.0179	0.017	0.0071	0.0155	0.0165
Th	0.0093	b.d.l.	b.d.l.	b.d.l.	b.d.l.	0.0304	0.01309	0.00088	0.0014	0.0044
U	0.0051	b.d.l.	b.d.l.	b.d.l.	b.d.l.	0.00271	0.00445	0.00022	0.0003	0.0037

Figure 1

Click here to download high resolution image

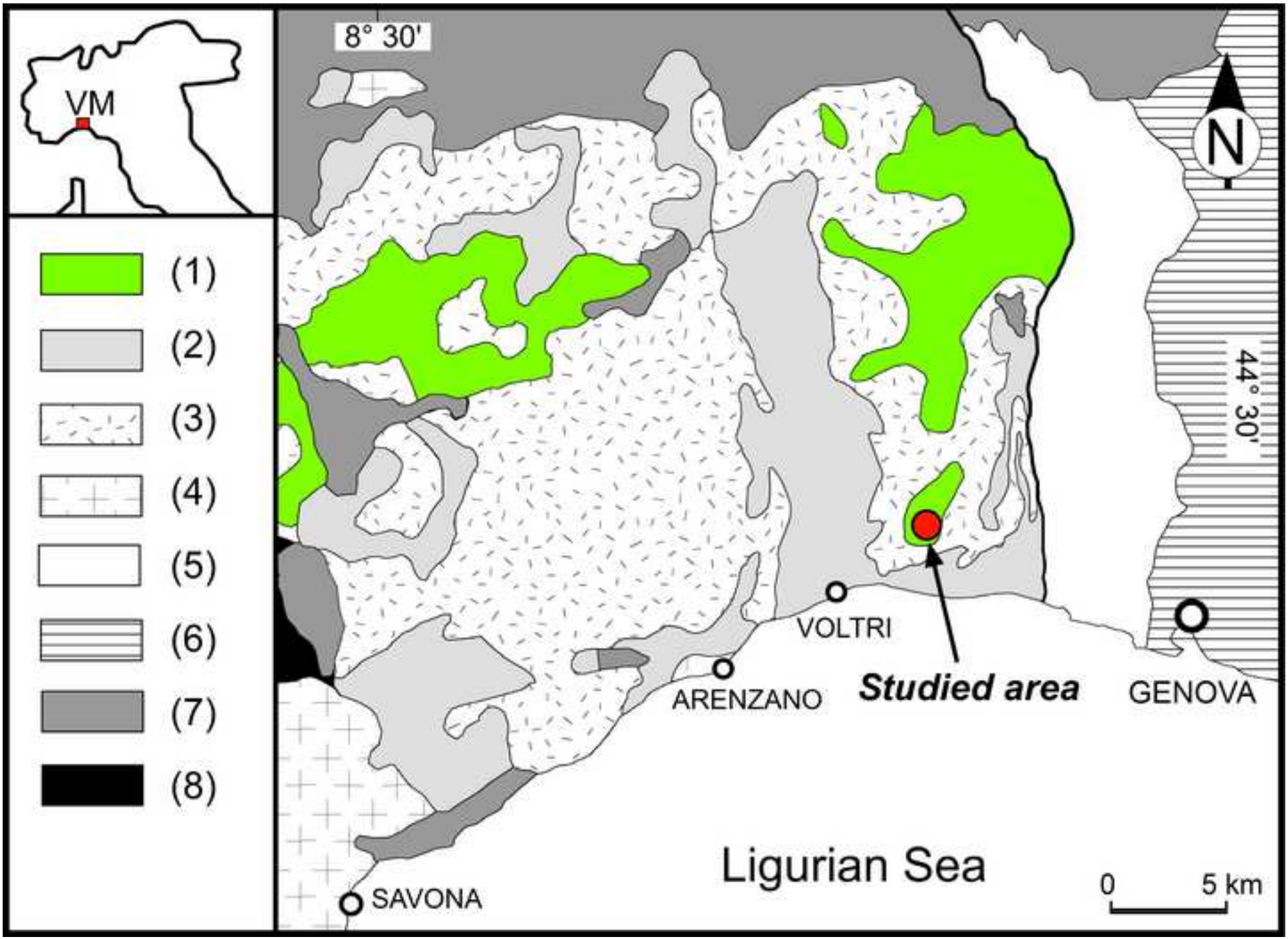

Figure 2

Click here to download high resolution image

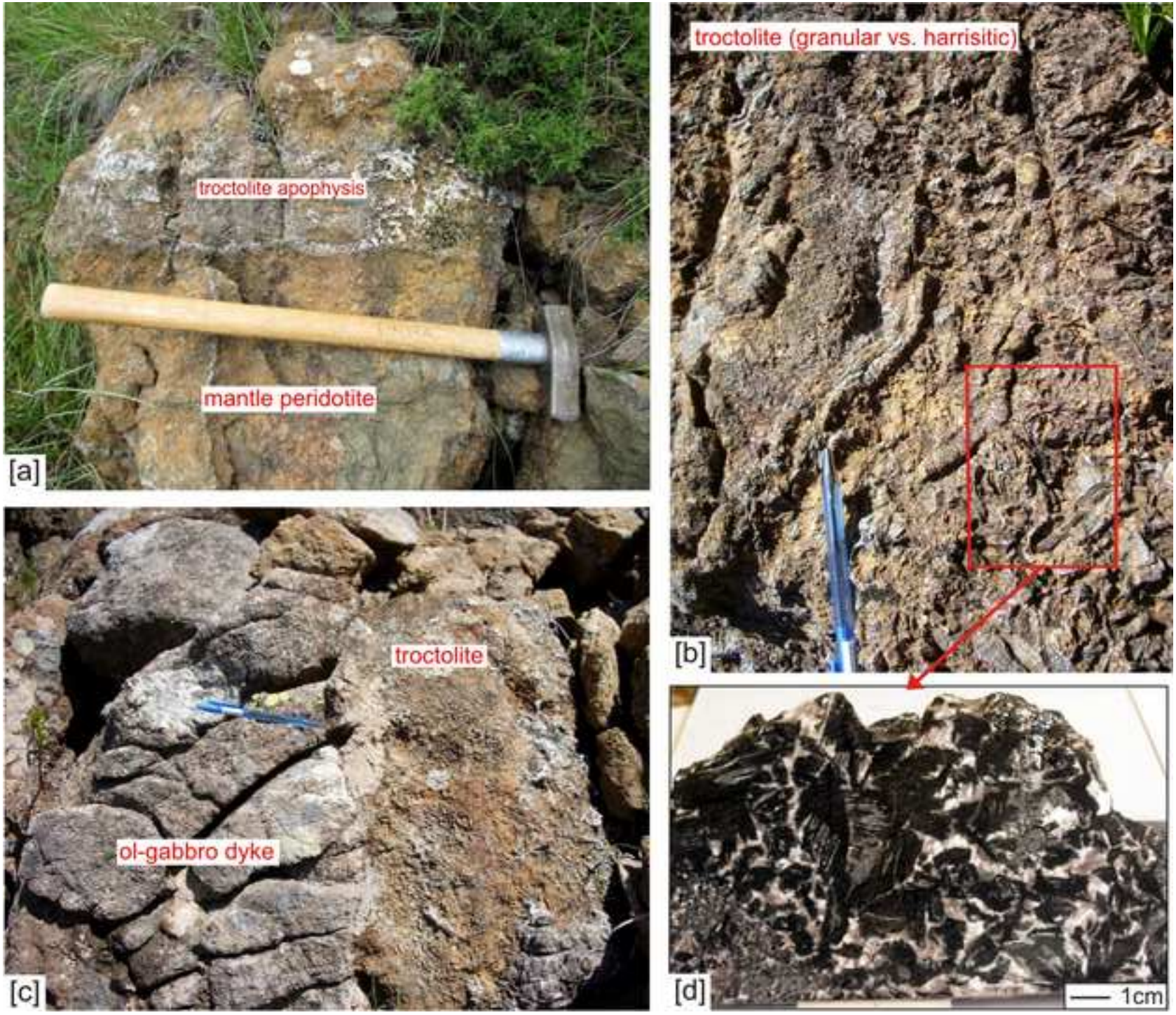

Figure 3

Click here to download high resolution image

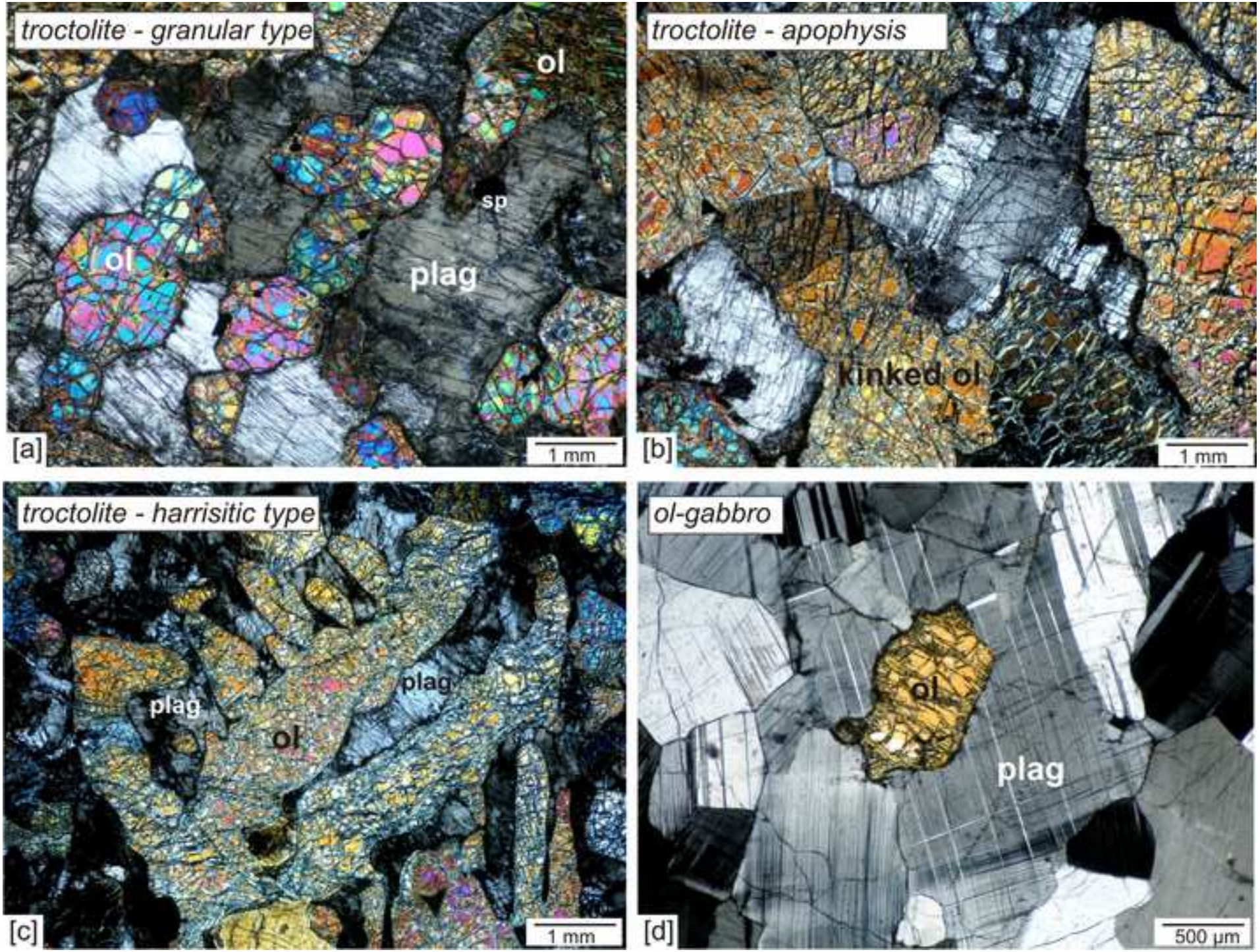

Figure 4

Click here to download high resolution image

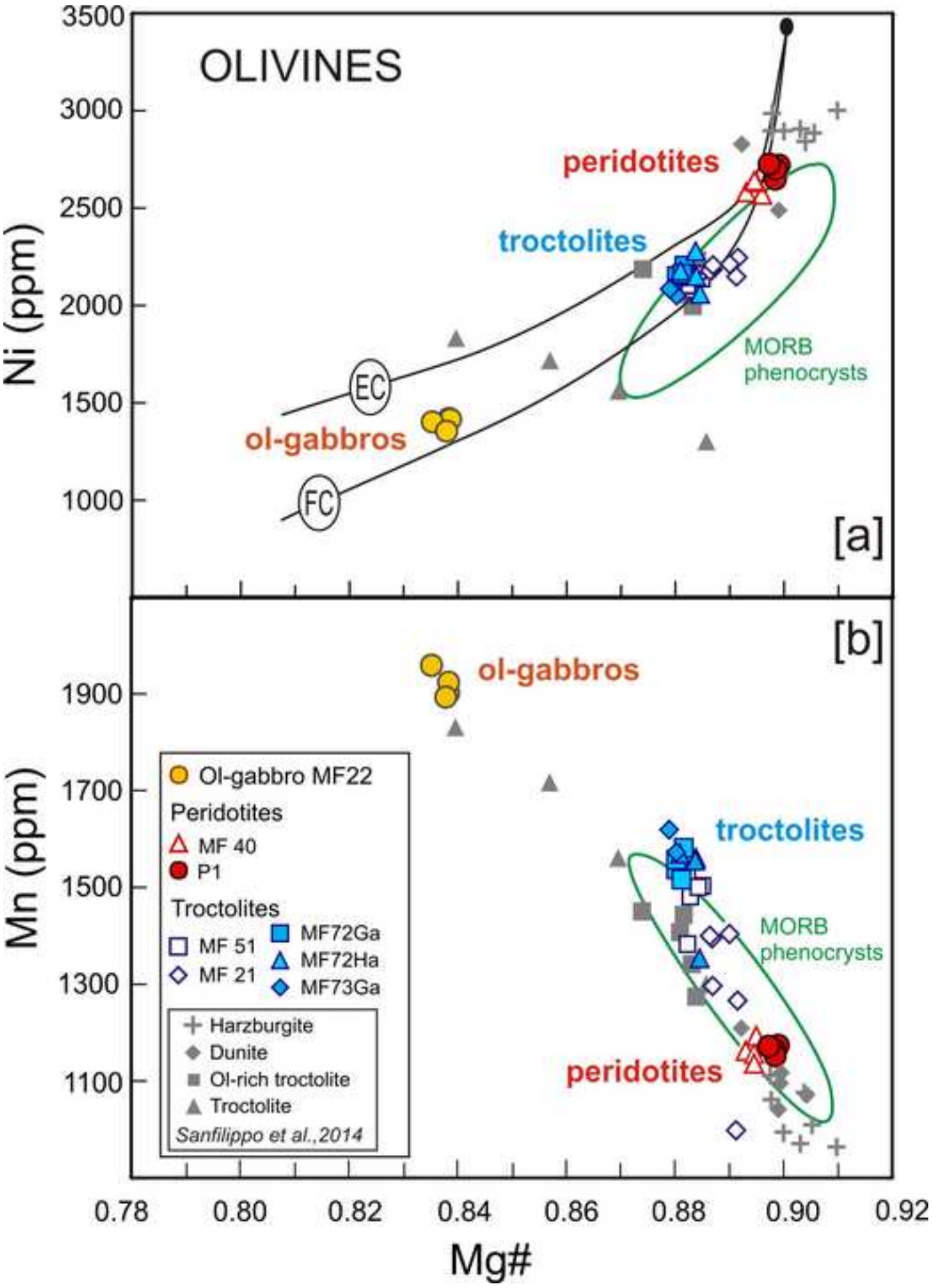

Figure 5

Click here to download high resolution image

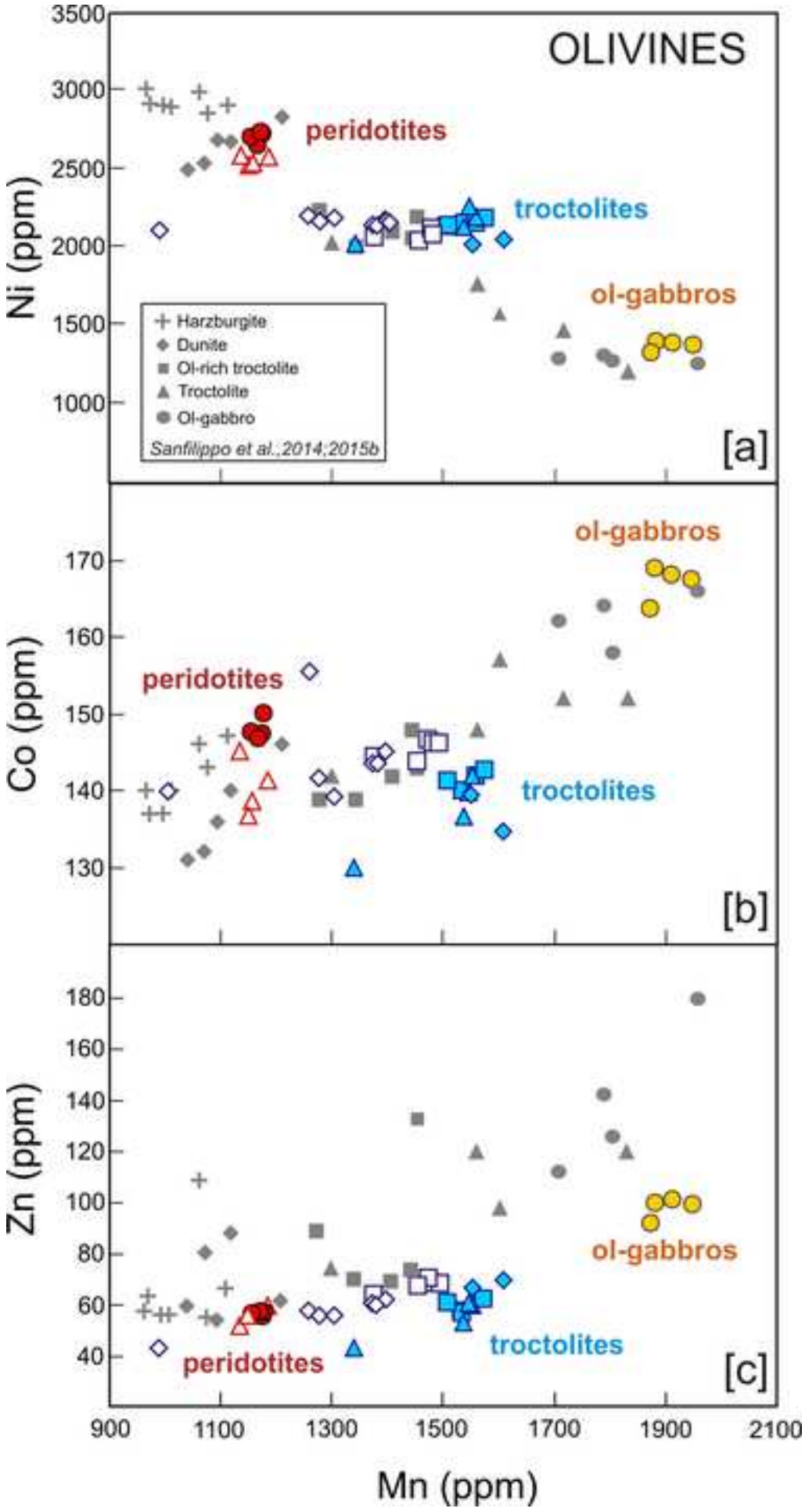

Figure 6

Click here to download high resolution image

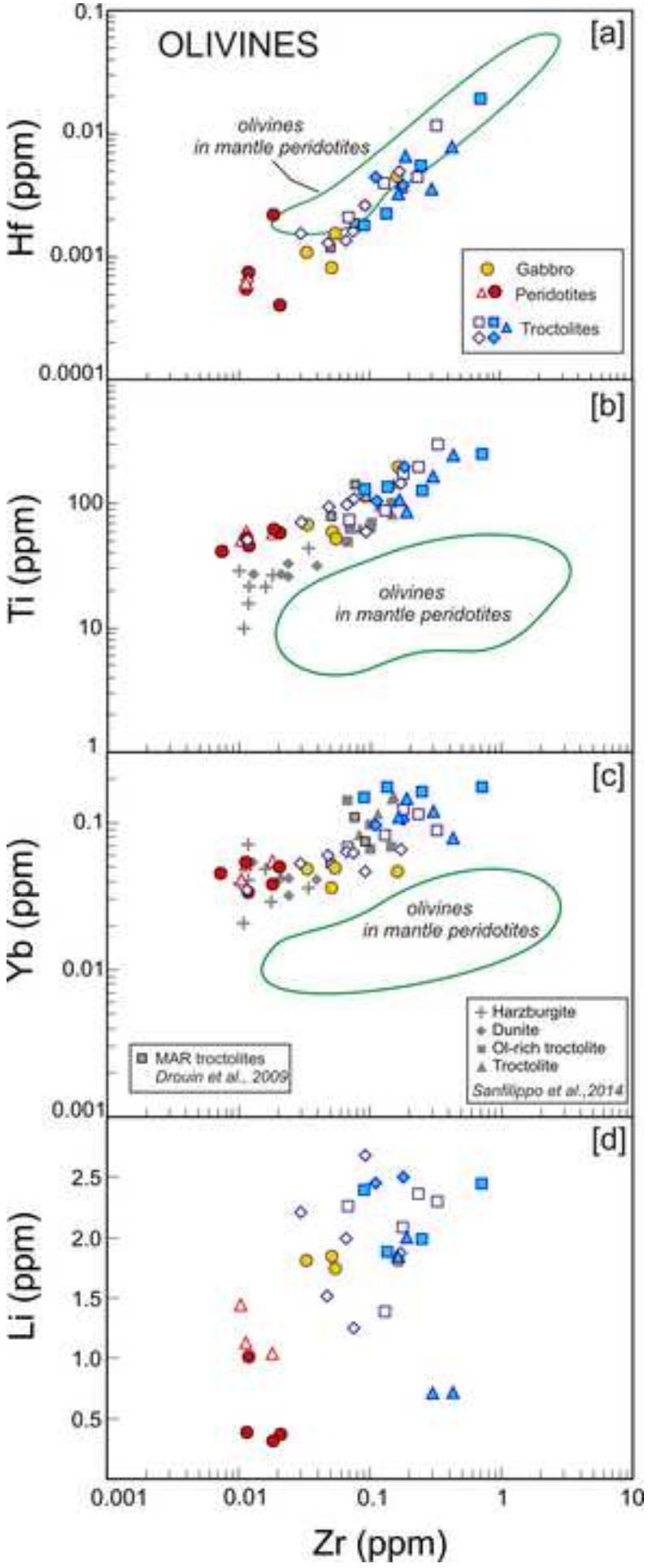

Figure 7

Click here to download high resolution image

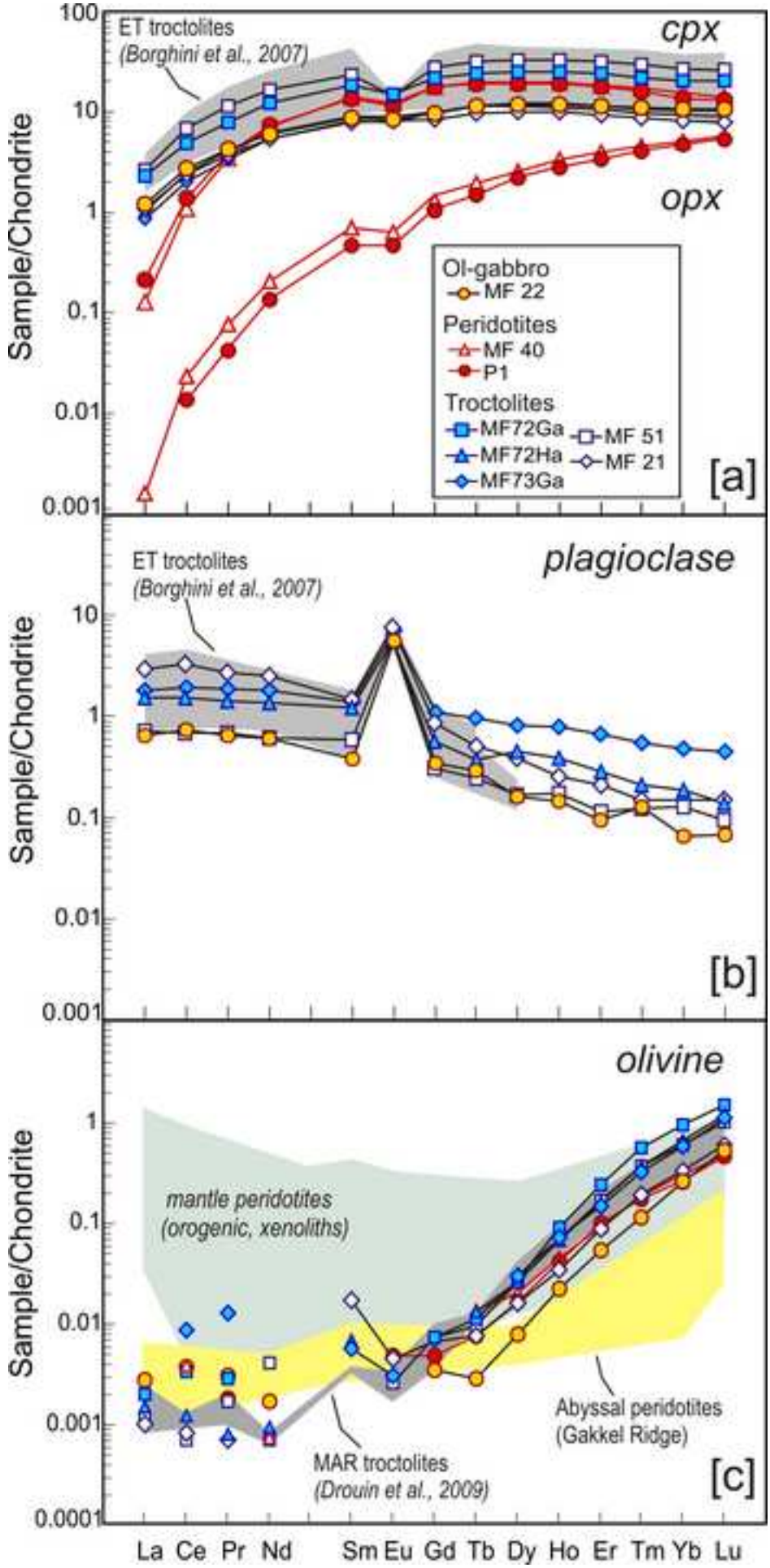

Figure 8

Click here to download high resolution image

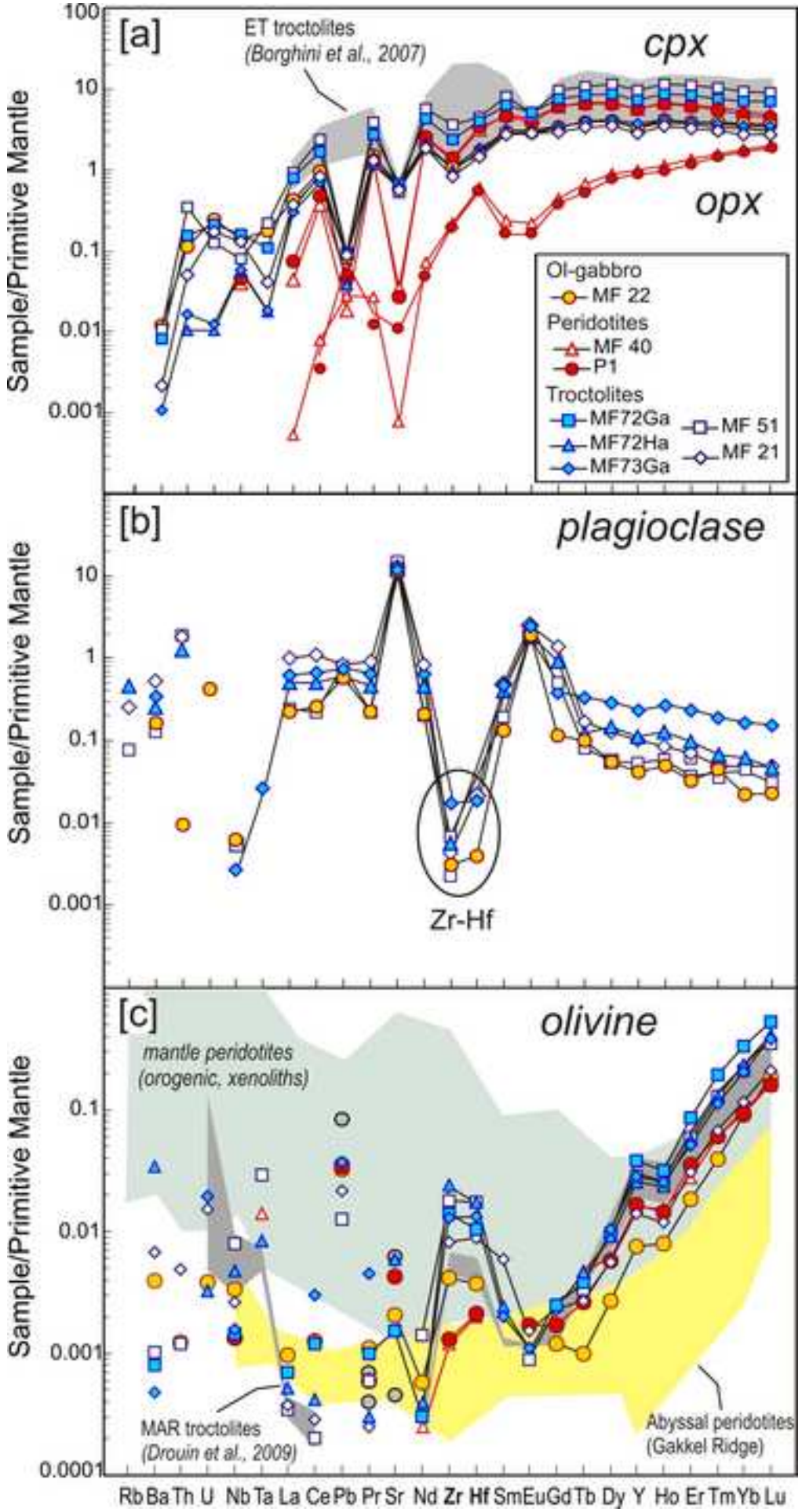

Figure 9

Click here to download high resolution image

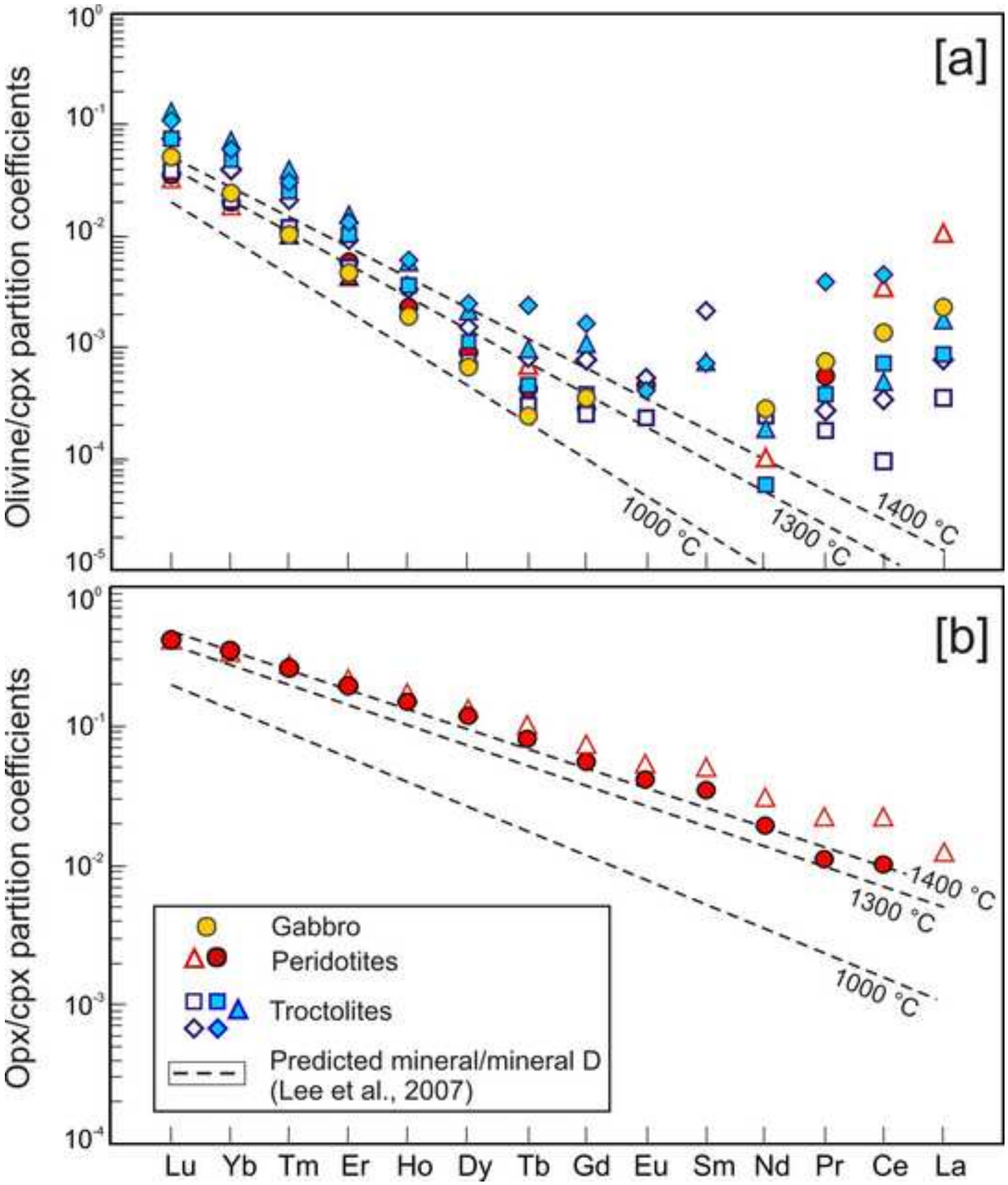

Figure 10

Click here to download high resolution image

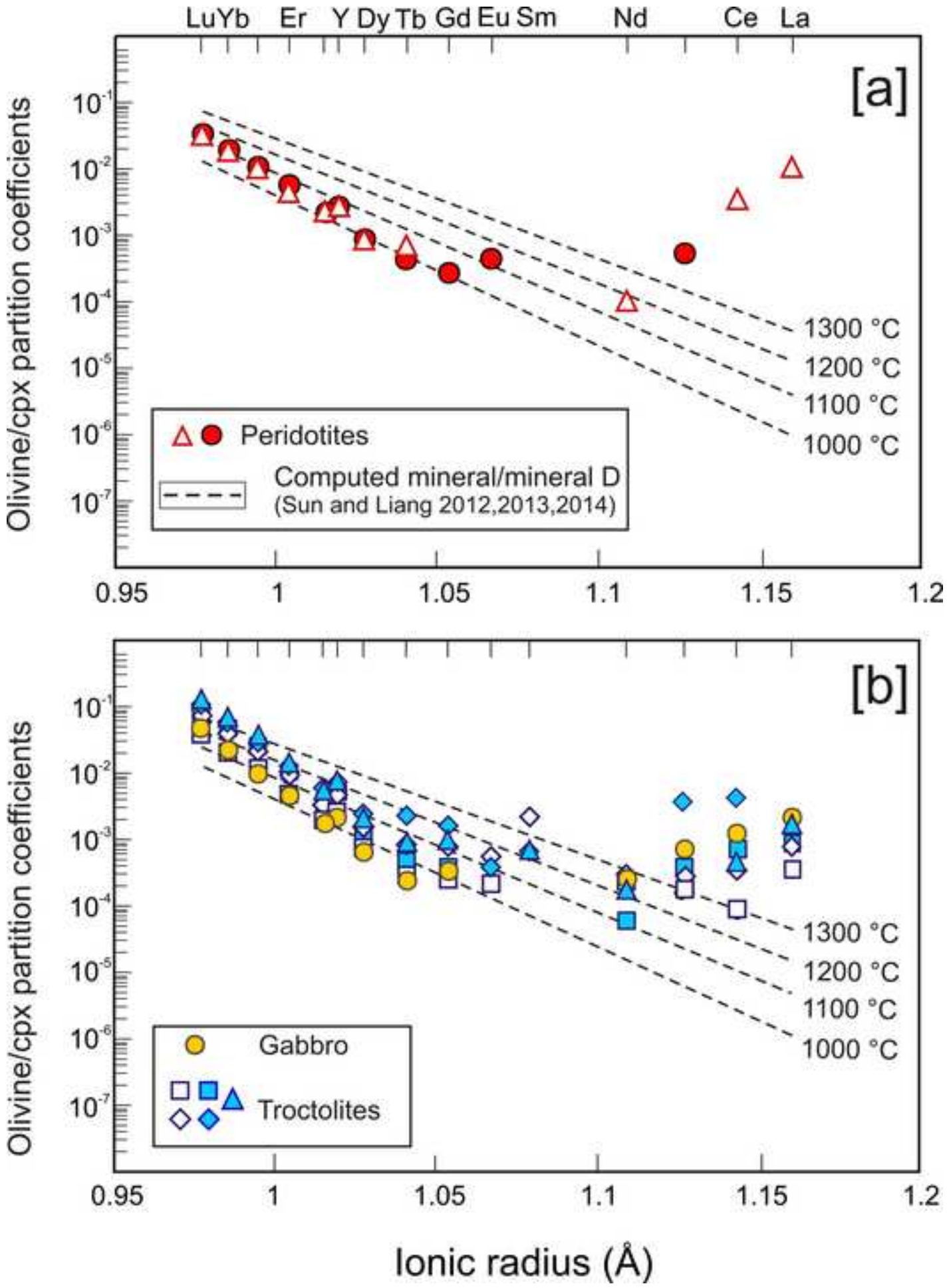

Figure 11

Click here to download high resolution image

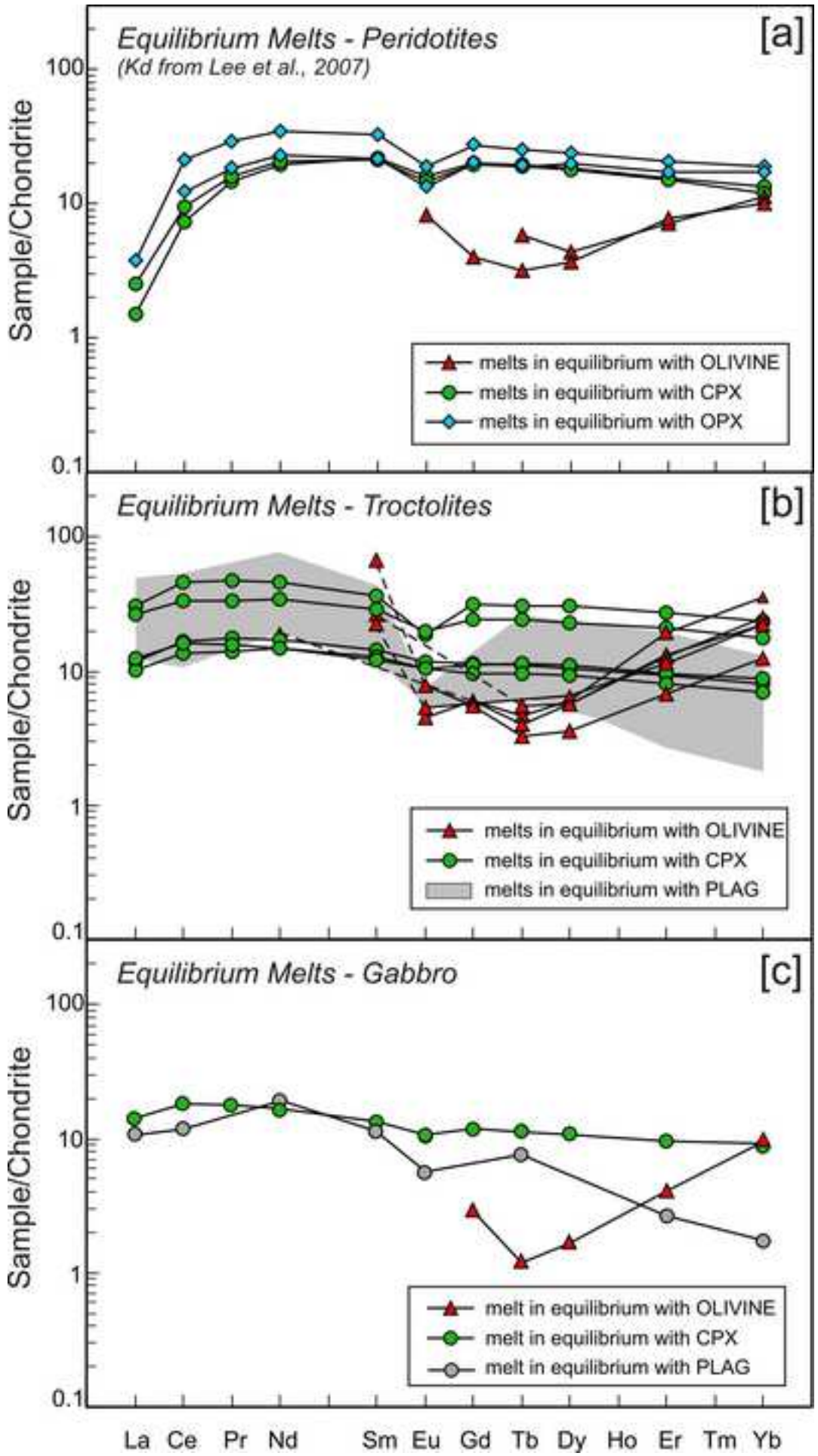

Figure 12

Click here to download high resolution image

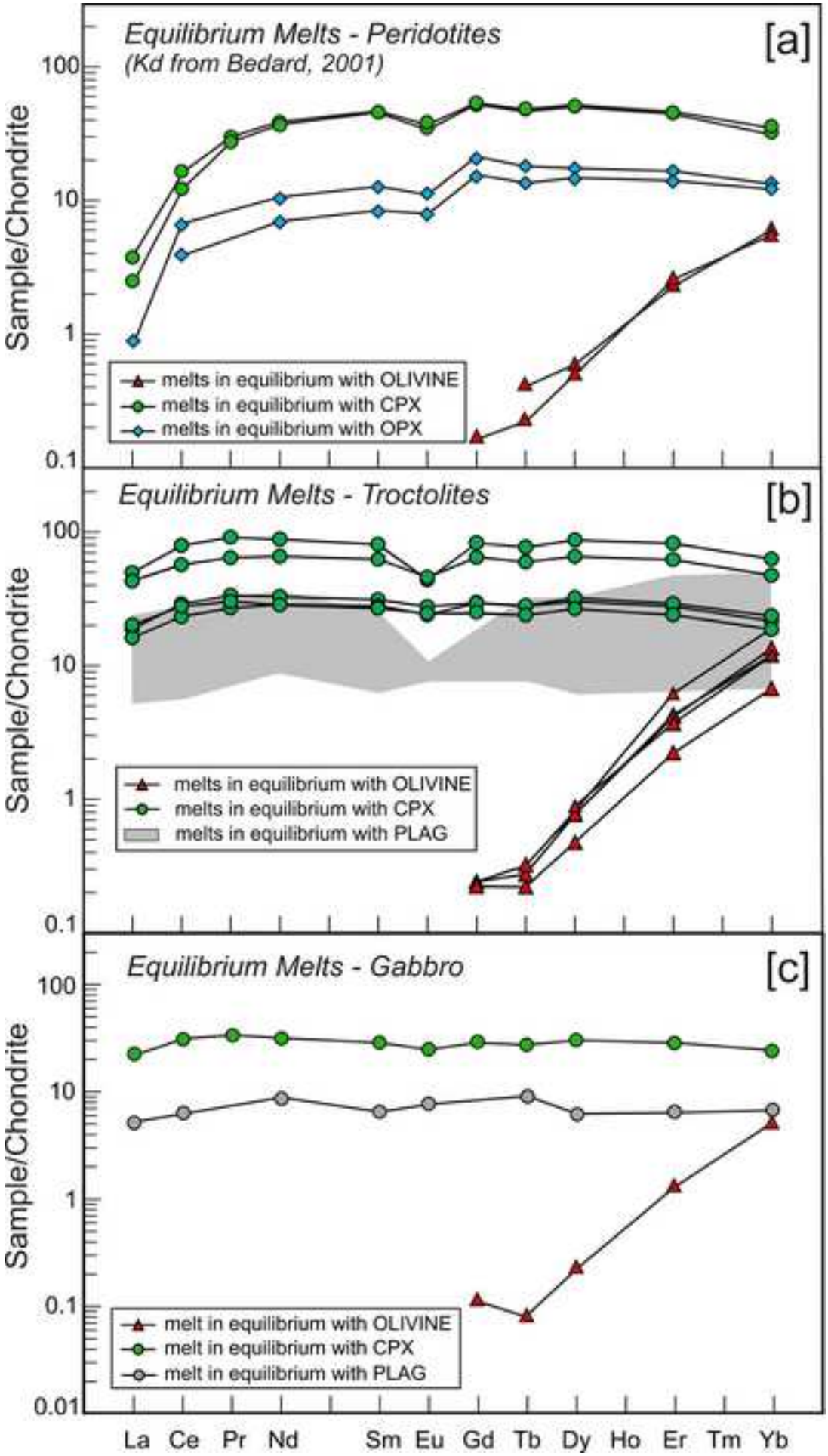

Figure 13

Click here to download high resolution image

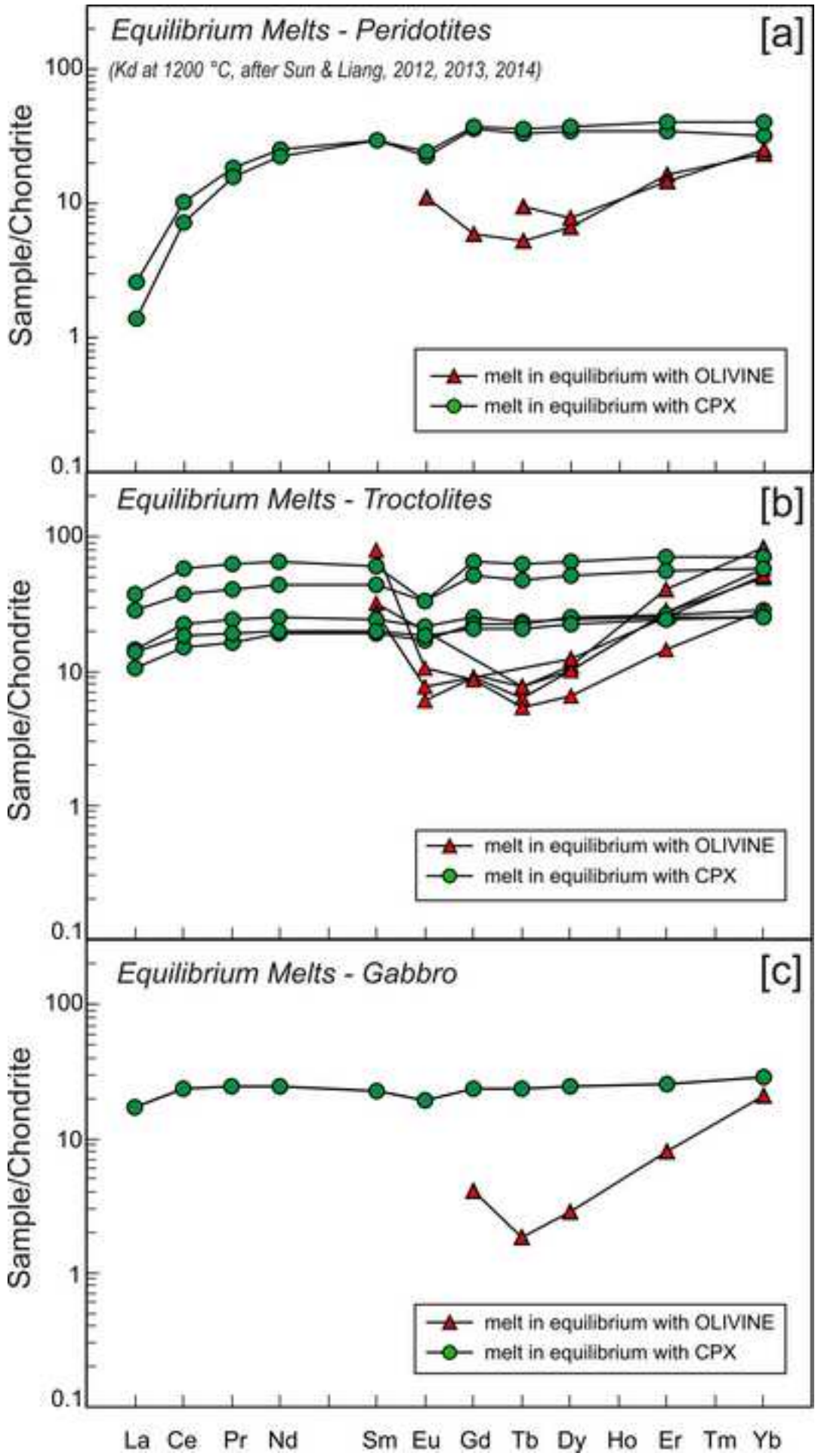

Figure 14

Click here to download high resolution image

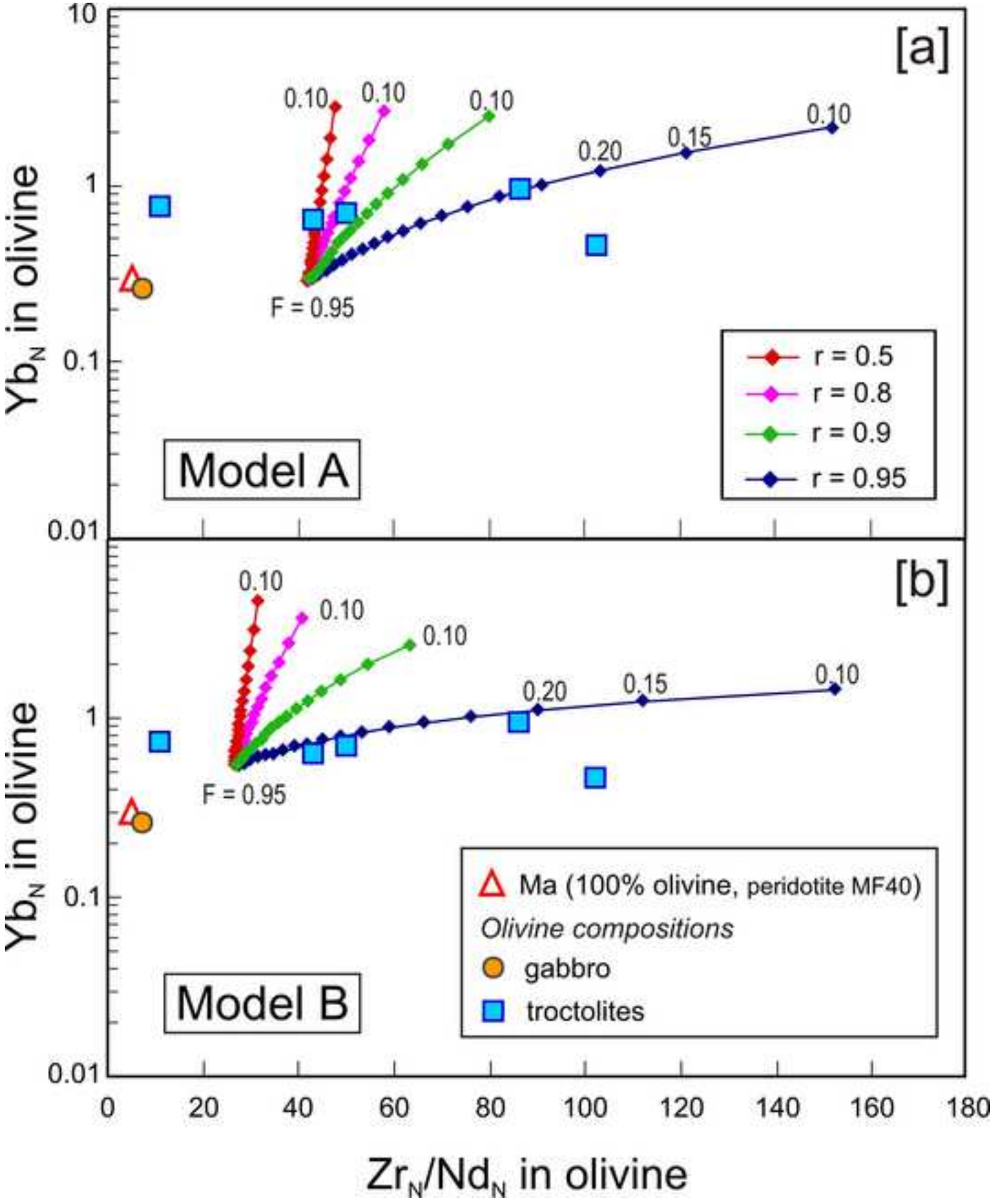

Supplementary Note 1

Click here to download Electronic Annex: Supplementary Note 1.pdf

Supplementary Table 1

Click here to download Electronic Annex: Supplementary Table 1.xlsx

Supplementary Table 2

Click here to download Electronic Annex: Supplementary Table 2.xlsx

Supplementary Table 3

Click here to download Electronic Annex: Supplementary Table 3.xlsx

Supplementary Figure 1

Click here to download Electronic Annex: Supplementary Figure 1.jpg

Supplementary Figure 2

Click here to download Electronic Annex: Supplementary Figure 2.jpg